Linköping studies in science and technology.
Dissertations, No. 1167

Molecular Quadratic Response Properties with Inclusion of Relativity

Johan Henriksson

Akademisk avhandling

som för avläggande av teknologie doktorsexamen vid Linköpings universitet kommer att offentligt försvaras i hörsal Planck, Fysikhuset, Linköpings universitet, fredagen den 11 april 2008, kl. 10.15. Opponent är Dr. Juha Vaara, Laboratory of Physical Chemistry, Department of Chemistry, University of Helsinki.

Abstract

This thesis concerns quadratic response properties, foremost their application to properties related to Jablonski diagrams such as resonant two-photon absorption and excited state absorption. Our main interest lie in optical power limitting applications, and in this context, molecules containing heavy metal atoms prove superior. Therefore, we are interested in the effects of relativity on these properties. In order to assess relativistic effects, a four-component relativistic framework is adopted.

To properly address the molecular properties of interest, not only relativistic effects are important, but also electron correlation. These two properties are not additive, but need to be addressed on the same footing, and, due to the size of the molecules under consideration, we present the implementation of quadratic response properties at the four-component density functional level of theory. For second-harmonic generation, we have demonstrated that correlation and relativity are not additive and that the inclusion of noncollinear magnetization is of little importance.

In the four-component framework, we also present the implementations of single and double residues of the first-order hyperpolarizability, i.e., the evaluation of resonant two-photon absorption cross section and excited state properties. Using these tools we discuss different levels of approximation to the relativistic Hamilto-

nian and we demonstrate that for two-photon absorption, a proper treatment of relativistic effects qualitatively alter the spectrum.

Finally, quantum chemistry in conjunction with electrodynamics is applied to investigate clamping levels in macroscopic samples. The microscopic properties of optically active chromophores are determined by quantum chemistry, and then, electrodynamics is successfully used in order to describe the interaction between chromophores embedded in a host material and laser light.

Department of Physics, Chemistry and Biology
Linköping University, SE-581 83 Linköping, Sweden

Linköping 2008

ISBN 978–91–7393–957–79 ISSN 0345–7524

Linköping studies in science and technology.
Dissertations, No. 1167

Molecular Quadratic Response Properties with Inclusion of Relativity

Johan Henriksson

Linköping University
INSTITUTE OF TECHNOLOGY

Department of Physics, Chemistry and Biology
Linköping University, SE-581 83 Linköping, Sweden

Linköping 2008

Author:
Johan Henriksson
Department of Physics, Chemistry and Biology
Linköping University, SE-581 83 Linköping, Sweden

Bibliographic information:
Henriksson, Johan:
Molecular Quadratic Response Properties
with Inclusion of Relativity
Linköping studies in science and technology.
Dissertations, No. 1167
ISBN 978–91–7393–957–79
ISSN 0345–7524

URL to electronic publication:
http://urn.kb.se/resolve?urn=urn:nbn:se:liu:diva-11035

Cover illustration:
Platinum acetylide compound used in optical power
limiting applications.

Printed in Sweden by Linköpings Tryckeriaktiebolag, Linköping 2008

Abstract

This thesis concerns quadratic response properties, foremost their application to properties related to Jablonski diagrams such as resonant two-photon absorption and excited state absorption. Our main interest lie in optical power limitting applications, and in this context, molecules containing heavy metal atoms prove superior. Therefore, we are interested in the effects of relativity on these properties. In order to assess relativistic effects, a four-component relativistic framework is adopted.

To properly address the molecular properties of interest, not only relativistic effects are important, but also electron correlation. These two properties are not additive, but need to be addressed on the same footing, and, due to the size of the molecules under consideration, we present the implementation of quadratic response properties at the four-component density functional level of theory. For second-harmonic generation, we have demonstrated that correlation and relativity are not additive and that the inclusion of noncollinear magnetization is of little importance.

In the four-component framework, we also present the implementations of single and double residues of the first-order hyperpolarizability, i.e., the evaluation of resonant two-photon absorption cross section and excited state properties. Using these tools we discuss different levels of approximation to the relativistic Hamiltonian and we demonstrate that for two-photon absorption, a proper treatment of relativistic effects qualitatively alter the spectrum.

Finally, quantum chemistry in conjunction with electrodynamics is applied to investigate clamping levels in macroscopic samples. The microscopic properties of optically active chromophores are determined by quantum chemistry, and then, electrodynamics is successfully used in order to describe the interaction between chromophores embedded in a host material and laser light.

Populärvetenskaplig sammanfattning

Då ljus färdas genom ett material kommer ljuset och materialet att ömsesidigt påverkar varandra. Ett materials färg är t.ex. relaterad till dess absorption. Vid låga ljusintensiteter kommer denna växelverkan att vara linjär, men då intensiteten ökar allt mer kommer ickelinjära effekter att bli märkbara. Ett exempel på detta är så kallad tvåfotonsabsorption, där ett material kan vara genomskinligt i normalt ljus men mörkt eller färgat då det träffas av högintensivt ljus, t.ex. från en laser.

Denna avhandling behandlar hur man kan använda kvantmekaniska beräkningar för att bestämma ickelinjära optiska effekter i olika molekyler. Ett starkt fokus ligger på hur dessa molekyler kan användas för att skydda optiska sensorer från att bli skadade av laserljus. Många av de molekyler som visat sig framgångsrika i dessa applikationer innehåller tunga metallatomer. I de tyngre grundämnena har relativistiska effekter en stor inverkan på egenskaperna. Om man bortser från relativistiska effekter skulle beräkningar visa att guld är silverfärgat, medan den korrekta färgen erhålls då dessa effekter tas i beaktande. Mot denna bakgrund har vi utvecklat metoder för att se hur relativistiska effekter påverkar ickelinjära optiska egenskaperna. Vidare illustreras en metod där kvantmekanik tillsammans med elektrodynamik används för att visa hur molekyler ingjutna i ett glasmaterial påverkar en ljuspuls som färdas genom materialet. Detta arbete visar hur man i ett kombinderade ramverk av två teorier kan simulera egenskaper hos ett makroskopiskt objekt genom att man känner till egenskaperna för dess mikroskopiska beståndsdelar.

Preface

This thesis is a compilation of work carried out since May 2003. Its first three chapters briefly cover the theoretical background of my work and serve as introduction to the papers included thereafter. The main work has been carried out in the Computational Physics group at the Department of Physics, Chemistry and Biology at Linköping University, but also during a three month stay at the Department of Chemistry at University of Southern Denmark.

I would like to take this opportunity to give a special thanks to some persons without whom these years would not have passed by as fast as they did. First, and foremost, I want to thank my advisor Patrick Norman for providing me with this great opportunity, which has not only introduced me to challenging tasks to work with, but also to many interesting persons and friends. He also deserves many thanks for his guidance, help, and patience during the work resulting in this thesis. I would also like to direct my gratitude to my collaborators, especially to Dr. Hans Jørgen Aa. Jensen and Dr. Trond Saue for the projects initiated by them and the secondments in their groups. To Hans Jørgen a special thanks for the arrangement of my three months at University of Southern Denmark as research assistant within the EU Marie Curie network NANOQUANT. Beyond the purely scientific, I would like to thank Ingegärd Andersson for taking care of most administrative matters and making paper work flow as smoothly as possible. Then, last but not least, my friends, both inside and outside the university. Hopefully no one will feel left out, but there are some who deserve a special mentioning; Ulf Ekström for our collaboration and discussions concerning our work on DALTON and DIRAC, Auayporn Jiemchooroj and Magnus Hultell for helpful comments on this thesis, Peter Jaksch and Michael Öster for all our discussions on various topics not only the ones concerning physics and mathematics, and, of course, to the PhD and Master students, past and present, in the Computational and Theoretical Physics groups who have participated in discussions and joined in on social activities at as well as outside work.

Finally, I would like to thank the National Graduate School in Scientific Com-

puting (grant no. 200-02-084), the EU Marie Curie network NANOQUANT, and the Swedish Defence Research Agency (FOI) for funding.

Johan Henriksson
Linköping, February 2008

Contents

CHAPTER 1

Introduction

> "Every attempt to employ mathematical methods in the study of chemical questions must be considered profoundly irrational and contrary to the spirit of chemistry. If mathematical analysis should ever hold a prominent place in chemistry—an aberration which is happily almost impossible—it would occasion a rapid and widespread degeneration of that science."
>
> Auguste Comte, *Cours de Philosophie Positive*, 1830

In light of the above quote by Auguste Comte, this thesis seems to make little sense; however, within a hundred years this statement would prove utterly wrong. The late 19^{th} and early 20^{th} century introduced radical changes in the views on physics and chemistry — on the macroscopic scale, the theory of relativity was introduced and, on the microscopic scale, quantum mechanics made its entry. In the light of these developments, Paul Dirac stated:[13]

> "The underlying physical laws necessary for the mathematical theory of a large part of physics and the whole of chemistry are thus completely known, and the difficulty is only that the exact application of these laws leads to equations much too complicated to be soluble. It therefore becomes desirable that approximate practical methods of applying quantum mechanics should be developed, which can lead to an explanation of the main features of complex atomic systems without too much computation."

The "approximate practical methods" called for are what this thesis is concerned with, more precisely in a context where relativity needs to be incorporated with quantum mechanics.

The definition of a "practical method" is, of course, intimately connected to the accuracy wanted and the computational resources at hand. In the early days of quantum mechanics, crude approximations were needed, but as computers were introduced and grew more complex and capable, so did the applicability of quantum

mechanical calculations. Worth noticing is that this development was predicted as early as 1838 when Charles Babbage, an English mathematician, philosopher, and mechanical engineer who originated the idea of a programmable computer, stated that with such a machine at hand

> "All of chemistry, and with it crystallography, would become a branch of mathematical analysis which, like astronomy, taking its constants from observation, would enable us to predict the character of any new compound and possibly the source from which its formation might be anticipated."

Over the last decades, the advances in computational methods and computer hardware have made Babbage's vision, to predict properties of novel materials, a reality. For example, today, computations are routinely used to aid interpretation of experimental data as well as predicting properties of new, functionalized, materials before they are even synthesized. In a world where smaller and smaller building blocks are considered when manufacturing devices, accurate computational predictions form valuable and cost effective tools. Some of these tools are treated in this thesis, and the common denominator of the different topics is the strive for a device protecting optical sensors from laser radiation.

1.1 Optical Power Limiting

In 1960, the first laser was constructed by Theodore Maiman at Hughes Research Laboratories.[34] Since then, lasers have developed considerably — the intensity has been largely increased, lasers have been made tunable so that they are not locked at a specific wavelength, devices get smaller, etc.[11] All these developments have made lasers powerful tools useful in many applications ranging from high quality spectroscopy through medicine to cutting tools. The intensity and focus of the laser beam, which makes lasers such a useful tool in many applications, poses a potential problem when it comes to optical sensors which might be dazzled, blinded, or even destroyed if subjected to laser radiation. In light of this, a need and demand for optical power limiting devices to protect optical sensors have emerged, and over recent years, the Swedish Defence Research Agency, FOI, has coordinated a collaboration with the goal to develop such a product. Within this collaboration, theoretical modeling of molecular materials has been employed as guidance for which materials to focus on.

The apparent issue when it comes to protecting optical sensors from laser damage is that light in this case is both the origin of information and the cause of damage. For apparent reasons, the source of harm cannot be screened permanently, since then, the optical information one strives to retrieve will also be lost. The key difference between useful and harmful light is the intensity, i.e., laser light is high-intensive, and, thus, it can damage sensors. The task at hand is to create a device (see Figure 1.1[33]) that will allow useful light to enter the system at intensities below the damage threshold, whereas it blocks high-intensive light beyond this threshold.

Since high-intensive lasers might damage a sensor in a single pulse, a self-activated part filter is called for since there is no time to activate a filter upon

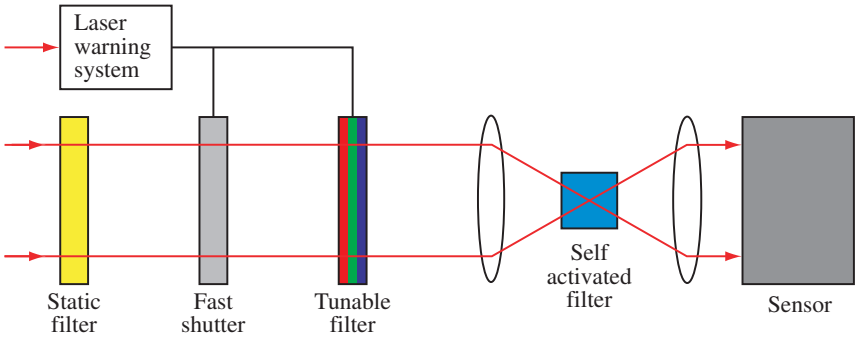

Figure 1.1. Schematic layout of a laser protection device under development by the Swedish Defence Research Agency.[33]

detection of an incident laser pulse. This has been successfully achieved using two-photon absorption and processes following,[9,36,41,44,50,51,52] which is further discussed in Section 1.2. Due to saturation, this self-activated part of the device will only be able to block a first pulse, or maybe the first few pulses, but it will not work against continuous lasers or consecutive pulses. Despite saturation, the self-activating part plays a crucial role as it enables for a second, controlled part of the device to be activated. For apparent reasons, the controlled filter has to have a response time shorter than the saturation of the self-activating one, which is why FOI has turned their attention to so-called spin-transition materials. These materials and their functions are outlined in Section 1.3.

1.2 Passive Protection and Jablonski Diagrams

Upon light irradiation, a molecule may absorb photons, resulting in an excited molecular state. Figure 1.2, a so-called Jablonski diagram, illustrates different optical properties of the platinum compound studied in Paper VI. As can be seen, one photon is not sufficient to bring this molecule into an excited singlet state, which means that the material will be transparent at low intensities, i.e., when one-photon absorption (OPA) is the dominating process. However, as the intensity increases, the probability of absorbing two or more photons simultaneously becomes significant. Thus, at high intensities, two-photon absorption (TPA) can bring the molecule into an excited state, which is the onset of the filter. Once in an excited state, a rapid relaxation to the lowest excited singlet state follows ($\tau \sim 1$ ps).[52] From this state, relaxation brings the molecule either back into its ground state ($\tau \sim 10$ ns) or via an intersystem crossing (ISC) into the triplet state manifold ($\tau \sim 100$ ns).[52] The triplet state has a significant lifetime ($\tau \sim 1$ μs),[37] and, thus, from here, it is possible to achieve significant OPA within the triplet manifold. This is known as excited state absorption (ESA). Utilizing materials with large TPA cross section and high yield in the ISC open the possibilities to create materials suitable for self-activating protections.

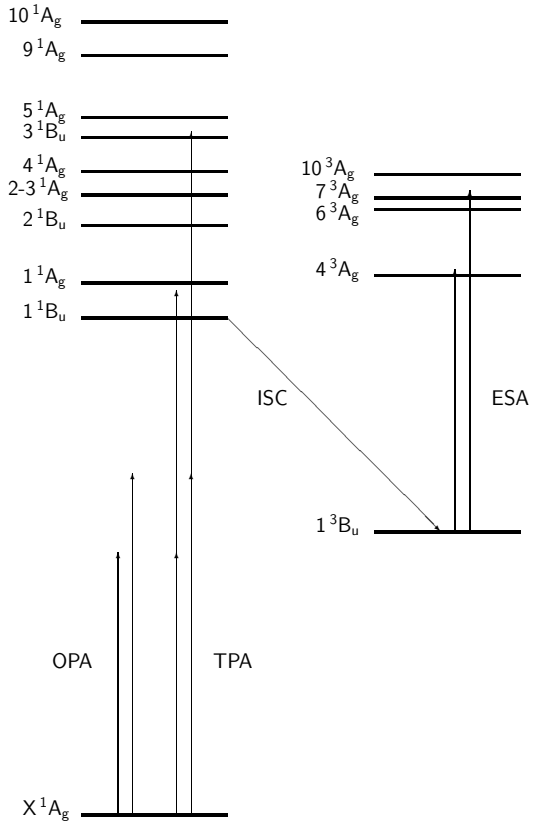

Figure 1.2. Jablonski diagram illustrating the absorption processes in a Pt(II) compound. For further details, see Paper VI.

Computational evaluation of properties related to the Jablonski diagram form the main part of this thesis, as will also be further illustrated in Chapter 3. The main focus lies on how relativity affects these properties and how it is included into the calculations. The need to account for this springs from the fact that materials containing heavy metal atoms provide superior ISC yields.[36]

1.3 Active Protection and Spin-transitions

The active part of the device sketched in Figure 1.1 is used to provide protection when the self-activated part saturates. The requirement that the controlled part is activated before saturation is reached, eliminates any mechanical solutions or solutions based on liquid crystals since their response times are orders of magnitude too slow. Instead of relying on reconfiguration of entire molecules, like liquid crystals, in order to change the optical properties of a material, the Swedish Defence Research Agency considers the possibility to use the much faster process

of electronic reconfiguration. If the electronic configuration of a molecule can be controlled by external perturbations, and if one configuration is colored whereas the other one is colorless, it will be possible to realize a fast controlled filter. The approach investigated by FOI is to use so-called spin-transition (ST) materials. The concept of such a spin-transition is illustrated in Figure 1.3, where it is shown how reversible transitions between two different electronic configurations can be brought about, all depending on external perturbations such as changes in temperature, pressure, light irradiation, etc. Below follows a brief introduction to the materials investigated by FOI and treated by us in Ref. 22.

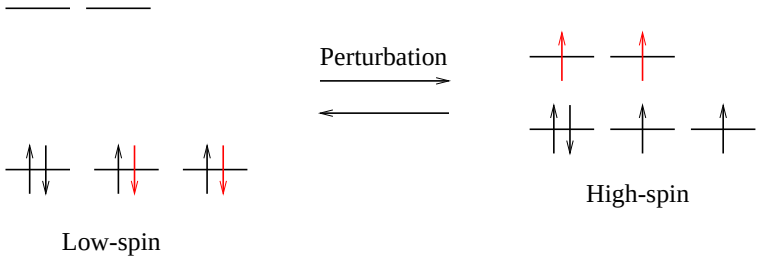

Figure 1.3. Schematic illustration of the electron configurations of the low-spin and high-spin states.

In atomic iron, the $3d$-orbitals are all degenerate, however, if ligands are attached in octahedric coordination, this degeneracy is lifted, and, in the O_h point group, the three $3d$-orbitals of symmetry t_{2g} will be lower in energy than the two of symmetry e_g.[6] These orbitals are illustrated in Figure 1.3. If six valence electrons are distributed among these $3d$-orbitals, in a weak ligand field, the splitting of the t_{2g}- and e_g-orbitals is small, and, thus, Hund's rules apply forming a quintet configuration with four open shells, a high-spin (HS) state. If, on the other hand, the ligand field is strong, the orbital splitting is large and all six electrons are found in the t_{2g}-orbitals forming a closed-shell, or low-spin (LS), state.[20] In the intermediate case, the state of the system depends on external perturbations. The different electronic structures of the two states are associated with different molecular properties, the most obvious being the change in magnetic properties.

From a practical point of view, the challenge lies in finding materials with suitable optical properties in the two states as well as a switching criterion that enables practical devices. Experiment can be largely aided by computational investigations since the synthesis of the considered spin-transition compounds is tedious. For example, if the absorption spectra of the different states can be calculated, only the most promising systems need to be synthesized, or, if one can assess the relative stability of the high- and low-spin states, candidates not capable of spin-transitions can be ruled out. These topics have been touched upon in Ref. 22, but will not be treated further in this thesis.

CHAPTER 2

Molecular Electronic-structure Theory

> "I think that I can safely say that nobody understands quantum mechanics."
>
> RICHARD FEYNMAN, *The Character of Physical Law*, 1965

The cornerstone, and starting point, when describing a quantum mechanical system is the quantum mechanical wave equation

$$i\hbar\frac{\partial}{\partial t}|\psi(t)\rangle = \hat{H}|\psi(t)\rangle. \tag{2.1}$$

This equation gives the possibility to describe matter by wave functions, but analytical solutions exist only for a very limited number of systems. The necessity for approximative solutions were, as quoted in the Introduction, pointed out by Dirac and further emphasized by Gilbert Lewis[31]

> "...in the Schrödinger equation we very nearly have the mathematical foundation for the solution of the whole problem of atomic and molecular structure..."
> [but]
> "...the problem of the many bodies contained in the atom and the molecule cannot be completely solved without a great further development in mathematical technique."

The tools needed to attack these problems are introduced in this chapter.

2.1 Self-consistent Field Theory

The wave equation (2.1) provides the tool for describing quantum mechanical systems, however, as pointed out, approximate methods are necessary and the key issue is to find good approximations. In the following, two different approaches

to tackle this problem are outlined; wave function and density functional theory (DFT) methods. The discussion will only focus on solving the electronic structure problem for fixed nuclear positions, i.e., the Born–Oppenheimer approximation is employed. This approximation states that the quantum mechanical wave equation, to good approximation, can be separated into an electronic part solved for fixed nuclear positions and a nuclear part where the electronic solution is utilized as potential energy surface. The justification for this lies in the fact that the much heavier nuclei move much slower than the electrons.

2.1.1 Wave Function Methods

In a fixed nuclear framework, the electronic Hamiltonian of a molecule is

$$\hat{H} = \sum_i \hat{h}_i + \sum_{i>j} \hat{g}_{ij}, \tag{2.2}$$

where $\hat{h}_i$ is the one-electron part of the Hamiltonian, $\hat{g}_{ij}$ is the two-electron part, and i and j are indices referring to electrons. Given a wave function, ψ, the energy of a system can be evaluated according to

$$E[\psi] = \frac{\langle\psi|\hat{H}|\psi\rangle}{\langle\psi|\psi\rangle}, \tag{2.3}$$

and if the wave function is constructed such that it contains variational parameters, it is possible to adjust these parameters until the minimum energy is found. Together with the variational principle,[19] which states that for any given wave function, ψ, the energy functional yields an upper bound of the true ground state energy E_0, i.e.,

$$E_0 \leq E[\psi], \tag{2.4}$$

where the equality holds if and only if ψ is the exact ground state wave function.[61] This maps a route toward finding approximate solutions in an iterative fashion.

Turning the attention to the wave function, in a quantum mechanical system containing N electrons, let these electrons be distributed among N orthogonal spin-orbitals, ϕ_i. The total wave function can now be constructed from these spin-orbitals under the restriction that a physical wave function is retrieved. One way to achieve this is by forming a so-called Slater determinant[61]

$$|\psi\rangle = \frac{1}{\sqrt{N!}} \begin{vmatrix} \phi_1(\mathbf{r}_1) & \phi_2(\mathbf{r}_1) & \cdots & \phi_N(\mathbf{r}_1) \\ \phi_1(\mathbf{r}_2) & \phi_2(\mathbf{r}_2) & \cdots & \phi_N(\mathbf{r}_2) \\ \vdots & \vdots & \ddots & \vdots \\ \phi_1(\mathbf{r}_N) & \phi_2(\mathbf{r}_N) & \cdots & \phi_N(\mathbf{r}_N) \end{vmatrix}, \tag{2.5}$$

where $\mathbf{r}$ denotes electron coordinates. If, for simplicity, the wave function is constructed from a single Slater determinant, i.e., neglecting electron correlation, we arrive at the Hartree–Fock equations[61]

$$\hat{F}\phi_i = \sum_j \lambda_{ij}\phi_j, \tag{2.6}$$

where λ_{ij} are Lagrangian multipliers and $\hat{F}$ is the Fock operator

$$\hat{F} = \hat{h} + \sum_j (\hat{J}_j - \hat{K}_j), \tag{2.7}$$

where $\hat{J}$ and $\hat{K}$ are the Coulomb and exchange operators, respectively.[61] Equation (2.6) can be diagonalized yielding the so-called canonical Hartree–Fock equations,

$$\hat{F}\phi'_i = \varepsilon_i \phi'_i, \tag{2.8}$$

where ε_i are the orbital energies.

So far, the spin-orbitals have only been treated as abstract entities, but in order to be useful in numerical calculations, a concrete form is required. In a molecule, the spin-orbitals will be so-called molecular orbitals, extended over the whole or parts of the molecule. Introducing a basis set (see Section 2.2 for further details) of atomic orbitals, χ_i, the molecular orbitals can be expressed as linear combinations thereof,

$$\phi_j = \sum_i c_{ij}\chi_i, \tag{2.9}$$

which finally turns the Hartree–Fock equations into a matrix equation known as the Roothaan–Hall equation,

$$FC = SCE, \tag{2.10}$$

where the Fock matrix elements are given by

$$F_{ij} = \langle \chi_i | \hat{F} | \chi_j \rangle, \tag{2.11}$$

the overlap matrix elements by

$$S_{ij} = \langle \chi_i | \chi_j \rangle, \tag{2.12}$$

all the expansion coefficients c_{ij} have been collected in C, and E is a diagonal matrix with the orbital energies, ε_i, as diagonal elements. Given a wave function, the Fock matrix can be constructed, and the generalized eigenvalue problem (2.10) yields a new C-matrix. This in turn updates the wave function according to Eq. (2.9), and the procedure is repeated until convergence is reached — the so-called self-consistent field method.

2.1.2 Density Functional Theory

Above, the wave function formalism was outlined, and as could be seen, every single electron is explicitly accounted for, i.e., N sets of electron coordinates have to be dealt with. If instead considering the electron density,

$$\rho(\mathbf{r}) = N \cdot \int \cdots \int |\psi|^2 d\mathbf{r}_2 \ldots d\mathbf{r}_N, \tag{2.13}$$

a quantity which is always described by three spatial coordinates, the complexity remains the same regardless of system size. Hence, a tempting thought is to base

a theory on the electron density instead of the wave function. This idea was raised in the very early days of quantum mechanics by both Thomas and Fermi, the so-called Thomas–Fermi theory (see for example Ref. 48 for a detailed discussion). However, this theory, and modifications thereof, proved inadequate and unable to compete with wave function methods. For over thirty years, density based methods were fighting an uphill battle, but this drastically changed in 1964 with the groundbreaking paper by Hohenberg and Kohn.[25] In this paper it is proven that the ground state electron density uniquely determines both the potential defining the system, $v(\mathbf{r})$, within an additive constant, as well as the number of electrons, N, and, thus, all ground state properties. Following this, the ground state energy can be written in terms of density functionals according to

$$\begin{aligned} E[\rho] =& T[\rho] + V_{ee}[\rho] + V_{ne}[\rho] \\ =& T[\rho] + V_{ee}[\rho] + \int v(\mathbf{r})\rho(\mathbf{r})d\mathbf{r} \\ =& F[\rho] + \int v(\mathbf{r})\rho(\mathbf{r})d\mathbf{r}, \end{aligned} \tag{2.14}$$

where the terms in the first line correspond to the kinetic energy of the electrons and the potential energy terms due to electron-electron and electron-nuclear interactions. Treating the electron-nuclear interaction separately leaves a universal functional, $F[\rho]$, valid for any potential and any number of electrons. Furthermore, Hohenberg and Kohn proved that for electronic ground states, the variational principle holds. Any given density $\rho \geq 0$ will, inserted into the energy functional, provide an upper bound of the ground state energy, E_0, i.e.,

$$E_0 \leq E[\rho]. \tag{2.15}$$

The paper by Hohenberg and Kohn provided a theoretical foundation for density functional methods, but practical problems still remained since knowledge of the functional form of $F[\rho]$ was required, or rather of the kinetic energy functional and the functional describing electron-electron interactions. This problem was addressed a year later, in 1965, by Kohn and Sham.[30] As a starting point, they reintroduced the concept of orbitals and considered a system of N noninteracting electrons in N orbitals ϕ_i. For such a system, it is possible to find the exact solution to the wave equation

$$\left[\hat{T} + v_s(\mathbf{r})\right]\phi_i = \varepsilon_i\phi_i, \tag{2.16}$$

where $\hat{T}$ is the kinetic energy operator and $v_s(\mathbf{r})$ is a potential chosen such that

$$\rho(\mathbf{r}) = \sum_i \langle\phi_i(\mathbf{r})|\phi_i(\mathbf{r})\rangle \tag{2.17}$$

yields the exact electron density of the corresponding interacting system. Using the orbitals introduced, the kinetic energy of the noninteracting system is given by

$$T_s[\rho] = \sum_i \left\langle \phi_i \left| \hat{T} \right| \phi_i \right\rangle. \tag{2.18}$$

Now, returning to Eq. (2.14), using the kinetic energy of the noninteracting system, T_s, and explicitly accounting for the Coulomb part of the electron-electron interaction, J, it is possible to rewrite the energy functional (2.14) as

$$E[\rho] = T_s[\rho] + J[\rho] + E_{xc}[\rho] + \int v(\mathbf{r})\rho(\mathbf{r})d\mathbf{r}, \tag{2.19}$$

where the exchange-correlation functional

$$E_{xc}[\rho] = (T[\rho] - T_s[\rho]) + (V_{ee}[\rho] - J[\rho]) \tag{2.20}$$

has been introduced. An exchange-correlation potential is now defined through

$$v_{xc}(\mathbf{r}) = \frac{\delta E_{xc}[\rho]}{\delta\rho(\mathbf{r})}, \tag{2.21}$$

which leads to the the Kohn–Sham equations

$$\left[\hat{h} + \int \frac{\rho(\mathbf{r}')}{|\mathbf{r} - \mathbf{r}'|}d\mathbf{r}' + v_{xc}(\mathbf{r})\right]\phi_i(\mathbf{r}) = \varepsilon_i\phi_i(\mathbf{r}). \tag{2.22}$$

It is easy to see the resemblance between these equations and the Hartree–Fock ones. The difference is that the exchange term in the Hartree–Fock equations has been replaced by the exchange-correlation term. Thus, it is realized that the machinery established for solving the Hartree–Fock equations, the self-consistent field method, is equally well applicable for solving the Kohn–Sham ones. It should finally be noted that knowledge of the exact exchange-correlation functional will yield the exact density, and, hence, the exact ground state properties of the system under consideration.

2.1.3 Relativistic Considerations

Up until now, no reference has been made to whether the quantum mechanical wave equation is nonrelativistic or relativistic. The theory as such has only been presented in terms of the Hamiltonian and its constituent operators. It is first when these operators are investigated, the differences, and, thus, the effects of a relativistic theory, show.

For a free particle, the Schrödinger equation, i.e., the nonrelativistic wave equation, takes the form

$$i\hbar\frac{\partial}{\partial t}\psi = -\frac{\hbar^2}{2m}\nabla^2\psi, \tag{2.23}$$

which is a first-order differential equation in time but second-order in space. The different orders of derivatives with respect to space and time prevent this equation from being Lorentz covariant, and, hence, it is not consistent with special relativity.[57]

Introducing the concept of the correspondence principle,[58] quantum mechanical operators are to correspond to observables in classical physics. From the action

of operators on plane waves, the quantum mechanical energy and momentum operators are assigned as

$$\hat{E} = i\hbar\frac{\partial}{\partial t} \quad \text{and} \quad \hat{p} = \frac{\hbar}{i}\nabla, \tag{2.24}$$

respectively, and it is seen that the Schrödinger equation for a free particle is in accordance with the energy expression, $E = p^2/2m$, from classical mechanics. Along these lines, attempts were made to reach a relativistic wave equation from the relativistic energy expression $E^2 = (cp)^2 + (mc^2)^2$. Such an approach was considered already by Schrödinger and later also by several others, leading to what today is known as the Klein–Gordon equation.[59] However, due to the second-order derivative in time, the probability density is not positive definite, and, therefore, the equation was discarded as unphysical.[a]

The negative probability density of the Klein–Gordon equation led Dirac toward an equation linear in both space and time, the equation known as the Dirac equation.[12] For a free electron, the Dirac equation is written as

$$i\hbar\frac{\partial}{\partial t}\psi = \left\{c\alpha^k\hat{p}_k + \beta mc^2\right\}\psi, \tag{2.25}$$

where Einstein summation is applied over the index k. A closer examination shows that the coefficients α and β are Hermitian matrices and that rank 4 is the smallest dimension satisfying the demands put upon them.[57] The matrices are given by

$$\alpha^i = \begin{pmatrix} 0 & \sigma^i \\ \sigma^i & 0 \end{pmatrix} \quad \text{and} \quad \beta = \begin{pmatrix} \mathbb{I}_2 & 0 \\ 0 & -\mathbb{I}_2 \end{pmatrix}, \tag{2.26}$$

where σ^i are the Pauli spin matrices. As compared to the Schrödinger equation where the wave functions are scalar functions, the solutions of the Dirac equation have four components, so-called four-spinors. The solutions spanning the four components fall into two categories, two with positive-energy solutions and two with negative ones. The interpretation of the different terms will be outlined below, following the discussion by Schwabl.[57]

Considering an electron at rest, it is seen that the components of the spinor give rise to two positive-energy solutions and two negative ones. (It should be noted that the occurrence of both positive- and negative-energy solutions requires that special attention is paid to the self-consistent field procedure.[54]) In order to continue the interpretation, an electromagnetic field is applied. Due to the vector potential, $\mathbf{A}$, this modifies the momentum operator according to

$$\hat{\mathbf{p}} \rightarrow \hat{\boldsymbol{\pi}} = \hat{\mathbf{p}} - \frac{e}{c}\mathbf{A} \tag{2.27}$$

and, furthermore, a term, $e\Phi$, related to the scalar potential is added. Hence, in an electromagnetic field, the Dirac equation is[57]

$$i\hbar\frac{\partial}{\partial t}\psi = \left\{c\alpha^k\pi_k + \beta mc^2 + e\Phi\right\}\psi. \tag{2.28}$$

[a] N.b., it was later discovered by Pauli and Weisskopf[49] that the Klein–Gordon equation properly describes massive particles with spin 0.

Going to the nonrelativistic limit, it is found that the negative-energy solutions are roughly a factor v/c smaller than the positive-energy solutions, and they are therefore referred to as small- and large-component solutions, respectively.[57] Focusing on the positive-energy solutions, it is seen that the Dirac equation reduces to the so-called Pauli equation,[58] which describes spin added *ad hoc* to nonrelativistic theory. Thus, the Dirac equation intrinsically describes spin, and the components of the four-spinor are

$$\psi = \begin{pmatrix} \psi^{L\alpha} \\ \psi^{L\beta} \\ \psi^{S\alpha} \\ \psi^{S\beta} \end{pmatrix}, \tag{2.29}$$

where α and β refer to spin and L and S refer to the large- and small-components.

Reductions of Relativistic Hamiltonians

Computationally, the four-component Dirac equation will, for technical reasons, be about two orders of magnitudes more demanding than its nonrelativistic counterpart.[26] Considerable efforts have been put into reducing these costs at the four-component level,[7,32,40,53,55,62,63] but still, these methods are computationally demanding. One of the key issues is the coupling between the large- and small-component bispinors of the four-spinor. Considering the Dirac equation, two types of operators can be identified — even ones that do not couple the large- and small-component parts, and odd ones that do. In chemical applications in general, the contributions from the small-component bispinor are small.[53] Therefore, methods have been sought that decouple the large- and small-component bispinors of the Dirac equation in order to achieve two two-component equations, where the interest lie in the large-component equation. In the literature, two approaches to decouple the positive energy solutions from the negative ones exist; elimination of the small-component and decoupling by a unitary transformation. Recently, it has been shown that these two methods are equivalent.[26] As for decoupling through a unitary transformation, the idea was introduced by Foldy and Wouthuysen,[17] and detailed accounts of this transformation is, for example, given in the books by Schabl[57] and Strange.[60] The basic idea is that successive application of a unitary transformation will form weaker and weaker couplings between the two components, i.e., reducing the influence of odd operators, at the same time as relativistic correction terms are added. The scalar relativistic correction terms are easily incorporated into nonrelativistic codes, whereas dedicated programs are needed in order to account for couplings between the two spin-components, e.g., spin-orbit coupling. Numerous modifications of the Foldy–Wouthuysen scheme have been proposed, e.g., the Douglas–Kroll–Heß,[14,23,24] Barysz–Sadlej–Snijders,[4,5] and infinite-order two-component[26] Hamiltonians.

2.2 Basis Sets

Above, the quantum chemical methods and the underlying equations have been dealt with. However, apart from Eq. (2.9), nothing has been said about the ba-

sis functions, χ, and basis sets thereof spanning the matrix equations. From a physical point of view, so-called Slater-type functions, $e^{-\alpha r}$, have the same radial dependence as hydrogen orbitals, but, from a computational point of view, they call for numerical integration. If, on the other hand, Gaussian-type functions, $e^{-\alpha r^2}$, are used, analytical evaluation of integrals is gained to the cost of the loss of the physical shape of the orbitals. The computational gain in using Gaussian-type orbitals (GTOs) is so high, that in practice, linear combinations of GTOs are used to describe the atomic orbitals. Figure 2.1 illustrates the radial distribution function for a hydrogen 1s-orbital. The true wave function, i.e., the Slater-type orbital (STO), the optimized Gaussian-type orbital (GTO), and an optimized orbital formed by a linear combination of two GTOs (the so-called STO-2G basis set) are plotted for comparison. The plot is only to show the concept, STO-2G is the very simplest Gaussian-type basis set there is, and the more complex and advanced the basis sets, the closer the resemblance to the true orbital. A detailed account of different basis sets is given in Ref. 21.

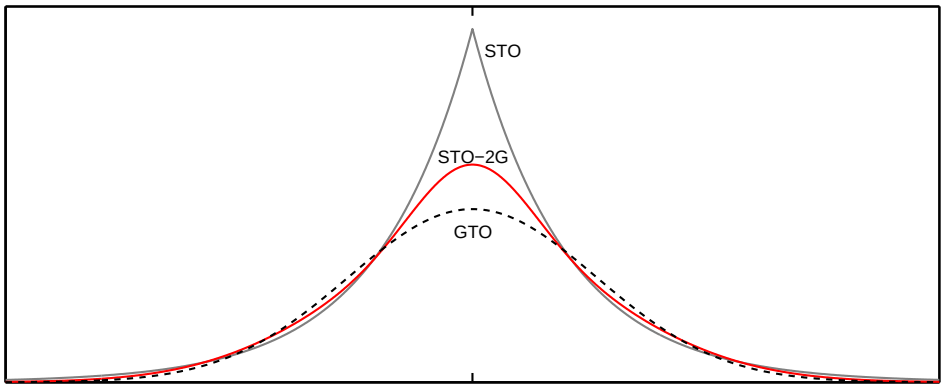

Figure 2.1. Illustration of hydrogenic wave functions for fixed angles and varying r.

In the nonrelativistic realm, the use of basis sets is straightforward since the wave functions are scalar functions. However, in the relativistic theory, special attention is called for due to the different components in the solutions. Consider two basis sets — one for the large-component and one for small-component spinors. From the Dirac equation for a free particle, Eq. (2.25), it is seen that the two basis sets are connected through the operator $\sigma^k p_k$. For basis sets where this connection is fulfilled, the kinetic energy has a maximum,[15] and, in the nonrelativistic limit, any other connection will underestimate the kinetic energy.[16] This gives rise to so-called kinetically balanced basis sets where the small-component basis sets are derived from the large-component ones. It should be noted that this also makes the use of contracted basis sets nontrivial in relativistic calculations, which is why uncontracted basis sets are widely used.[16]

2.2.1 Effective Core Potentials

The cost of an electronic structure calculation using the self-consistent field methods outlined depends on the number of electrons treated and the size of the basis sets used. As the number of basis functions increases, so does the computational cost. However, for heavy elements, most of the electrons are situated in the core region and do not contribute significantly to most chemical and spectroscopic properties. Thus, when dealing with such elements, vast savings would be achieved if the effect of the core electrons could be emulated by a potential leaving only the valence electrons to be explicitly accounted for. Effective core potentials (ECPs) provide such an approach.

The concept of effective core potentials was introduced by Kahn and Goddard in 1972.[29] They suggested to replace core electrons with an effective potential

$$U(\mathbf{r}) = \sum_{l,m} U_l(r)|lm\rangle\langle lm|, \tag{2.30}$$

where $U_l(r)$ is a potential depending on the angular momentum quantum number l and $|lm\rangle\langle lm|$ is the angular momentum projection operator (projector). In principle, the summation over l is infinite, however, in practice $U_l(r) \approx U_L(r)$ for $l > L$, where L is taken to be the largest l quantum number in the core.[38] Using the closure relation, this results in the potential

$$U(\mathbf{r}) = U_L(r) + \sum_{l=0}^{L} \sum_{m=-l}^{l} \left[U_l(r) - U_L(r)\right] |lm\rangle\langle lm|, \tag{2.31}$$

where the first part is referred to as the local part and the second one as the nonlocal part. In accordance with Kahn *et al.*[28] the potential fitting is applied to $U_L(r)$ and $[U_l(r) - U_L(r)]$ separately, resulting in different sets of parameters for the local part and each l of the nonlocal part according to

$$r^2 \left[U_L(r) - \frac{N_c}{r}\right] = \sum_i d_{iL} r^{n_i} \exp(-\xi_i r^2), \tag{2.32}$$

where N_c is the number of core electrons, and

$$r^2 \left[U_l(r) - U_L(r)\right] = \sum_i d_{il} r^{n_i} \exp(-\xi_i r^2), \tag{2.33}$$

respectively.

To show ECPs at work, calculations on neon and argon have been performed at the Hartree–Fock level, and the radial distribution function is illustrated in Figure 2.2. In order to make comparisons between ECP and all-electron calculations, the all-electron basis set is also used as valence basis set for the ECP. It is clearly seen that the valence region is properly described by the ECP. Now, the question arises what happens if an electric field is applied. To show this, a static electric field, $\mathbf{E} = E\mathbf{e}_z$, is applied to argon, inducing a dipole moment in the z-direction, μ_z. At a field strength $E = 0.1$ a.u., the all-electron calculation

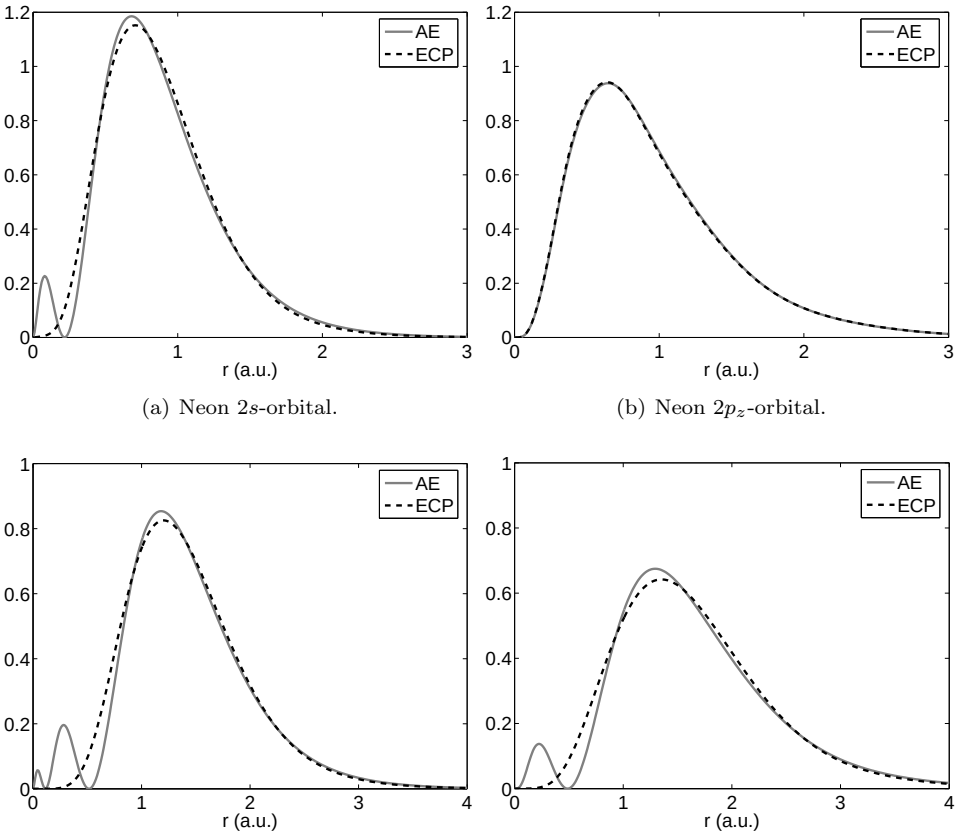

(a) Neon 2s-orbital.

(b) Neon 2p_z-orbital.

(c) Argon 3s-orbital.

(d) Argon 3p_z-orbital.

Figure 2.2. Comparison between the radial distribution functions for the valence orbitals in neon and argon obtained with all-electron and ECP Hartree–Fock calculations.

yields $\mu_z = 0.656$ a.u., whereas the ECP calculation yields $\mu_z = 0.653$ a.u. Thus, it is seen that the ECP manages to describe polarization well. The corresponding 3s-orbital is depicted in Figure 2.3, where $|\psi|^2$ has been plotted along the z-axis.

Effective core potentials are of prime interest for heavy elements since these have large numbers of electrons. It is also in heavy elements that relativistic effects are prominent — the heavier the atom, the larger the relativistic effect. This opens for a second important role of ECPs, namely to include indirect relativistic effects. If the potentials are optimized based on relativistic calculations, relativistic effects will be built into the potential, and, thus, also be included when applied in nonrelativistic calculations.

In Paper V we have compared nonrelativistic calculations using ECPs to nonrelativistic and relativistic all-electron calculations. We come to the conclusion that ECPs outperform nonrelativistic calculations also for sensitive properties such as the hyperpolarizability. E.g., the errors in hyperpolarizability of *meta*-di-

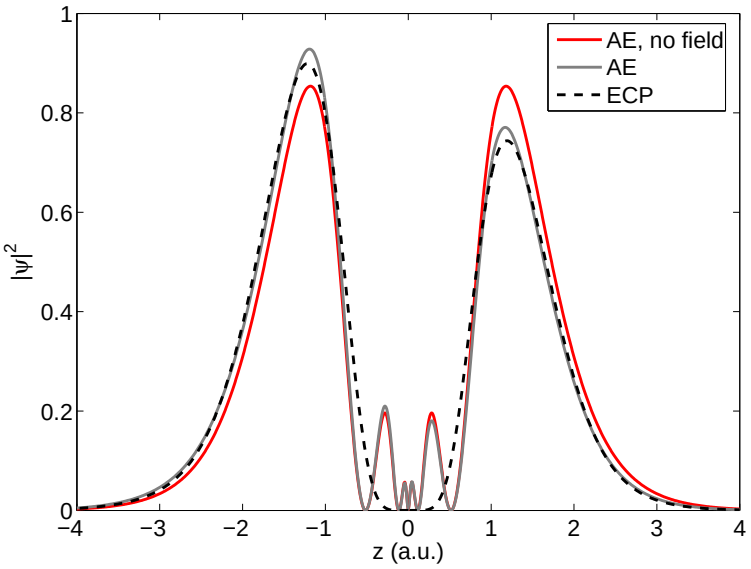

Figure 2.3. $|\psi|^2$ of the 3s-orbital in argon plotted along the z-axis when an electric field $\mathbf{E} = E\mathbf{e}_z$, $E = 0.1$ a.u. has been applied.

iodobenzene compared to full relativistic calculations are reduced from 18% to 7% when an ECP is used to describe iodine in the nonrelativistic calculation. However, when it comes to for example two-photon absorption, the relativistic effects introduced by the ECPs are no longer sufficient to provide good agreement with relativistic calculations. Typically, we see comparable integrated cross sections, but the nonrelativistic calculations are more narrowbanded. In nonrelativistic calculations, triplet excitations are strictly spin-forbidden, whereas at the relativistic level they attain significant cross sections. This drastically broadens the spectra, an effect we have attributed to spin-orbit coupling.

2.3 Response Theory

In Section 2.1, the route to solving the wave equation has been outlined for a molecular system described by a time-independent Hamiltonian; now, attention turns to systems subjected to time-dependent perturbations. Due to the perturbations, the solutions are no longer stationary and the molecular properties are affected accordingly. The changes in molecular properties, the responses, due to perturbations can, given a variational wave function, be treated using so-called response theory, for which the work by Olsen and Jørgensen [47] is considered the starting point. A reformulation of response theory, including not only variational electronic structure methods but also nonvariational ones, was introduced by Christiansen *et al.* [8] Recently, response theory has also been extended to the near-resonant and resonant regimes by Norman *et al.* [42,43] In the following, only the basic ideas of

response theory will be treated and for further detail the reader is referred to the references listed above.

Consider a time-dependent perturbation of the form

$$\hat{V}^t = \int_{-\infty}^{\infty} \hat{V}^\omega e^{-i\omega t} d\omega, \tag{2.34}$$

which is adiabatically switched on at $t = -\infty$. Under the influence of this perturbation, the time-evolution of the electronic reference state can be parameterized using a unitary exponential operator according to [47,56]

$$|\tilde{0}(t)\rangle = e^{i\hat{\kappa}(t)}|0\rangle, \quad \hat{\kappa}(t) = \sum_{a,i} \left(\kappa_{ai} \hat{a}_a^\dagger \hat{a}_i + \kappa_{ai}^* \hat{a}_i^\dagger \hat{a}_a \right), \tag{2.35}$$

where a nonredundant parameterization includes electron transfer from occupied orbitals (i) to unoccupied orbitals (a). In the relativistic case a also includes negative energy orbitals (sometimes referred to as positronic orbitals), and the corresponding transfer amplitudes are denoted $\kappa^{e\text{-}e}$ and $\kappa^{e\text{-}p}$, respectively. In order to solve the time dependence of the state transfer parameters, following the work by Olsen and Jørgensen, [47] the parameters are expanded in a power series over the perturbation and the Ehrenfest theorem is then solved for each order in the perturbation. Since the time evolution of the molecular state is now known, the expectation value of any operator $\hat{\Omega}$ can be expanded in powers of the perturbation, and the different response functions are identified as the Fourier coefficients in this expansion, [47] i.e.,

$$\begin{aligned}
\langle \tilde{0}|\hat{\Omega}|\tilde{0}\rangle =& \langle 0|\hat{\Omega}|0\rangle \\
&+ \int \langle\langle \hat{\Omega}; \hat{V}^{\omega_1} \rangle\rangle e^{-i\omega_1 t}\, d\omega_1 \\
&+ \frac{1}{2} \int \langle\langle \hat{\Omega}; \hat{V}^{\omega_1}, \hat{V}^{\omega_2} \rangle\rangle e^{-i(\omega_1+\omega_2)t}\, d\omega_1 d\omega_2 \\
&+ \frac{1}{3!} \int \langle\langle \hat{\Omega}; \hat{V}^{\omega_1}, \hat{V}^{\omega_2}, \hat{V}^{\omega_3} \rangle\rangle e^{-i(\omega_1+\omega_2+\omega_3)t}\, d\omega_1 d\omega_2 d\omega_3 \\
&+ \dots
\end{aligned} \tag{2.36}$$

2.3.1 Electric Field Induced Response Functions

In the applications we focus on, molecules interact with visible or near-visible light, or electromagnetic radiation. The wavelengths of interest are much more extended than the molecules considered, and, hence, to good approximation, the electric vector potential can be assumed to be constant over the entire molecule. This assumption has two implications for the coupling of the electromagnetic field to the molecular properties. First, the electric field is constant over the entire molecule which implies that in an expansion over electric multipole moments, only the molecular dipole moment will couple to the field. Second, no magnetic interactions will be included. Therefore, this is called the electric dipole approximation. [10]

Having established the electric dipole approximation, to second order, the expectation value of the dipole moment becomes

$$\begin{aligned}\langle\tilde{0}|\hat{\mu}|\tilde{0}\rangle =& \langle 0|\hat{\mu}_\alpha|0\rangle \\ &- \int \langle\!\langle \hat{\mu}_\alpha; F^{\omega_1}\hat{\mu}_\beta^{\omega_1}\rangle\!\rangle e^{-i\omega_1 t}\, d\omega_1 \\ &+ \frac{1}{2}\int \langle\!\langle \hat{\mu}_\alpha; F^{\omega_1}\hat{\mu}_\beta^{\omega_1}, F^{\omega_2}\hat{\mu}_\gamma^{\omega_2}\rangle\!\rangle e^{-i(\omega_1+\omega_2)t}\, d\omega_1 d\omega_2 \\ &+ \ldots, \end{aligned} \tag{2.37}$$

which can be compared to the expression [46]

$$\mu(t) = \mu_0 + F^{\omega_1}\alpha_{\alpha\beta}(-\omega_1;\omega_1) + \frac{1}{2}F^{\omega_1}F^{\omega_2}\beta_{\alpha\beta\gamma}(\omega_\sigma;\omega_1,\omega_2) + \ldots, \tag{2.38}$$

where $\omega_\sigma = -(\omega_1+\omega_2)$. It is seen that the first term in the expansion (2.37) is the permanent dipole moment of the molecule, the second term, the linear response function, $\langle\!\langle \hat{\mu}_\alpha; \hat{\mu}_\beta\rangle\!\rangle$, is associated with the polarizability of the system, [46]

$$\alpha_{\alpha\beta}(-\omega;\omega) = -\langle\!\langle \hat{\mu}_\alpha; \hat{\mu}_\beta\rangle\!\rangle_\omega, \tag{2.39}$$

and the third term, the quadratic response function, represents the first-order hyperpolarizability, or for short hyperpolarizability, [46]

$$\beta_{\alpha\beta\gamma}(\omega_\sigma;\omega_1,\omega_2) = \langle\!\langle \hat{\mu}_\alpha; \hat{\mu}_\beta, \hat{\mu}_\gamma\rangle\!\rangle_{\omega_1,\omega_2}. \tag{2.40}$$

As an illustrative example, consider a lithium hydride (LiH) molecule and assume an electric field of the form $\mathbf{E} = F_z^\omega \sin(\omega t)$. At a weak electric field strength ($F_z^\omega = 5\cdot 10^{-5}$ a.u.), the dipole moment follows the oscillations of the electric field, as seen in the mid panel of Figure 2.4. In this plot, the time-dependent dipole moment is plotted both to linear and quadratic order, however, the nonlinear contributions are too small to be noticeable. If, on the other hand, the electric field strength is increased by two orders of magnitude, as shown in the lower panel, the nonlinear effects are clearly visible. The dipole moment variations still follow the variations in the electric field, however, in an unsymmetric way. All the above calculations were carried out in the nonrelativistic realm and far away from resonances (the frequency of the electric field is 35% of the lowest singlet state transition frequency of LiH). Figure 2.5 shows $\beta_{x;z,x}(-2\omega;\omega,\omega)$ for water. It is seen that in resonant regions, the response theory formulations by Olsen and Jørgensen [47] and Christiansen *et al.* [8] diverges due to the infinite lifetime approximation. The thin vertical lines indicate the singlet excited state energy at ω_e and the corresponding two-photon resonance at $\omega_e/2$. To treat resonant regions, the finite lifetime formulation by Norman *et al.* [42,43] has to be adopted, as is illustrated by the solid line in Figure 2.5. It should be noted that in relativistic calculations, triplet state transitions are allowed, and, thus, the response functions diverge in these regions as well.

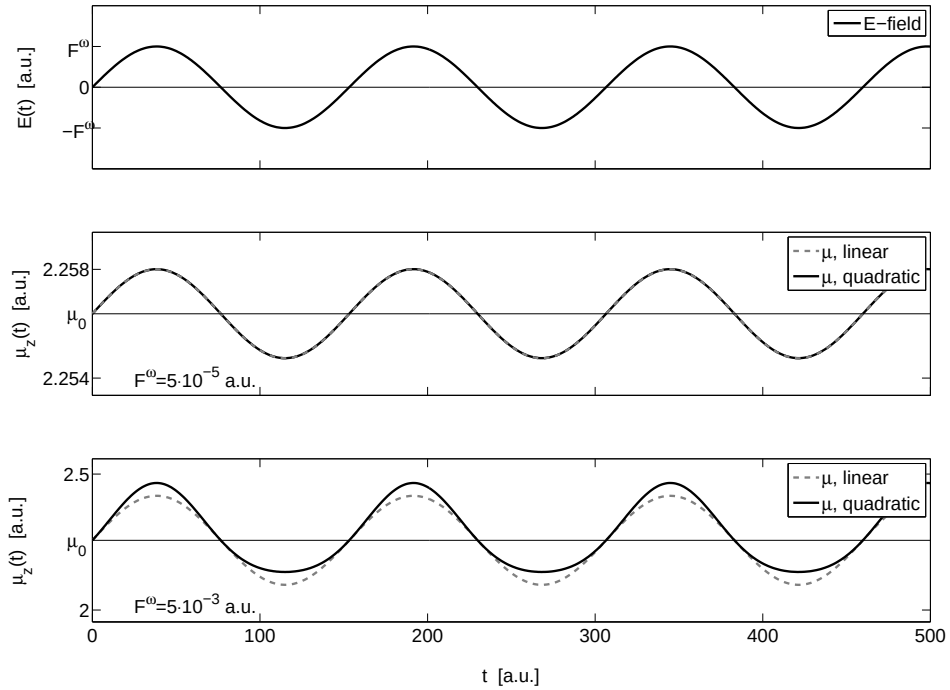

Figure 2.4. LiH molecule in a time-dependent electric field $\mathbf{E} = F_z^\omega \sin(\omega t)$. The uppermost plot shows the time-dependence of the electric field. In the middle, the time-dependent dipole moment is shown in a weak electric field, and it is seen that the nonlinear influence is negligible. In the lower plot, the field strength has been increased such that the nonlinear effects can be clearly seen. The solid line represents the dipole moment up to second order contributions in the electric field strength, whereas the dashed line shows only the linear contribution.

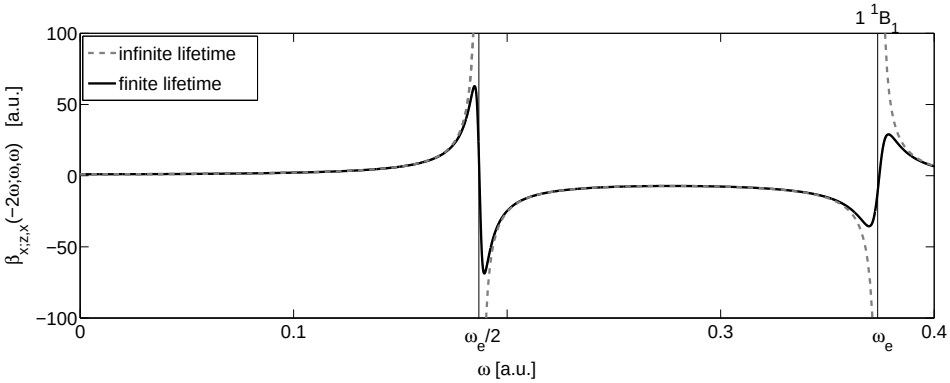

Figure 2.5. The dispersion of $\beta_{x;z,x}(-2\omega;\omega,\omega)$ for water. The dashed line adopts the infinite lifetime approximation, and, thus, breaks down at resonance, whereas the solid line shows the effect when finite lifetimes are accounted for.

Through the polarizability, the refraction index and absorption are accessible from the real and imaginary parts, respectively, and at resonance, the transition moments for one-photon absorption, $M_\alpha^{0\to f}$ are given by[46]

$$\lim_{\omega\to\omega_f}(\omega_f-\omega)\left\{-\langle\langle\hat{\mu}_\alpha;\hat{\mu}_\beta\rangle\rangle_\omega\right\}=M_\alpha^{0\to f}\langle f|\hat{\mu}_\beta|0\rangle. \tag{2.41}$$

Going to the nonlinear regime, analogously, evaluating the residue of the quadratic response function yields the two-photon transition matrix elements[46]

$$\lim_{\omega_2\to\omega_f}(\omega_f-\omega_2)\langle\langle\hat{\mu}_\alpha;\hat{\mu}_\beta,\hat{\mu}_\gamma\rangle\rangle_{\omega_1,\omega_2}=S_{\alpha\beta}^{0\to f}(\omega_\sigma)\langle f|\hat{\mu}_\gamma|0\rangle \tag{2.42}$$

whereas from the double residue,

$$\begin{aligned}&\lim_{\substack{\omega_1\to\omega_{f_1}\\ \omega_2\to\omega_{f_2}}}(\omega_{f_1}-\omega_1)(\omega_{f_2}-\omega_2)\langle\langle\hat{\mu}_\alpha;\hat{\mu}_\beta,\hat{\mu}_\gamma\rangle\rangle_{\omega_1,\omega_2}\\ =&\langle 0|\hat{\mu}_\beta|f_1\rangle\langle f_1|\overline{\hat{\mu}}_\alpha|f_2\rangle\langle f_2|\hat{\mu}_\gamma|0\rangle,\end{aligned} \tag{2.43}$$

the entity $\langle f_1|\overline{\hat{\mu}}_\alpha|f_2\rangle$ is identified as the excited state dipole moment if $|f_1\rangle=|f_2\rangle$ and the excited state transition moment if $|f_1\rangle\neq|f_2\rangle$.

Using the transition moments and transition matrix elements above, the cross section for a transition, i.e., its probability, can be evaluated. For the one-photon case this is given by the so-called oscillator strength, and, in order to compare with gas phase results an orientationally averaged value is given by

$$\delta_{\mathrm{OPA}}=\frac{2}{3}\omega_{0f}\sum_\alpha M_\alpha^{0\to f}\left[M_\alpha^{0\to f}\right]^*. \tag{2.44}$$

In the two-photon case the situation is more complex. For a randomly oriented sample, the two-photon absorption cross section is[35,39]

$$\begin{aligned}\delta_{\mathrm{TPA}}=\frac{1}{30}\sum_{\alpha,\beta}\Big\{&FS_{\alpha\alpha}^{0\to f}\Big(\frac{\omega_f}{2}\Big)\left[S_{\beta\beta}^{0\to f}\Big(\frac{\omega_f}{2}\Big)\right]^*\\ &+GS_{\alpha\beta}^{0\to f}\Big(\frac{\omega_f}{2}\Big)\left[S_{\alpha\beta}^{0\to f}\Big(\frac{\omega_f}{2}\Big)\right]^*\\ &+HS_{\alpha\beta}^{0\to f}\Big(\frac{\omega_f}{2}\Big)\left[S_{\beta\alpha}^{0\to f}\Big(\frac{\omega_f}{2}\Big)\right]^*\Big\},\end{aligned} \tag{2.45}$$

where F, G, and H are factors depending on the polarization of the two photons. If both photons come from the same monochromatic source, in the linearly polarized case $F=G=H=2$, whereas in the circularly polarized one $F=-2$ and $G=H=-3$. With these properties defined, it is now possible to address the absorption spectra, and, thus, the properties of the Jablonski diagram as discussed in Section 1.2.

The quadratic response function and its residues form the foundation for all papers included in this thesis. Paper II is the most fundamental one, dealing with the implementation of the quadratic response functions at the four-component relativistic density functional level of theory. In previous work by Norman and

Jensen[45] the quadratic response function has been implemented at the four-component relativistic Hartree–Fock level. With this as a starting point, the extension to DFT, i.e., the contribution from the exchange-correlation functional, is dealt with.

Papers III and IV deal with the implementation of the residues of the quadratic response function. The implementations described are based on the quadratic response function for a Kramers-restricted Hartree–Fock wave function,[45] however, the implementations as such are open-ended and require no modifications to be compatible with DFT, and, thus, the recent implementation described in Paper II.

In Paper V, a detailed investigation of the influence of relativity on quadratic response functions and two-photon absorption is carried out. The quadratic response functions are evaluated at different levels of approximation ranging from nonrelativistic calculations through effective core potentials to a full four-component treatment using the Dirac–Coulomb Hamiltonian. The effects, benefits, and shortcomings of core potentials has already been discussed in Section 2.2.1.

Finally, in Paper VI, quantum mechanical absorption calculations are used together with electromagnetic pulse propagation in order to describe the macroscopic behavior of optically active materials. This will be discussed in greater detail in Chapter 3, where the essence of this work is put into an illustrative example.

CHAPTER 3

Clamping Levels in Optical Power Limiting

"Erwin kann mit seinem Psi
kalkulieren wie noch nie.
Doch wird jeder gleich einsehn:
Psi lässt sich nicht recht verstehn."

ERICH HÜCKEL

"Erwin with his psi can do
calculations quite a few.
But one thing has not been seen:
Just what does psi really mean?"

English translation by FELIX BLOCH

Our quantum mechanical calculations treat isolated molecules at zero temperature. Solvation effects and finite temperatures can be accounted for in different ways, but has not been included into our investigations. When it comes to the coupling to phenomena on the macroscopic scale, e.g., the interaction between chromophores embedded in a host material and an electromagnetic field, little is known. The framework for the latter situation has been laid down in the work by Gel'mukhanov and co-workers.[1,2,18] This work introduces pulse propagation through a medium containing optically active molecules. A proof of principle is presented in Paper VI and the following chapter is an illustrative example of this concept based on this paper as well as the continuation thereof.[3]

At time t_0, a laser pulse approaches an optically active material and at time t_1 it has passed through the material, see Figure 3.1. If the properties of the incident laser pulse and the material are known, the question arises: What are the properties of the pulse at t_1? As the laser pulse propagates through the material, which consists of randomly oriented optically active

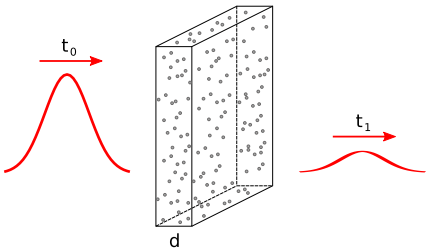

Figure 3.1. At time t_0, a laser pulse approaches an optically active material. As it passes through the material, the pulse interacts with the materials, and as it has passed through the material at time t_1, its properties have been altered.

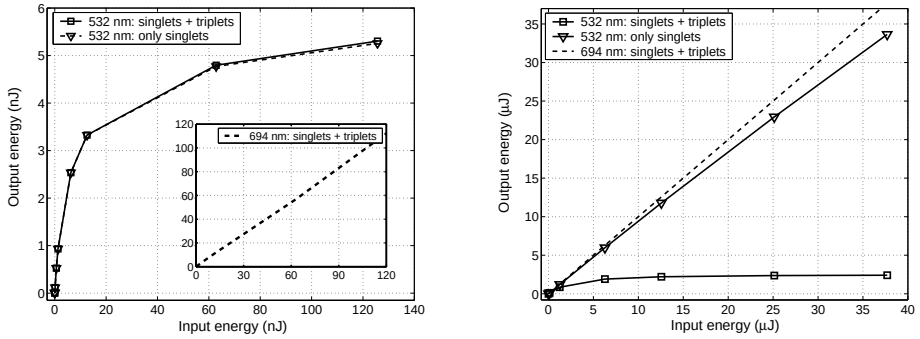

Figure 3.2. Simulated clamping levels for the Pt(II) compound seen in Figure 3.3(E). The simulations are performed for 1 mm thick sample with a chromophore concentration of 0.02 M. Two wavelengths, 532 and 694 nm, are considered. On the left, the pulse duration is 100 fs, whereas on the right it is 10 ns. The need to include excited state absorption also in the triplet state manifold is clearly seen.

molecules, chromophores, embedded in a host material, its properties are altered. Assuming that the pulse is a plane wave, this interaction is described by the paraxial wave equation[27] which couples the amplitude function, $\mathcal{E}(\mathbf{r}, t)$, of the electric field to the polarization of the material, $\mathcal{P}(\mathbf{r}, t)$. The polarization of the material has, of course, one contribution from the host material and one from the chromophores, where the former is assumed to have no influence on the nonlinear characteristics of the material. The part associated with the chromophores depends on the molecular properties, and it is here the link to quantum chemistry enters. The parameters of the Jablonski diagram determined by calculations enters as input to the Liouville equation, and through the density matrix formulation of quantum mechanics, the polarization due to the chromophores is determined, as described in Paper VI. The interplay between the macroscopic laser field and the microscopic properties of the chromophores is now determined.

In, for example, the work by McKay *et al.*,[36] it is shown experimentally that π-conjugated platinum(II) compounds work as broadband power limiters. Therefore, the Swedish Defence Research Agency has considered materials in this family of molecules for power limiting applications. One such material that has proved promising in experiments is the one seen in Figure 3.3(E). Therefore, this molecule was used as test case in the proof of principle presented in Paper VI. The properties of the Jablonski diagram, see Figure 1.2, have been evaluated by first principles quantum chemical calculations, and the simulated clamping levels for different pulses are shown in Figure 3.2. Two different wavelengths, 532 and 694 nm, are considered for two different pulse durations, and it is obvious that this particular chromophore is only suitable for the shorter of the two wavelengths. However, of greater interest and importance is the results for the longer pulse, see the right panel. At 532 nm, two utterly different results are achieved depending on whether or not excited state absorption in the triplet state manifold is included. On the one hand, as triplets are excluded, linear transmittance is seen, whereas on the

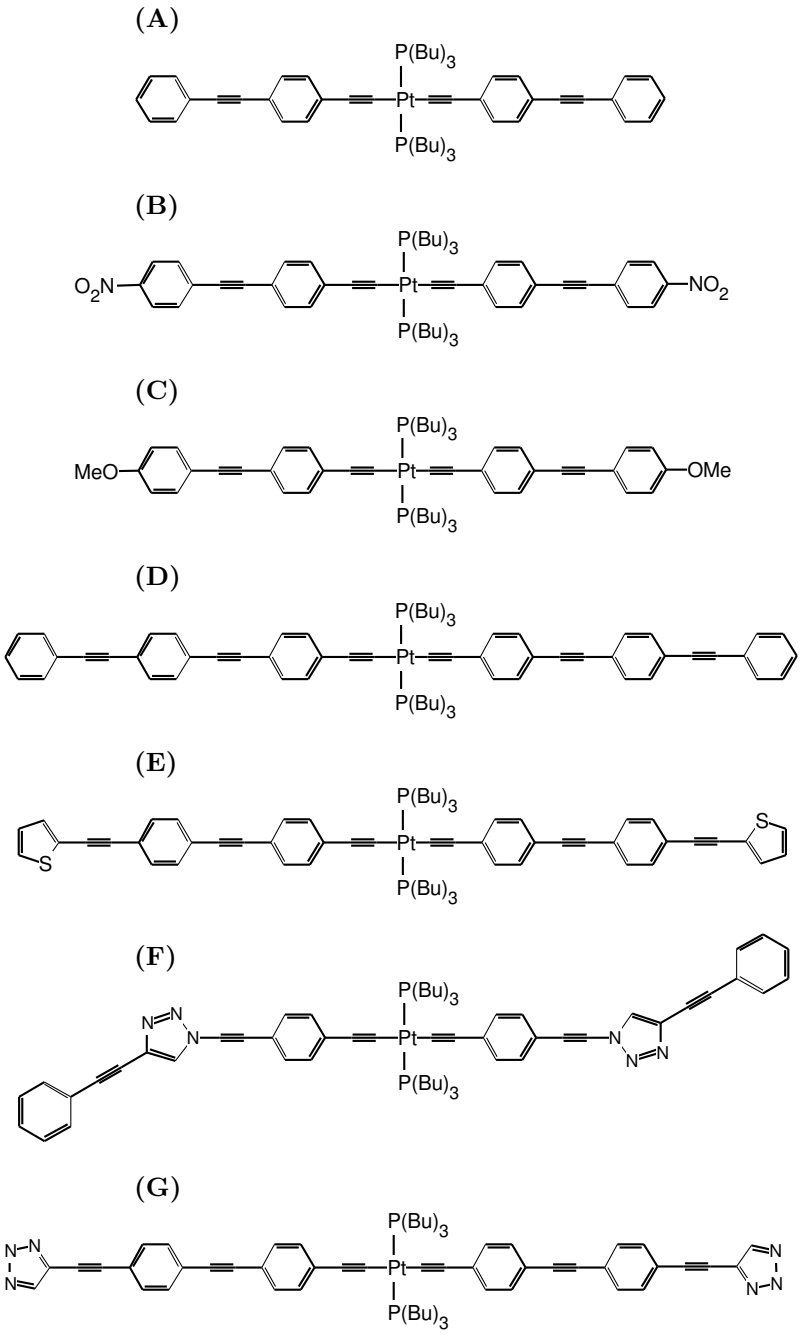

Figure 3.3. Molecular structure of Pt(II)-compounds used in clamping level simulations.

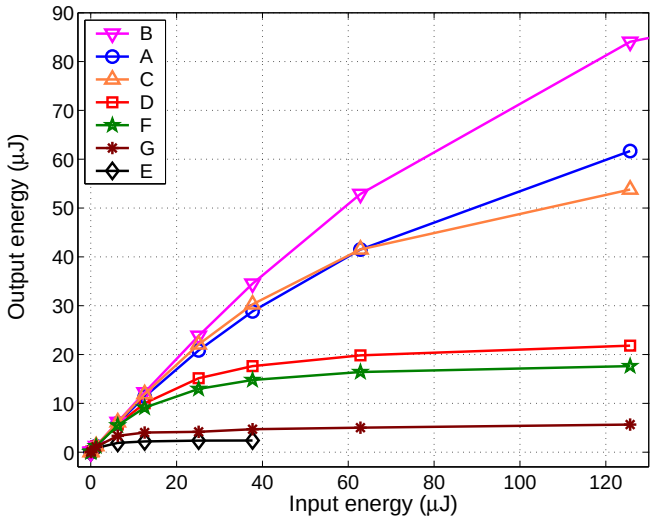

Figure 3.4. Simulated clamping levels for the Pt(II) compounds in Figure 3.3. The simulations consider 1 mm thick samples with a chromophore concentrations of 0.02 M subjected to 10 ns long laser pulses at 532 nm.

other hand, when they are included, a rapid clamping is achieved. This behavior is attributed to excited state triplet absorption close to 532 nm. The calculated clamping level is in good agreement with experiments carried out by FOI. Unfortunately, these results are classified and a direct comparison cannot be presented.

The above results show the significance of the combined theoretical framework based on quantum mechanics in conjunction with pulse propagation based on electrodynamics. Molecular quantum mechanics alone is not able to predict the clamping levels, e.g., the extent of the importance of the triplet state excitations cannot be forseen. Now, a direct connection can be made between macroscopic clamping levels and microscopic properties of the chromophores, which enables the possibility to design molecular materials suitable for a particular purpose. Not only does this provide the means to address clamping levels from molecular properties, but it also enables the ability to find which molecular properties to look for in order to achieve a certain clamping level in a given frequency range.

The molecule investigated in Paper VI show excellent clamping levels, but experimentally it is difficult to solvate in order to manufacture doped sol-gel glass materials. Therefore, an extended survey [3] was pursued where a number of similar chromophores were investigated, see Figure 3.3. Yet again, a sample thickness of 1 mm and a chromophore concentration of 0.02 M was used. The simulated clamping levels for a 10 ns laser pulse are depicted in Figure 3.4. The seven investigated materials split up in two distinct groups, where molecules with longer ligand chains attached to the platinum have lower clamping levels. All four compounds (D, E, F, and G) have triplet excited states at or close to 532 nm, whereas such features are missing in the other three compounds.

This chapter, compiled from our work in Paper VI and Ref. 3, point out the capabilities of computational chemistry of today. A large number of properties can be accurately addressed on a computational basis, in many cases to a much reduced cost, not only financially but also time wise. In the light of this, the developments presented in this thesis form a natural step toward more accurate assessments of properties, enabling even greater detail to be treated. Still, large areas need to be charted out and understood in order properly account for certain effects, but I think it is safe to say that we are at a point where we approach the visions of Charles Babbage (see p. 2). The development we see in computational sciences is rather a useful complement to experiments than, as stated by Comte (see p. 1), a "degradation of that science".

Bibliography

1. A. Baev, F. Gel'mukhanov, V. Kimberg, and H. Ågren. Nonlinear propagation of string multi-mode fields. *Journal of Physics B: Atomic, Molecular and Optical Physics*, 36:3761–3774, 2003.

2. Alexander Baev, Faris Gel'mukhanov, Peter Maćak, Yi Luo, and Hans Ågren. General theory for pulse propagation in two-photon active media. *Journal of Chemical Physics*, 117(13):6214–6220, October 2002.

3. Alexander Baev, Pontus Welinder, Robert Erlandsson, Johan Henriksson, Patrick Norman, and Hans Ågren. A quantum mechanical-electrodynamical approach to nonlinear properties: Application to optical power limiting with platinum-organic compounds. *Journal of Nonlinear Optical Physics and Materials*, 16(2):157–169, June 2007.

4. Maria Barysz and Andrzej J. Sadlej. Two-component methods of relativistic quantum chemistry: from the Douglas–Kroll approximation to the exact two-component formalism. *Journal of Molecular Structure: THEOCHEM*, 573(1–3):181–200, October 2001.

5. Maria Barysz, Andrzej J. Sadlej, and Jaap G. Snijders. Nonsingular Two/One-Component Relativistic Hamiltonians Accurate Through Arbitrary High Order in α^2. *International Journal of Quantum Chemistry*, 65(3):225–239, 1997.

6. Fred Basolo and Ronlad C. Johnson. *Coordination Chemistry*. Science Reviews, second edition, 1986. ISBN 0-905927-47-8.

7. Leonardo Belpassi, Francesco Tarantelli, Antonio Sgamellotti, and Harry M. Quiney. Electron density fitting for the Coulomb problem in relativistic density-functional theory. *Journal of Chemical Physics*, 124:124104, March 2006.

8. Ove Christiansen, Poul Jørgensen, and Christof Hättig. Response Functions from Fourier Component Variational Perturbation Theory Applied to a Time-Averaged Quasienergy. *International Journal of Quantum Chemistry*, 68(1):1–52, 1998.

9. Thomas M. Cooper, Daniel G. McLean, and Joy E. Rogers. Molecular structure–spectroscopic property relations in a series of transition metal-containing phenylacetylene oligomers. *Chem. Phys. Lett.*, 349:31–36, November 2001.

10. D. P. Craig and T. Thirunamachandra. *Molecular quantum electrodynamics: an introduction to radiation molecule interactions*. Dover Publications Inc., Mineola, 1998. ISBN 0-486-40214-2.

11. Mark Csele. *Fundamentals of Light Sources and Lasers*. John Wiley & Sons, Inc., Hoboken, 2004. ISBN 0-471-47660-9.

12. P. A. M. Dirac. The Quantum Theory of the Electron. *Proceedings of the Royal Society of London. Series A, Containing Papers of a Mathematical and Physical Character*, A117:610–624, February 1928.

13. P. A. M. Dirac. Quantum Mechanics of Many-Electron Systems. *Proceedings of the Royal Society of London. Series A, Containing Papers of a Mathematical and Physical Character*, 123(792):714–733, April 1929.

14. Marvin Douglas and Norman M. Kroll. Quantum electrodynamical corrections to the fine structure of helium. *Annals of Physics*, 82(1):89–155, 1974.

15. K. G. Dyall, I. P. Grant, and S. Wilson. Matrix representation of operator products. *Journal of Physics B: Atomic and Molecular Physics*, 17(4):493–504, February 1984.

16. Kenneth G. Dyall and Knut Fægri, Jr. *Introduction to Relativistic Quantum Chemistry*. Oxford University Press, Inc., New York, 2007. ISBN 978-0-19-514086-6.

17. Leslie L. Foldy and Siegfried A. Wouthuysen. On the Dirac Theory of Spin 1/2 Particles and Its Non-Relativistic Limit. *Physical Review*, 78(1):29–36, April 1950.

18. F. Gel'mukhanov, A. Baev, P. Macák, Y. Luo, and H. Ågren. Dunamics of two-photon absorption by molecules and solutions. *Journal of the Optical Society of America B*, 19(5):937–945, May 2002.

19. Herbert Goldstein. *Classical Mechanics*. Addison–Wesley Publishing Company, Reading, 2nd edition, 1980. ISBN 0-201-02918-9.

20. Philipp Gütlich. Spin Crossover in Iron(II)-Complexes. *Structure and bonding*, 44:83–195, 1981.

21. Trygve Helgaker, Poul Jørgensen, and Jeppe Olsen. *Molecular Electronic-Structure Theory*. John Wiley & Sons, Ltd, Chichester, 2004. ISBN 0-471-96755-6.

22. Johan Henriksson, Susanna Nyrell, and Patrick Norman. Theoretical design of optical switches using the spin transition phenomenon. *Computing Letters*, 2:237, 2006.

23. Bernd A. Heß. Applicability of the no-pair equation with free-particle projection operators to atomic and molecular structure calculations. *Physical Review A*, 32(2):756–763, August 1985.

24. Bernd A. Heß. Relativistic electronic-structure calculations employing a two-component no-pair formalism with external-field projection operators. *Physical Review A*, 33(6):3742–3748, June 1986.

25. P. Hohenberg and W. Kohn. Inhomogeneous Electron Gas. *Physical Review*, 136(3B):B 864–871, November 1964.

26. Miroslav Iliaš and Trond Saue. An infinite-order two-component relativistic Hamiltonian by a simple one-step transformation. *Journal of Chemical Physics*, 126:064102, February 2007.

27. John David Jackson. *Classical Electrodynamics*. John Wiley & Sons, Inc., New York, 3rd edition, 1999. ISBN 0-471-30932-X.

28. Luis R. Kahn, Paul Baybutt, and Donald G. Truhlar. *Ab initio* effective core potentials: Reduction of all-electron molecular structure calculations to calculations involving only valence electrons. *Journal of Chemical Physics*, 65(10):3826–3853, November 1976.

29. Luis R. Kahn and William A. Goddard III. *Ab Initio* Effective Potentials for Use in Molecular Calculations. *Journal of Chemical Physics*, 56(6):2685–2701, March 1972.

30. W. Kohn and L. J. Sham. Self-Consistent Equations Including Exchange and Correlation Effects. *Physical Review*, 140(4A):A 1133–1138, November 1965.

31. Gilbert N. Lewis. The Chemical Bond. *Journal of Chemical Physics*, 1(1):17–28, 1933.

32. Wenjian Liu, Gongyi Hong, Dadi Dai, Lemin Li, and Michael Dolg. The Beijing four-component density functional program package (BDF) and its application to EuO, EuS, YbO and YbS. *Theoretical Chemistry Accounts*, 96(2):75–83, July 1997.

33. Cesar Lopes, Sören Svensson, Stefan Björkert, and Lars Öhrström. Swedish patent no. 0600828-6.

34. T. H. Maiman. Stimulated Optical Radiation in Ruby. *Nature*, 187(4736):493–494, August 1960.

35. W. M. McClain. Excited State Symmetry Assignment Through Polarized Two-Photon Absorption Studies of Fuilds. *Journal of Chemical Physics*, 55(6):2789–2796, September 1971.

36. T. J. McKay, J. A. Bolger, J. Staromlynska, and J. R. Davy. Linear and nonlinear optical properties of platinum-ethynyl. *Journal of Chemical Physics*, 108(13):5537–5541, April 1998.

37. T. J. McKay, J. Staromlynska, J. R. Davy, and J. A. Bolger. Cross sections for excited-state absorption in a Pt:ethynyl complex. *Journal of the Optical Society of America B*, 18(3):358–362, March 2001.

38. Larry E. McMurchie and Ernest R. Davidson. Calculation of Integrals over *ab initio* Pseudopotentials. *Journal of Computational Physics*, 44:289–301, 1981.

39. P. R. Monson and W. M. McClain. Polarization Dependence of the Two-Photon Absorption of Tumbling Molecules with Application to Liquid 1-Chloronaphthalene and Benzene. *Journal of Chemical Physics*, 53(1):29–37, July 1970.

40. Takahito Nakajima and Kimihiko Hirao. Pseudospectral approach to relativistic molecular theory. *Journal of Chemical Physics*, 121(8):3438–3445, August 2004.

41. Patrick Norman and Hans Ågren. First Principles Quantum Modeling of Optical Power Limiting Materials. *Journal of Computational and Theoretical Nanoscience*, 1(4):343, 2004.

42. Patrick Norman, David M. Bishop, Hans Jørgen Aa. Jensen, and Jens Oddershede. Near-resonant absorption in the time-dependent self-consistent field and multiconfigurational self-consistent field approximations. *Journal of Chemical Physics*, 115(22):10323–10334, December 2001.

43. Patrick Norman, David M. Bishop, Hans Jørgen Aa. Jensen, and Jens Oddershede. Nonlinear response theory with relaxation: The first-order hyperpolarizability. *Journal of Chemical Physics*, 123:194103, November 2005.

44. Patrick Norman, Peter Cronstrand, and Jerry Ericsson. Theoretical study of linear and nonlinear absorption in platinum-organic compounds. *Chemical Physics*, 285(2–3):207–220, December 2002.

45. Patrick Norman and Hans Jørgen Aa. Jensen. Quadratic response functions in the time-dependent four-component Hartree–Fock approximation. *Journal of Chemical Physics*, 121(13):6145–6154, October 2004.

46. Patrick Norman and Kenneth Ruud. *Non-Linear Optical Properties of Matter: From molecules to condensed phases*, chapter 1, pages 1–49. Challenges and Advances in Computational Chemistry and Physics, Volume 1. Kluwer Academic Publishers Group, Dordrecht, 2006. ISBN 1-4020-4849-1.

47. Jeppe Olsen and Poul Jørgensen. Linear and nonlinear response functions for an exact state and for an MCSCF state. *Journal of Chemical Physics*, 82(7):3235–3264, April 1985.

48. Robert G. Parr and Weitao Yang. *Density-Functional Theory of Atoms and Molecules*. International series of monographs on chemistry. Oxford University Press, New York, 1989. ISBN 0-19-509276-7.

49. W. Pauli and V. Weisskopf. Über die Quantisierung der skalaren relativistischen Wellengleichung. *Helvetica Physica Acta*, 7:709–731, 1934.

50. Joy E. Rogers, Thomas M. Cooper, Paul A. Fleitz, Douglas J. Glass, and Daniel G. McLean. Photophysical Characterization of a Series of Platinum(II)-Containing Phenyl–Ethyl Oligomers. *Journal of Physical Chemistry A*, 106(43):10108–10115, 2002.

51. Joy E. Rogers, Kiet A. Nguyen, David C. Hufnagle, Daniel G. McLean, Weijie Su, Kristi M. Gossett, Aaron R. Burke, Sergei A. Vinogradov, Ruth Pachter, and Paul A. Fleitz. Observation and Interpretation of Annulated Porphyrins: Studies on the Pohotophysical Properties of *meso*-Tetraphenylmetalloporphyrins. *Journal of Physical Chemistry A*, 107(51):11331–11339, 2003.

52. Joy E. Rogers, Jonathan E. Slagle, Daniel G. McLean, Richard L. Sutherland, Bala Sankaran, Ramamurthi Kannan, Loon-Seng Tan, and Paul A. Fleitz. Understanding the One-Photon Photophysical Properties of a Two-Photon Absorbing Chromophore. *Journal of Physical Chemistry A*, 108(26):5514–5520, 2004.

53. T. Saue, K. Fægri, T Helgaker, and O. Gropen. Principles of direct 4-component relativistic SCF: application to caesium auride. *Molecular Physics*, 91(5):937–950, August 1997.

54. T. Saue and L. Visscher. *Theoretical Chemistry and Physics of Heavy and Superheavy Elements*, chapter 6, pages 211–267. Progress in Theoretical Chemistry and Physics, Volume 11. Kluwer Academic Publishers, Dordrecht, 2003. ISBN 1-020-1371-X.

55. Trond Saue and Hans Jørgen Aa. Andersen. Quartenion symmetry in relativistic molecular calculations: The Dirac–Hartree–Fock method. *Journal of Chemical Physics*, 111(14):6211–6222, October 1999.

56. Trond Saue and Trygve Helgaker. Four-Component Relativistic Kohn–Sham Theory. *Journal of Computational Chemistry*, 23(8):814–823, June 2002.

57. Franz Schwabl. *Advanced Quantum Mechanics*. Springer-Verlag, Heidelberg, 1999. ISBN 3-540-64478-4.

58. Franz Schwabl. *Quantum Mechanics*. Springer-Verlag, Heidelberg, 3rd edition, 2002. ISBN 3-540-43109-8.

59. Silvan S. Schweber. *An Introduction to Relativistic Quantum Field Theory*. Dover Publications, Inc., Mineola, 2005. ISBN 0-486-44228-4.

60. Paul Strange. *Relativistic Quantum Mechanics*. Cambridge University Press, New York, 1998. ISBN 0-521-56583-9.

61. Attila Szabo and Neil S. Ostlund. *Modern Quantum Chemistry: Introduction to Advanced Electronic Structure Theory*. Dover Publications, Inc., Mineola, 1996. ISBN 0-486-69186-1.

62. S. Varga, E Engel, W.-D. Sepp, and B. Fricke. Systematic study of the Ib diatomic molecules Cu_2, Ag_2, and Au_2 using advanced relativistic density functionals. *Physical Review A*, 59(6):4288–4294, June 1999.

63. Lucas Visscher. Approximate molecular relativistic Dirac–Coulomb calculations using a simple Coulombic correction. *Theoretical Chemistry Accounts*, 98(2–3):68–70, December 1997.

List of Publications

I. Johan Henriksson, Trond Saue, and Patrick Norman. Quadratic response functions in the relativistic four-component Kohn–Sham approximation. *The Journal of Chemical Physics*, 128:024105, 2008.

II. Radovan Bast, Trond Saue, Johan Henriksson, and Patrick Norman. Role of noncollinear magnetization for the first-order electric-dipole hyperpolarizability at the four-component Kohn–Sham density functional theory level. *In manuscript*.

III. Johan Henriksson, Patrick Norman, and Hans Jørgen Aa. Jensen. Two-photon absorption in the relativistic four-component Hartree–Fock approximation. *The Journal of Chemical Physics*, 122:114606, 2005.

IV. Erik Tellgren, Johan Henriksson, and Patrick Norman. First order excited state properties in the four-component Hartree–Fock approximation; the excited state electric dipole moments in CsAg and CsAu. *The Journal of Chemical Physics*, 126:064313, 2007.

V. Johan Henriksson, Ulf Ekström, and Patrick Norman. On the evaluation of quadratic response functions at the four-component Hartree-Fock level: Nonlinear polarization and two-photon absorption in bromo- and iodobenzene. *The Journal of Chemical Physics*, 124:214311, 2006.

VI. Alexander Baev, Patrick Norman, Johan Henriksson, and Hans Ågren. Theoretical Simulations of Clamping Levels in Optical Power Limiting. *The Journal of Physical Chemistry B*, 110:20912, 2006.

Papers not included in this thesis

VII. Alexander Baev, Pontus Welinder, Robert Erlandsson, Johan Henriksson, Patrick Norman, and Hans Ågren. A quantum mechanical-electrodynamical approach to nonlinear properties: Application to optical power limiting with platinum-organic compounds. *Journal of Nonlinear Optical Physics and Materials*, 16:157, 2007.

VIII. Johan Henriksson, Susanna Nyrell, and Patrick Norman. Theoretical design of optical switches using the spin transition phenomenon. *Computing Letters*, 2:237, 2006.

I

Paper I

Quadratic response functions in the relativistic four-component Kohn–Sham approximation

Johan Henriksson
Trond Saue
Patrick Norman

The Journal of Chemical Physics **128**, 024105 (2008)

THE JOURNAL OF CHEMICAL PHYSICS **128**, 024105 (2008)

Quadratic response functions in the relativistic four-component Kohn-Sham approximation

Johan Henriksson
Department of Physics, Chemistry and Biology, Linköping University, SE-581 83 Linköping, Sweden

Trond Saue
Institut de Chimie, UMR 7177 CNRS et Université Louis Pasteur, 4 rue Blaise Pascal, F-67000 Strasbourg, France

Patrick Norman[a)]
Department of Physics, Chemistry and Biology, Linköping University, SE-581 83 Linköping, Sweden

(Received 5 October 2007; accepted 31 October 2007; published online 10 January 2008)

A formulation and implementation of the quadratic response function in the adiabatic four-component Kohn-Sham approximation is presented. The noninteracting reference state is time-reversal symmetric and formed from Kramers pair spinors, and the energy density is gradient corrected. Example calculations are presented for the optical properties of disubstituted halobenzenes in their *meta* and *ortho* conformations. It is demonstrated that correlation and relativistic effects are not additive, and it is shown that relativity alone reduces the $\mu\bar{\beta}$-response signal by 62% and 75% for *meta*- and *ortho*-bromobenzene, respectively, and enhances the same response by 17% and 21% for *meta*- and *ortho*-iodobenzene, respectively. Of the employed functionals, CAM-B3LYP shows the best performance and gives hyperpolarizabilities β distinctly different from B3LYP. © *2008 American Institute of Physics*. [DOI: 10.1063/1.2816709]

I. INTRODUCTION

In the presence of external (or internal) perturbing electromagnetic fields, the molecular polarization (or magnetization) can be expressed as a Taylor series in terms of the field strengths and the coupling parameters relate to spectroscopic properties (see, for instance, the book by Boyd).[1] Over the past 20 years, increasingly accurate and efficient computational methods have been developed to determine the linear as well as nonlinear molecular response parameters and, today, theoretical calculations are routinely used for the interpretation of experimental spectra as well as for material functionalization and optimization. If we are concerned with the correction to the molecular polarization that depends quadratically on the perturbing electric-field strengths, we note fundamental nonlinear optical processes, such as the second-harmonic generation and the electro-optical Pockels effect, and an important device such as the optical parametric oscillator. Moreover, static magnetic fields can be used to induce birefringences in nonchiral systems and, in this context, the quadratic response parameters (or *quadratic response functions*) are pertinent to spectroscopies such as magnetic circular dichroism and the Faraday effect.

In nonrelativistic quantum chemistry, quadratic response functions have been formulated and implemented at the electron uncorrelated level in the so-called time-dependent Hartree-Fock (HF) approximation[2–6]—this approximation is sometimes also referred to as the time-dependent coupled perturbed Hartree-Fock level or the random phase approximation—as well as at the electron correlated level employing second-order Møller-Plesset,[7] multiconfiguration self-consistent field (MCSCF),[2,6] and coupled cluster[8–10] reference states. More recently, the quadratic response function has also been formulated in the second-order polarization propagator approach[11] and formulated and implemented in Kohn-Sham density functional theory (DFT).[12,13] Successful use of these computational techniques has been demonstrated in numerous publications in the literature and, furthermore, it has been shown that a residue analysis of the response functions at the electronic transition frequencies of the system enables the calculation of observables in absorption spectroscopies and properties of electronically excited states.[2] At small frequency detunings of the perturbing fields, however, one must be cautious since the dispersion of the response functions is severely overestimated in this region due to the divergences at resonances. This issue has been considered in a series of publications by Norman *et al.*, and a *resonance convergent* formulation of response theory up to second order has been proposed and implemented at the HF, MCSCF, and DFT levels of theory.[14] It stands clear that, in the nonrelativistic realm, there exist sophisticated and highly accurate methodologies and program implementations for the determination of the linear and nonlinear responses in the electronic density to time-dependent electromagnetic field perturbations.

In photonics, it is well-known that the use of organometallic compounds can give unprecedented performance in certain applications,[15] but it is clear that, from a theoretical perspective, the inclusion of one or several heavy atoms calls for the treatment of relativistic effects in one way or another. It is possible to consider these effects by perturbation theory and, in the nonrelativistic framework, to add relativistic cor-

a)Electronic mail: panor@ifm.liu.se.

rections to the perturbation operator that describes the coupling to the external electromagnetic fields. This approach has been adopted to determine, e.g., phosphorescence,[16,17] electron spin resonance,[18] and nuclear magnetic resonance parameters[19] but, although these calculations employ quadratic response functions, they are all examples of second-order molecular properties since one of the perturbation operators in the response functions refers to an intrinsic field. In order to address a third-order molecular property in a relativistic-perturbational approach, one would need to evaluate a cubic response function which is computationally more complex, and we are not aware of such work. Apart from the increased computational complexity, a relativistic-perturbational approach is also limited by the fact that it is not applicable when relativistic effects are large and, therefore, must be included in the zeroth-order Hamiltonian.

There exist a number of ways to include relativistic effects in the zeroth-order molecular Hamiltonian. One can replace the core electron densities by effective potentials and include only the valence electrons in the parametrization of the wave function.[20] The parameters of the effective core potentials (ECPs) may be optimized against accurate relativistic atomic densities and later used in regular nonrelativistic calculations. The ECP approach indirectly accounts for scalar relativistic as well as spin-orbit effects in the atomic cores, and it can be applied to all elements of the Periodic Table while providing a reasonable accuracy (see Refs. 21–23 for evaluations of this method for third-order molecular properties). The obvious limitation is the neglect of direct (rather than indirect via the core potential) relativistic effects in the valence electron density. The severity of this approximation varies strongly for different molecular properties; not only does it vary with respect to the order of the molecular property but it also varies substantially for different properties of the same order. The most striking example when spin-orbit effects in the valence electron density are of prominent importance in the calculation of a quadratic response function is given by the two-photon absorption spectra (which relate to a first-order residue of the quadratic response function). It was demonstrated by Henriksson *et al.*[24] that even for a light element such as neon, the inclusion of spin-orbit interactions is necessary to obtain a qualitatively correct two-photon absorption spectrum.

At the all-electron level of theory, spin-free scalar relativistic corrections may be added to the one-electron Hamiltonian and, with the neglect of the picture change in the perturbation operators, response properties can be determined without further modifications of the nonrelativistic code. In this way, the hyperpolarizabilities of a series of group IIb sulfides were determined[25] in the spin-averaged Douglas-Kroll approximation, as introduced by Hess,[26,27] and the same approach has later been benchmarked against four-component calculations and then showing significant discrepancies for the hyperpolarizabilities of iodine and tellurium hydrides.[21] Full inclusion of scalar relativistic and spin-orbit effects in the calculation of third-order molecular properties was accomplished with the implementation of the quadratic response function (and its first- and second-order residues) in the time-dependent four-component Hartree-Fock approximation.[24,28,29] While accurate with respect to relativistic effects, it is expected that the applicability of this method is severely limited due to the large effects of electron correlation on nonlinear response properties and since it is inappropriate to treat relativity and electron correlation separately. In the present work, we therefore develop and implement the quadratic response function in the time-dependent four-component Kohn-Sham DFT approximation. Our work should be seen as an extension of the previous mentioned work in the HF approximation[24,28,29] as well as the work on the linear response function in the DFT approximation.[30]

In Sec. II A, we give a brief review of the four-component Kohn-Sham approximation and the derivation of the quadratic response function but, since these general aspects are largely covered in our previous work,[29,30] we focus primarily on a presentation of the details of the implementation that are unique to the extension made here (see Sec. II B). In Sec. III, we illustrate our implementation with an example calculation of the first-order electric-dipole hyperpolarizability for dibromo- and di-iodo-substituted benzene using a set of standard density functionals. We emphasize that although the implementation is completely general, we here present results for nonoscillating external perturbations which require functionals of the charge density only. For dynamic properties, we would like to perform a detailed investigation of also adding the induced noncollinear magnetization as a functional variable, and this work is in progress.

II. THEORY AND METHODOLOGY

A. Time-dependent four-component Kohn-Sham approximation

In the time-dependent four-component Kohn-Sham DFT approximation, the noninteracting reference system is described by a determinant of spinors $\phi_p(\mathbf{r})$. The time-reversal symmetric reference state of the isolated system $|0_s\rangle$ is variationally optimized with the use of an electronic Hamiltonian for the interacting system in which the kinetic energy is given by the free-particle Dirac Hamiltonian and the electron-electron repulsion is approximated by the instantaneous Coulomb interaction. This approximate form of the two-electron part of the relativistic Hamiltonian is improved on by the inclusion of the Gaunt term, or the full Breit interaction, but the introduction of current-current interactions in DFT requires a general consideration before introduced here.[31] Time-reversal symmetry of $|0_s\rangle$ is enforced by the occupation of Kramers pairs of spinors (corresponding to the closed-shell state in a nonrelativistic theory)—a pair of spinors are related by the time-reversal operator,

$$\Phi_{\bar{p}}(\mathbf{r}) = \hat{\mathcal{K}}\phi_p(\mathbf{r}), \quad \hat{\mathcal{K}} = \begin{bmatrix} 0_2 & -\mathbf{I}_2 \\ \mathbf{I}_2 & 0_2 \end{bmatrix} \hat{\mathcal{K}}_0, \tag{1}$$

where $\hat{\mathcal{K}}_0$ denotes the complex conjugation operator. The eigenvalues of the spinors are divided into two sets that are separated by *circa* twice the electron rest energy, and spinors corresponding to the upper and lower sets are sometimes referred to as electronic and positronic orbitals, respectively (although they all represent electron wave functions). The

reference state includes only electronic orbitals and is optimized in a minmax sense.[32]

When subjected to an external time-dependent electromagnetic field, the reference state becomes time dependent in a way that is not described by a trivial phase factor but involves electronic transitions to virtual orbitals. We parametrize this time dependence in a nonredundant and unitary way as follows:[2,31]

$$|\tilde{0}_s(t)\rangle = \exp[-\hat{\kappa}(t)]|0_s\rangle, \quad \hat{\kappa}(t) = \kappa_{ai}\hat{a}_a^\dagger\hat{a}_i - \kappa_{ai}^*\hat{a}_i^\dagger\hat{a}_a. \tag{2}$$

Here and in the following, we have made use of the Einstein summation convention for repeated indices and $a,b,\ldots,i,j,\ldots$, and $p,q,\ldots$ are indices of virtual, occupied, and general molecular orbitals, respectively. In general, the summation over virtual orbitals in Eq. (2) includes the positronic orbitals and the corresponding electron transfer amplitudes are at times denoted by κ_{ai}^- (to be distinguished from rotations among electronic orbitals with amplitudes κ_{ai}^+). In calculations of electric-field induced valence properties, such as the electric-dipole hyperpolarizability, the effect of redressing of the electronic states due to the inclusion of the κ_{ai}^- parameters in the propagator is small and can be ignored with the benefit of memory savings.[23]

For weak, periodic external fields, we can use the quasienergy formalism to determine the time dependence of the κ parameters[33]—a technique which was also used for the derivation and implementation of the linear response function at this level of theory[30] (see, however, Ref. 34 for a discussion about the validity of this approach). The relevant time-averaged Kohn-Sham quasienergy functional can be written as

$$Q[\rho] = T_s[\rho] + V[\rho] + J[\rho] + Q_{xc}[\rho] + S_s[\rho], \tag{3}$$

where the time-dependent electron density is introduced as ρ and depends implicitly on the κ parameters. The response functions are defined as derivatives of the quasienergy with respect to the Fourier amplitudes of the external electromagnetic field, and the third-order response, or the quadratic response function, is given by

$$\langle\langle \hat{A};\hat{B},\hat{C}\rangle\rangle_{\omega_B,\omega_C} = \left.\frac{d^3Q}{d\varepsilon_A(\omega_A)d\varepsilon_B(\omega_B)d\varepsilon_C(\omega_C)}\right|_{\varepsilon=0}. \tag{4}$$

In evaluating this derivative, we note that the sum of terms in Eq. (3) excluding Q_{xc} corresponds formally to Hartree-Fock theory without exchange interaction. We can, therefore, benefit from the implementation of the quadratic response function reported in Ref. 29 and use it with a mere turnoff of the exchange interaction (or partial turnoff for hybrid functionals) together with the addition of the contribution from Q_{xc}. We will adopt the adiabatic approximation and employ the time-dependent exchange-correlation functional as a substitute for Q_{xc},

$$Q_{xc}[\rho] \to E_{xc}[\rho] = \int e_{xc}(\rho,\zeta)d\tau. \tag{5}$$

The energy density is here assumed to be a function of ρ and the square norm of the electron density gradient $\zeta=\nabla\rho\cdot\nabla\rho$, and a time averaging is implied here as well. The time averaging will impose that the response function [Eq. (4)] is nonzero only when $\omega_A=-(\omega_B+\omega_C)$. In the next section, we will present the detailed expressions needed for the implementation of the part in Eq. (4) that is due to E_{xc}.

B. Implementation of the exchange-correlation contribution to the quadratic response function

In the evaluation of the third-order derivative of E_{xc} with respect to the amplitudes of the external fields, we will use chain rule differentiation of the energy density $e(\rho,\zeta)$. We will view the electron density as dependent on the κ parameters and determine the response of the latter to the external perturbation from the variational condition $\delta Q[\rho]=0$. Since the $2n+1$ rule applies in the present case, it will be sufficient to determine the first-order response in κ with respect to $\varepsilon(\omega)$ in order to determine the quadratic response function. We note that the details and code implementation concerned with the determination of this linear response have already been considered in Ref. 30. The structure of the implementation of the quadratic response function at the Hartree-Fock level is such that first, the formation of a generalized electronic gradient

$$\left.\frac{\partial}{\partial\kappa_{ai}}\frac{d^2E_{xc}}{d\varepsilon_B d\varepsilon_C}\right|_{\varepsilon=0} \tag{6}$$

is made and, thereafter, this gradient is contracted with the response of the κ_{ai} parameters with respect to the external field.[29] In order to comply with this structure, we therefore seek an explicit expression for the quantity in Eq. (6).

This exchange-correlation contribution will be added to the generalized gradient as due to the Coulomb interaction and which is denoted as $E^{[3]}N^BN^C$ in Ref. 29. Let us now turn to the differentiation of E_{xc} and first consider the partial derivatives that will appear. In doing so, we will make use of the fact that $\varepsilon\to 0$ implies that $\kappa\to 0$ and vice versa and, although partial differentiation is to be made independently for κ_{ai} and κ_{ai}^*, we restrict the presentation to include only one of them.

With the use of the density operator,

$$\hat{\rho} = \Omega_{pq}\hat{a}_p^\dagger\hat{a}_q, \quad \Omega_{pq} = \phi_p^\dagger(\mathbf{r})\phi_q(\mathbf{r}), \tag{7}$$

the electron density can be written as

$$\rho(\mathbf{r}) = \langle\tilde{0}_s|\hat{\rho}|\tilde{0}_s\rangle = \Omega_{pq}\langle 0_s|e^{\hat{\kappa}}\hat{a}_p^\dagger\hat{a}_q e^{-\hat{\kappa}}|0_s\rangle. \tag{8}$$

Expanding the density matrix elements with use of the Baker-Campbell-Hausdorff expansion yields

$$\rho = \sum_{n=0}^{\infty}\rho^{(n)}, \quad \rho^{(n)} = \frac{\Omega_{pq}}{n!}\langle 0_s|\hat{\boldsymbol{\kappa}}^n\hat{a}_p^\dagger\hat{a}_q|0_s\rangle, \tag{9}$$

where the action of the superoperator $\hat{\boldsymbol{\kappa}}$ is the formation of a commutator according to $\hat{\boldsymbol{\kappa}}\hat{A}=[\hat{\kappa},\hat{A}]$. The differentiation of the density with respect to the external fields gives

$$\rho^{ABC\cdots} := \left.\frac{\partial^n\rho}{\partial\varepsilon_A\partial\varepsilon_B\partial\varepsilon_C\cdots}\right|_{\varepsilon=0} = \Omega_{ai}^{BC\cdots}\frac{\partial\kappa_{ai}}{\partial\varepsilon_A}, \tag{10}$$

where we have introduced

$$\Omega_{ai}^{BC\cdots} := \frac{\partial^n \rho^{(n)}}{\partial\kappa_{ai}\partial\kappa_{bj}\partial\kappa_{ck}\cdots}\frac{\partial\kappa_{bj}}{\partial\varepsilon_B}\frac{\partial\kappa_{ck}}{\partial\varepsilon_C}\cdots . \tag{11}$$

In order to account for gradient-corrected density functionals, we also introduce the following partial derivatives of ζ with respect to the external field:

$$\zeta^B := \left.\frac{\partial\zeta}{\partial\varepsilon_B}\right|_{\varepsilon=0} = 2\nabla\rho\cdot\nabla\rho^B, \tag{12}$$

$$\zeta^{BC} := \left.\frac{\partial^2\zeta}{\partial\varepsilon_B\partial\varepsilon_C}\right|_{\varepsilon=0} = 2(\nabla\rho\cdot\nabla\rho^{BC} + \nabla\rho^B\cdot\nabla\rho^C). \tag{13}$$

The numerical grid-integration kernel in the program assumes the integrand to be written on the form

$$s\Omega_{pq} + \mathbf{v}\cdot\nabla\Omega_{pq},$$

where the scalar s and vectorial $\mathbf{v}$ functions as well as the atomic orbital density matrix corresponding to Ω_{pq} are to be specified for a given property integration. Let us illustrate how this works for the electronic gradient,

$$\left.\frac{\partial E_{\mathrm{xc}}}{\partial\overset{*}{\kappa}_{ai}}\right|_{\kappa=0} = \int\left[\frac{\partial e_{\mathrm{xc}}}{\partial\rho}\left.\frac{\partial\rho}{\partial\overset{*}{\kappa}_{ai}}\right|_{\kappa=0} + \frac{\partial e_{\mathrm{xc}}}{\partial\zeta}\left.\frac{\partial\zeta}{\partial\overset{*}{\kappa}_{ai}}\right|_{\kappa=0}\right]d\tau = -\int f_{\mathrm{xc};ai}\,d\tau, \tag{14}$$

in which appears the exchange-correlation part of the Kohn-Sham matrix,

$$f_{\mathrm{xc};pq} = s_f\Omega_{pq} + \mathbf{v}_f\cdot\nabla\Omega_{pq}, \qquad s_f = \frac{\partial e_{\mathrm{xc}}}{\partial\rho}, \quad \mathbf{v}_f = \frac{1}{|\nabla\rho|}\frac{\partial e_{\mathrm{xc}}}{\partial|\nabla\rho|}\nabla\rho. \tag{15}$$

Continuing to linear response, we get

$$\frac{\partial}{\partial\overset{*}{\kappa}_{ai}}\left.\frac{\partial E_{\mathrm{xc}}}{\partial\varepsilon_B}\right|_{\varepsilon=0} = -\int(f_{\mathrm{xc};ai}^B + g_{\mathrm{xc};ai}^{[B]})d\tau, \tag{16}$$

where the integrand consists of the exchange-correlation part of the one-index transformed Kohn-Sham matrix,

$$f_{\mathrm{xc};pq}^B = s_f\Omega_{pq}^B + \mathbf{v}_f\cdot\nabla\Omega_{pq}^B, \tag{17}$$

and a remainder that equals to

$$g_{\mathrm{xc};pq}^{[B]} = s_g\Omega_{pq} + \mathbf{v}_g\cdot\nabla\Omega_{pq},$$

$$s_g^{[B]} = \frac{\partial^2 e_{\mathrm{xc}}}{\partial\rho^2}\rho^B + \frac{\partial^2 e_{\mathrm{xc}}}{\partial\rho\partial\zeta}\cdot 2(\nabla\rho\cdot\nabla\rho^B), \tag{18}$$

$$\mathbf{v}_g^{[B]} = \left[\frac{\partial^2 e_{\mathrm{xc}}}{\partial\rho\partial\zeta}\rho^B + \frac{\partial^2 e_{\mathrm{xc}}}{\partial\zeta^2}\cdot 2(\nabla\rho\cdot\nabla\rho^B)\right]\cdot 2\nabla\rho + \frac{\partial e_{\mathrm{xc}}}{\partial\zeta}\cdot 2\nabla\rho^B.$$

We will reach our desired expression for the quadratic response by performing a differentiation of Eq. (16) with respect to the external field. We collect the final result of this derivation in the form

$$\frac{\partial}{\partial\overset{*}{\kappa}_{ai}}\left.\frac{d^2E_{\mathrm{xc}}}{d\varepsilon_B d\varepsilon_C}\right|_{\varepsilon=0} = -\int(f_{\mathrm{xc};ai}^{BC} + g_{\mathrm{xc};ai}^{[C]B} + g_{\mathrm{xc};ai}^{[B]C} + h_{\mathrm{xc};ai}^{[BC]})d\tau, \tag{19}$$

where we recognize the doubly one-index transformed exchange-correlation part of the Kohn-Sham matrix $f_{\mathrm{xc};pq}^{BC}$ as well as matrices $g_{\mathrm{xc};ai}^{[C]B}$ and $g_{\mathrm{xc};ai}^{[B]C}$ which are one-index transformed versions of Eq. (18) with respect to B and C, respectively. The remainder is collected into

$$h_{\mathrm{xc};pq}^{[BC]} = s_h\Omega_{pq} + \mathbf{v}_h\cdot\nabla\Omega_{pq},$$

$$s_h = \sum\mathcal{P}_{B,C}\left\{\frac{\partial^3 e_{\mathrm{xc}}}{\partial\rho^3}\rho^B\rho^C + 2\frac{\partial^3 e_{\mathrm{xc}}}{\partial\rho^2\partial\zeta}\rho^B\cdot 2(\nabla\rho\cdot\nabla\rho^C) + \frac{\partial^3 e_{\mathrm{xc}}}{\partial\rho\partial\zeta^2}\cdot 2(\nabla\rho\cdot\nabla\rho^B)\cdot 2(\nabla\rho\cdot\nabla\rho^C) + \frac{\partial^2 e_{\mathrm{xc}}}{\partial\rho^2}\rho^{BC} + \frac{\partial^2 e_{\mathrm{xc}}}{\partial\rho\partial\zeta}\cdot 2[(\nabla\rho\cdot\nabla\rho^{BC}) + (\nabla\rho^B\cdot\nabla\rho^C)]\right\}, \tag{20}$$

$$\mathbf{v}_h = \sum\mathcal{P}_{B,C}\left\{\left[\frac{\partial^3 e_{\mathrm{xc}}}{\partial\zeta^3}\cdot 2(\nabla\rho\cdot\nabla\rho^B)\cdot 2(\nabla\rho\cdot\nabla\rho^C) + 2\frac{\partial^3 e_{\mathrm{xc}}}{\partial\rho\partial\zeta^2}\rho^B\cdot 2(\nabla\rho\cdot\nabla\rho^C) + \frac{\partial^3 e_{\mathrm{xc}}}{\partial\rho^2\partial\zeta}\rho^B\rho^C + \frac{\partial^2 e_{\mathrm{xc}}}{\partial\rho\partial\zeta}\rho^{BC} + \frac{\partial^2 e_{\mathrm{xc}}}{\partial\zeta^2}\cdot 2[(\nabla\rho\cdot\nabla\rho^{BC}) + (\nabla\rho^B\cdot\nabla\rho^C)]\right]\cdot 2\nabla\rho + \left[\frac{\partial^2 e_{\mathrm{xc}}}{\partial\rho\partial\zeta}\rho^C + \frac{\partial^2 e_{\mathrm{xc}}}{\partial\zeta^2}\cdot 2(\nabla\rho\cdot\nabla\rho^C)\right]\cdot 4\nabla\rho^B + \frac{\partial e_{\mathrm{xc}}}{\partial\zeta}\cdot 2\nabla\rho^{BC}\right\},$$

where the operator $\Sigma\mathcal{P}_{B,C}$ denotes the sum over permutations between B and C. An implementation of Eq. (19) has been added to the DIRAC program[35] and below, we will present an example calculation of the electric-dipole hyperpolarizability which corresponds to a quadratic response function [Eq. (4)] evaluated for electric-dipole operators. The implementation is general in the sense that it merely assumes the perturbations to be due to one-electron operators and our work is, therefore, in principle, applicable to a series of electromagnetic properties. However, the introduction of a magnetic perturbation breaks the time-reversal symmetry of the system and requires the consideration of spin polarization in the formalism. In fact, even the application of time-dependent electric fields will induce electronic currents and thereby magnetic fields, so also the evaluation of dynamic polarizabilities should take spin polarization into account. We will return to this topic in a future work.

III. EXAMPLE CALCULATIONS

A. Computational details

All calculations in the present work were performed for molecular structures that were optimized at the one-component Kohn-Sham DFT level of theory using the hybrid B3LYP exchange-correlation functional;[36] for H, C, and Br,

the 6-31G* basis set was used,[37,38] and for iodine, the Stuttgart ECP was used.[39] Structure optimizations were performed in the C_{2v} point group with the GAUSSIAN program.[40] The molecules are placed with the z axis as principle axis and in the yz plane with the heavy atoms along the negative z direction.

The all-electron property calculations were performed with a locally modified version of the DIRAC program,[35] and those where an ECP was used for Br or I were performed with a version of the DALTON program[41] to which an implementation of the Coulomb attenuated B3LYP (Ref. 42) (CAM-B3LYP) has been added.[43] The property calculations based on single determinant reference states (all-electron as well as ECP based) were performed with fully uncontracted basis sets that are based on the exponents from Sadlej's polarization basis set[44] with further addition of polarization and diffuse functions. The basis sets were augmented using the formula

$$\zeta_{N+j} = \left[\frac{\zeta_N}{\zeta_{N-1}}\right]^j \zeta_N, \quad j \in [1, N_{\text{aug}}], \tag{21}$$

where N_{aug} is the number of augmentation functions added and ζ_N and ζ_{N-1} refer to the two most diffuse exponents in the original basis sets. The only exception to this rule is the f shell of the iodine basis set, which was not augmented. To the basis set of bromine, we added four f functions based on the four most diffuse p exponents in the original basis set. The sizes of the singly augmented large component basis sets used in the property calculations were $[7s5p]$, $[11s7p5d]$, $[16s13p10d4f]$, and $[20s16p13d4f]$ for H, C, Br, and I, respectively, and the small-component basis functions were generated from those of the large component with the use of the restricted kinetic-balance condition. In all four-component calculations, we have ignored the interactions between the small component densities, i.e., the $(SS|SS)$ integrals. This approximation has virtually no influence on the presented results, as demonstrated in Ref. 23, and will not be further discussed here. All DFT functionals were employed self-consistently and with their proper derivatives to the required orders in the perturbations.

For comparison, wave function correlated results were obtained at the coupled cluster level with inclusion of single and double electron excited configurations (CCSD). For these calculations, we adopted the contracted Sadlej basis set[44] for hydrogen and carbon but augmented with the same diffuse functions as described above. For bromine and iodine, we employed the valence basis set of the Stuttgart ECPs (Ref. 39) but augmented and polarized using the functions from the Sadlej basis set and Eq. (21). The sizes of the heavy atom basis sets in the CCSD calculations were $[6s6p5d4f]/[4s4p3d2f]$ (bromine) and $[6s6p8d2f]/[4s4p3d1f]$ (iodine).

B. Results and discussion

With a molecular dipole moment aligned with the z axis, the relevant experimental observable for second-harmonic generation is $\mu\bar{\beta}$,[45] where

$$\bar{\beta}(-2\omega;\omega,\omega) = \frac{1}{5}\sum_{\alpha=x,y,z}(\beta_{z\alpha\alpha} + 2\beta_{\alpha z\alpha}). \tag{22}$$

In previous studies, we have shown that relativistic effects in heavy atom substituted π-conjugated systems are pronounced for the dipole moment as well as the first-order hyperpolarizability (but not for the linear polarizability);[22,23] for bromobenzene, the effects are predominantly scalar relativistic in nature but for iodobenzene, scalar relativistic and spin-orbit effects are about equally important.[23] Whereas changes due to relativity in the dipole moment can be attributed to changes in the chemical bond polarities, the effects on the hyperpolarizabilities are not as easily interpreted. The sum-over-states expression for β, which reads as

$$\beta_{\alpha\beta\gamma}(-\omega_\sigma;\omega_1,\omega_2) = \hbar^{-2}\sum \mathcal{P}_{-\sigma,1,2}\sum_{k,l}{}' \frac{\langle 0|\hat{\mu}_\alpha|k\rangle\langle k|\bar{\hat{\mu}}_\beta|l\rangle\langle l|\hat{\mu}_\gamma|0\rangle}{(\omega_k - \omega_\sigma)(\omega_l - \omega_2)}, \tag{23}$$

reveals an intricate dependence of the hyperpolarizability on interexcited state transition moments and excited-to-ground state dipole moment differences, in addition to a dependence on the linear absorption spectrum via the ground-to-excited state transition dipole moments and excitation energies. The permutation operator introduced in Eq. (23) permutes the pairs of dipole moment operators and optical frequencies $(\hat{\mu}_\alpha, -\omega_\sigma)$, $(\hat{\mu}_\beta, \omega_1)$, and $(\hat{\mu}_\gamma, \omega_2)$, and $\bar{\hat{\mu}}$ denotes the electric-dipole fluctuation operator. One thing that becomes clear from the sum-over-states expression is the separation between scalar relativistic and spin-orbit effects, since the latter can be attributed to the coupling between states in the singlet and triplet manifolds. The nonrelativistic and relativistic linear absorption spectra presented in Ref. 23 show significant spin-forbidden absorption only for the iodobenzenes, and scalar relativistic and spin-orbit effects on β are also of comparable magnitude in this case, whereas the spin-orbit effects are small on the same property for the bromobenzenes.

The same argumentation can be made for the linear polarizability. In fact, α depends only on the observables in the linear absorption spectrum, namely, transition energies and intensities. The absence of relativistic effects that are seen in Tables I and II for this property is, therefore, puzzling but has been previously noted also for the thiophene homologs which serve as important building blocks in optical materials.[22]

In the present work, we focus at a formulation of the quadratic response function at the electron correlated four-component level of theory. We give here a presentation of the response function which is quite different from the sum-over-states expression in Eq. (23) but is rather seen as energy derivatives. Since the correlation energy depends on the electron density, its value per electron will basically be larger, the heavier the atom. What makes property calculations at the Hartree-Fock level at all reasonable for heavy atoms are the facts that the molecular property is a measure of the energy difference with respect to external fields and that the induced fluctuations in the core electron densities are very small—in the valence region, where density fluctuations are larger, the

TABLE I. Optical properties for disubstituted bromobenzenes at the Hartree-Fock, Kohn-Sham, and post-HF levels of theory. Different exchange-correlation functionals are considered for the inclusion of electron correlation effects. All quantities are given in a.u.

Method		μ_z	α_{xx}	α_{yy}	α_{zz}	β_{zxx}	β_{zyy}	β_{zzz}
				meta-dibromobenzene				
LDA	NR	0.6149	72.79	166.1	124.2	26.13	−168.8	32.79
	ECP	0.5728	73.93	168.2	125.5	32.10	−167.4	44.76
	4C	0.5903	73.00	166.5	124.5	29.04	−163.4	41.00
BLYP	NR	0.6105	73.62	167.2	125.1	29.96	−155.6	44.22
	ECP	0.5902	73.60	167.0	125.0	30.82	−147.1	47.97
	4C	0.5864	73.85	167.6	125.3	33.13	−149.8	53.01
B3LYP	NR	0.6435	71.86	161.2	121.7	21.16	−117.7	36.31
	ECP	0.6203	72.01	161.4	121.8	22.92	−112.6	40.95
	4C	0.6186	72.03	161.5	121.9	23.63	−112.6	43.41
CAM-B3LYP	NR	0.6626	70.85	156.5	119.4	17.76	−88.99	34.92
	ECP	0.6333	71.22	157.1	119.7	20.07	−85.60	40.32
	4C	0.6361	71.00	156.8	119.6	19.81	−84.30	41.08
HF	NR	0.7482	69.78	150.5	115.8	3.57	−48.97	27.85
	ECP	0.7291	69.9	150.8	116.0	4.91	−47.30	31.27
	4C	0.7218	69.81	150.8	115.9	4.55	−45.50	31.64
CCSD	ECP	0.6344	72.18	156.6	120.3	12.87	−82.70	33.06
				ortho-dibromobenzene				
LDA	NR	0.8925	71.93	131.4	150.9	41.73	−62.10	−164.4
	ECP	0.8208	73.00	132.9	152.3	50.83	−55.44	−152.1
	4C	0.8513	72.14	131.6	151.0	46.44	−56.28	−152.8
BLYP	NR	0.8814	72.71	132.1	151.6	47.09	−52.58	−148.8
	ECP	0.8479	72.70	132.0	151.5	48.14	−46.90	−138.6
	4C	0.8409	72.94	132.4	151.9	52.40	−46.22	−136.6
B3LYP	NR	0.9395	71.01	128.3	147.1	33.37	−39.78	−113.5
	ECP	0.9008	71.16	128.4	147.2	35.71	−35.25	−105.3
	4C	0.8977	71.18	128.5	147.2	37.29	−34.45	−103.3
CAM-B3LYP	NR	0.9739	70.03	125.5	143.5	27.66	−28.81	−80.26
	ECP	0.9248	70.37	125.9	143.9	30.96	−24.62	−72.58
	4C	0.9296	70.17	125.7	143.7	31.01	−23.97	−71.05
HF	NR	1.1147	69.10	121.4	138.8	6.72	−9.99	−35.62
	ECP	1.0826	69.21	121.6	138.9	8.45	−7.56	−31.41
	4C	1.0709	69.13	121.5	138.9	8.30	−6.61	−29.79
CCSD	ECP	0.9310	71.34	126.5	144.1	20.50	−28.65	−82.57

effects of electron correlation are smaller. As a rule of thumb for the polarizability of molecules containing first- and second-row elements, the isotropic value is typically underestimated by some 5% at the Hartree-Fock level of theory, whereas anisotropies suffer from larger errors.[46] For the hyperpolarizabilities, on the other hand, the effects of electron correlation are known to be both large and unsystematic.

In Tables I and II, we present the optical properties of disubstituted bromobenzene and iodobenzene, respectively, in their *meta* and *ortho* conformations. We employ a series of four standard density functionals in the correlated four-component calculations, namely, local-density approximation (LDA), BLYP, B3LYP, and CAM-B3LYP, and the ordering of functionals in the tables reflects the consensus of increasing accuracy as due to gradient and exact exchange corrections. An apparent consequence of the use of the more sophisticated density functionals is the improved quality of the orbital energies and, since the difference in orbital energies between virtual and occupied orbitals appears on the diagonal of the electronic Hessian, it will correspond to improved excitation energies in the response function approach as well. In Ref. 47, it was also well illustrated how the inclusion of exact exchange in the density functional affects linear response calculation of excitation energies. It is the exact exchange that provides the Coulomb attraction between the hole and the electron in these calculations, and the more spatially separated the hole and electron orbitals are, the greater the need for exact exchange in the functional is. The present systems are by no means extreme charge-transfer systems but, at the same time, it is clear that the halogen

TABLE II. Optical properties for disubstituted iodobenzenes at the Hartree-Fock, Kohn-Sham, and post-hF levels of theory. Different exchange-correlation functionals are considered for the inclusion of electron correlation effects. All quantities are given in a.u.

Method		μ_z	α_{xx}	α_{yy}	α_{zz}	β_{zxx}	β_{zyy}	β_{zzz}
				meta-di-iodobenzene				
LDA	NR	0.6337	94.24	214.0	149.1	85.17	−175.1	140.6
	ECP	0.5674	95.86	216.1	150.6	96.74	−166.0	167.0
	4C	0.5661	94.61	215.1	149.5	96.78	−151.2	171.4
BLYP	NR	0.6240	95.86	216.0	150.5	95.56	−150.4	166.4
	ECP	0.5885	95.16	214.3	149.7	96.71	−128.2	174.8
	4C	0.5575	96.32	217.4	151.1	108.7	−125.6	200.3
B3LYP	NR	0.6501	93.55	208.1	146.5	79.16	−88.74	151.1
	ECP	0.6076	93.30	207.4	146.2	82.61	−73.72	162.0
	4C	0.5806	93.79	209.9	146.9	89.19	−64.85	179.0
CAM-B3LYP	NR	0.6618	91.88	201.2	143.4	68.39	−37.66	141.1
	ECP	0.6057	92.17	201.6	143.7	73.46	−25.95	155.5
	4C	0.5867	91.99	202.2	143.7	76.96	−15.23	165.7
HF	NR	0.7537	91.23	196.1	140.5	56.17	12.08	140.0
	ECP	0.7074	91.14	196.5	140.5	59.36	22.27	150.5
	4C	0.6793	90.91	197.2	140.5	61.26	31.21	157.2
CCSD	ECP	0.5822	96.54	205.1	147.6	80.97	−46.26	180.7
				ortho-di-iodobenzene				
LDA	NR	0.8877	92.07	166.3	182.7	125.0	−42.42	−46.42
	ECP	0.7777	93.59	167.9	184.0	142.3	−26.39	−16.02
	4C	0.7766	92.45	166.6	182.9	143.9	−19.06	−2.32
BLYP	NR	0.8639	93.49	167.7	183.9	136.7	−24.59	−16.73
	ECP	0.8071	92.87	166.1	182.7	138.2	−8.59	5.99
	4C	0.7544	93.94	168.1	184.2	157.9	1.05	29.70
B3LYP	NR	0.9103	91.31	162.4	178.6	113.4	1.21	25.32
	ECP	0.8411	91.11	161.6	178.0	118.1	14.86	45.94
	4C	0.7962	91.57	162.7	178.8	129.7	25.04	67.06
CAM-B3LYP	NR	0.9336	89.74	158.1	174.1	97.05	22.97	66.22
	ECP	0.8415	90.03	158.2	174.2	104.6	36.07	86.91
	4C	0.8105	89.88	158.3	174.3	110.4	45.22	104.3
HF	NR	1.0740	89.19	154.3	170.2	78.37	53.66	123.4
	ECP	0.9973	89.13	154.2	170.1	82.94	65.23	139.0
	4C	0.9519	88.93	154.3	170.4	86.26	72.80	151.2
CCSD	ECP	0.8023	94.14	162.7	177.7	117.3	23.97	89.22

atoms will play the role of donors in excitations to the π^* orbitals. We, therefore, anticipate that the use of the CAM-B3LYP can have an impact on results, and we would argue that these results are the best ones at the four-component level of theory. We would also like to draw attention to the systematic decrease in α when comparing results obtained with the series of functionals BLYP, B3LYP, and CAM-B3LYP. This trend is directly coupled to an increasing portion of exact exchange and thereby increased excitation energies of the system.

When measured against the four-component CAM-B3LYP results, the correlation contributions to β_{zxx}, β_{zyy}, and β_{zzz} of *meta*-bromobenzene amount to 15.3, −38.8, and 9.4 a.u., respectively, and for *meta*-iodobenzene, the corresponding values are 15.7, −46.4, and 8.5 a.u. In both cases, there is thus a strong error cancellation for the Hartree-Fock values of the observable $\bar{\beta}$ since electron correlation lowers the value of the *zyy* component but increases the values of the other two components. This illustrates how unsystematic correlation effects can be for the first-order hyperpolarizability. On the other hand, we note that the correlation effects on the hyperpolarizabilities of the two *meta* systems are close in magnitude. That again indicates that it is the correlation energy in the valence region that matters for this property, and that this energy is almost the same in the two systems. If we make the same comparison for the two *ortho* systems, we see correlation contributions of 22.7, −17.4, and −41.3 a.u. for the three nonzero β components of bromobenzene and 24.1, −27.6, −46.9 a.u. for the three components of iodobenzene.

We have argued that the ordering of DFT results in the tables reflects the quality. In order to get a more objective measure of the performance of the various functionals, we have also determined the optical properties using a nonrelativistic wave function correlated approach in conjunction with the Stuttgart relativistic ECPs. Due to the computational cost associated with the CCSD method, we are forced to employ a reduced basis set and, given the fact that the basis set requirements are stronger in wave function than in density functional approaches, we cannot use the CCSD results as benchmarks. Furthermore, the lack of inclusion of relativistic effects in the valence region will make the results based on ECPs error prone for the iodobenzenes. For the β-tensor elements of bromobenzenes, the largest discrepancy between ECP and four-component results at the CAM-B3LYP level is as small as 1.5 a.u. (or 2%), whereas for the iodobenzenes, this error bar is 17.4 a.u. It is, therefore, reasonable to use the bromobenzene CCSD results for the evaluation of the various density functionals. For each individual β component of the bromobenzenes, the best agreement with the CCSD results is obtained with use of the CAM-B3LYP functional but, at the same time, it is clear that discrepancies between the correlated results can be as large as 10 a.u. (see the *zzz* component of *ortho*-bromobenzene).

The calculations of the hyperpolarizabilities of the halobenzenes amply demonstrate that electron correlation effects can be very large for this property. Of greater concern to the present work, however, is the fact that relativistic effects on the hyperpolarizability are substantial for the bromobenzenes and large for the iodobenzenes. The development of electron correlated propagator methods with proper inclusion of relativity is particular important since the two effects are not additive. Without exception for the β tensor, the relativistic effects at the correlated level of theory exceed those at the uncorrelated level of theory, e.g., the relativistic effects for β_{zxx}, β_{zyy}, and β_{zzz} at the CAM-B3LYP level amount to 13.3, 22.2, and 38.1 a.u., respectively, whereas at the Hartree-Fock level, the corresponding values are 7.9, 19.2, and 27.8 a.u. The relativistic corrections are without exception positive, thereby increasing the value of $\bar{\beta}$.

IV. CONCLUSIONS

A derivation and implementation of the quadratic response function at the four-component density functional level of theory has been presented. The adiabatic, Kramers-restricted Kohn-Sham approximation has been adopted with consideration made of gradient-corrected functionals. We exemplify the significance of this work with calculations of the optical properties of disubstituted halobenzenes and thereby illustrate internal heavy atom effects on the hyperpolarizabilities in π-conjugated systems. Our best results are obtained with the use of the Coulomb attenuated B3LYP functional,[42] which here provides notably different hyperpolarizability values from B3LYP. It is shown that correlation as well as relativistic effects on β are large for the systems under investigation. Relativity alone reduces the $\mu\bar{\beta}$-response signals by 62% and 75% for *meta*- and *ortho*-bromobenzene, respectively, and enhances the same response by 17% and 21% for *meta*- and *ortho*-iodobenzene, respectively (these values are based on the CAM-B3LYP results). The results in the present work also demonstrates the well-known fact that correlation and relativistic effects are not additive and that our work is called for.

ACKNOWLEDGMENTS

We acknowledge the use of computational resources at the National Supercomputer Centre (NSC) in Linköping, Sweden.

[1] R. W. Boyd, *Nonlinear Optics*, 2nd ed. (Academic, New York, 2003).
[2] J. Olsen and P. Jørgensen, J. Chem. Phys. **82**, 3235 (1985).
[3] H. Sekino and R. Bartlett, J. Chem. Phys. **85**, 976 (1986).
[4] S. Karna and M. Dupuis, J. Comput. Chem. **12**, 487 (1991).
[5] J. Rice, R. Amos, S. Colwell, N. Handy, and J. Sanz, J. Chem. Phys. **93**, 8828 (1990).
[6] H. Hettema, H. Jensen, P. Jørgensen, and J. Olsen, J. Chem. Phys. **97**, 1174 (1992).
[7] J. Rice and N. Handy, Int. J. Quantum Chem. **43**, 91 (1992).
[8] C. Hättig, O. Christiansen, H. Koch, and P. Jørgensen, Chem. Phys. Lett. **269**, 428 (1997).
[9] J. Gauss, O. Christiansen, and J. Stanton, Chem. Phys. Lett. **296**, 117 (1998).
[10] P. Rozyczko and R. Bartlett, J. Chem. Phys. **107**, 10823 (1997).
[11] J. Olsen, P. Jørgensen, T. Helgaker, and J. Oddershede, J. Phys. Chem. A **109**, 11618 (2005).
[12] S. van Gisbergen, J. Snijders, and E. Baerends, J. Chem. Phys. **109**, 10644 (1998); **111**, 6652(E) (1999).
[13] P. Salek, O. Vahtras, T. Helgaker, and H. Ågren, J. Chem. Phys. **117**, 9630 (2002).
[14] P. Norman, D. M. Bishop, H. J. Aa. Jensen, and J. Oddershede, J. Chem. Phys. **123**, 194103 (2005).
[15] D. Roberto, R. Ugo, E. Tessore, F. Lucenti, S. Quici, S. Vezza, P. Fantucci, I. Invernizzi, S. Bruni, I. Ledoux-Rak, and J. Zyss, Organometallics **21**, 161 (2002).
[16] O. Vahtras, H. Ågren, P. Jørgensen, H. J. Aa. Jensen, T. Helgaker, and J. Olsen, J. Chem. Phys. **97**, 9178 (1992).
[17] I. Tunell, Z. Rinkevicius, O. Vahtras, P. Salek, T. Helgaker, and H. Ågren, J. Chem. Phys. **119**, 11024 (2003).
[18] M. Engström, O. Vahtras, and H. Ågren, Chem. Phys. Lett. **328**, 483 (2000).
[19] P. Manninen, K. Ruud, P. Lantto, and J. Vaara, J. Chem. Phys. **122**, 114107 (2005).
[20] L. R. Kahn, P. Baybutt, and D. G. Truhlar, J. Chem. Phys. **65**, 3826 (1976).
[21] P. Norman, B. Schimmelpfennig, K. Ruud, H. J. Aa. Jensen, and H. Ågren, J. Chem. Phys. **116**, 6914 (2002).
[22] B. Jansik, B. Schimmelpfennig, P. Norman, H. Ågren, and K. Ohta, J. Mol. Struct.: THEOCHEM **633**, 237 (2003).
[23] J. Henriksson, U. Ekström, and P. Norman, J. Chem. Phys. **124**, 214311 (2006).
[24] J. Henriksson, P. Norman, and H. J. Aa. Jensen, J. Chem. Phys. **122**, 114106 (2005).
[25] S. Raptis, M. Papadopoulos, and A. Sadlej, J. Chem. Phys. **111**, 7904 (1999).
[26] M. Douglas and N. Kroll, Ann. Phys. (N.Y.) **82**, 89 (1974).
[27] G. Jansen and B. Hess, Phys. Rev. A **39**, 6016 (1989).
[28] E. Tellgren, J. Henriksson, and P. Norman, J. Chem. Phys. **126**, 064313 (2007).
[29] P. Norman and H. J. Aa. Jensen, J. Chem. Phys. **121**, 6145 (2004).
[30] P. Salek, T. Helgaker, and T. Saue, Chem. Phys. **311**, 187 (2005).
[31] T. Saue and T. Helgaker, J. Comput. Chem. **23**, 814 (2002).
[32] T. Saue, K. Fægri, T. Helgaker, and O. Gropen, Mol. Phys. **91**, 937 (1997).
[33] O. Christiansen, P. Jørgensen, and C. Hättig, Int. J. Quantum Chem. **68**, 1 (1998).
[34] N. T. Maitra and K. Burke, Chem. Phys. Lett. **441**, 167 (2007).
[35] H. J. Aa. Jensen, T. Saue, L. Visscher, V. Bakken, E. Eliav, T. Enevoldsen, T. Fleig, O. Fossgaard, T. Helgaker, J. Laerdahl *et al.*, DIRAC, a relativistic *ab initio* electronic structure program, release as DIRAC4.0,

2004.
[36] A. D. Becke, J. Chem. Phys. **98**, 5648 (1993).
[37] W. J. Hehre, R. Ditchfield, and J. A. Pople, J. Chem. Phys. **56**, 2257 (1972).
[38] V. A. Rassolov, J. A. Pople, M. A. Ratner, and T. L. Windus, J. Chem. Phys. **109**, 1223 (1998).
[39] M. Kaupp, P. Schleyer, H. Stoll, and H. Preuss, J. Am. Chem. Soc. **113**, 6012 (1991).
[40] M. J. Frisch, G. W. Trucks, H. B. Schlegel *et al.*, GAUSSIAN 03, revision B05, Gaussian, Inc., Pittsburgh, PA, 2003.
[41] DALTON, a molecular electronic structure program, release 2.0, 2005 (see http://www.kjemi.uio.no/software/dalton/dalton.html).
[42] T. Yanai, D. P. Tew, and N. C. Handy, Chem. Phys. Lett. **393**, 51 (2004).
[43] M. J. G. Peach, T. Helgaker, P. Salek, T. W. Keal, O. B. Lutnæs, D. J. Tozer, and N. C. Handy, Phys. Chem. Chem. Phys. **8**, 558 (2006).
[44] A. J. Sadlej, Collect. Czech. Chem. Commun. **53**, 1995 (1988).
[45] D. Shelton and J. Rice, Chem. Rev. (Washington, D.C.) **94**, 3 (1994).
[46] S. A. C. McDowell, R. D. Amos, and N. C. Handy, Chem. Phys. Lett. **235**, 1 (1995).
[47] A. Dreuw and M. Head-Gordon, J. Am. Chem. Soc. **126**, 4007 (2004).

Paper II

II

Role of noncollinear magnetization for the first-order electric-dipole hyperpolarizability at the four-component Kohn–Sham density functional theory level

Radovan Bast
Trond Saue
Johan Henriksson
Patrick Norman

In manuscript

THE JOURNAL OF CHEMICAL PHYSICS **128**, 024105 (2008)

Quadratic response functions in the relativistic four-component Kohn-Sham approximation

Johan Henriksson
Department of Physics, Chemistry and Biology, Linköping University, SE-581 83 Linköping, Sweden

Trond Saue
Institut de Chimie, UMR 7177 CNRS et Université Louis Pasteur, 4 rue Blaise Pascal, F-67000 Strasbourg, France

Patrick Norman[a)]
Department of Physics, Chemistry and Biology, Linköping University, SE-581 83 Linköping, Sweden

(Received 5 October 2007; accepted 31 October 2007; published online 10 January 2008)

A formulation and implementation of the quadratic response function in the adiabatic four-component Kohn-Sham approximation is presented. The noninteracting reference state is time-reversal symmetric and formed from Kramers pair spinors, and the energy density is gradient corrected. Example calculations are presented for the optical properties of disubstituted halobenzenes in their *meta* and *ortho* conformations. It is demonstrated that correlation and relativistic effects are not additive, and it is shown that relativity alone reduces the $\mu\bar{\beta}$-response signal by 62% and 75% for *meta*- and *ortho*-bromobenzene, respectively, and enhances the same response by 17% and 21% for *meta*- and *ortho*-iodobenzene, respectively. Of the employed functionals, CAM-B3LYP shows the best performance and gives hyperpolarizabilities β distinctly different from B3LYP. © *2008 American Institute of Physics*. [DOI: 10.1063/1.2816709]

I. INTRODUCTION

In the presence of external (or internal) perturbing electromagnetic fields, the molecular polarization (or magnetization) can be expressed as a Taylor series in terms of the field strengths and the coupling parameters relate to spectroscopic properties (see, for instance, the book by Boyd).[1] Over the past 20 years, increasingly accurate and efficient computational methods have been developed to determine the linear as well as nonlinear molecular response parameters and, today, theoretical calculations are routinely used for the interpretation of experimental spectra as well as for material functionalization and optimization. If we are concerned with the correction to the molecular polarization that depends quadratically on the perturbing electric-field strengths, we note fundamental nonlinear optical processes, such as the second-harmonic generation and the electro-optical Pockels effect, and an important device such as the optical parametric oscillator. Moreover, static magnetic fields can be used to induce birefringences in nonchiral systems and, in this context, the quadratic response parameters (or *quadratic response functions*) are pertinent to spectroscopies such as magnetic circular dichroism and the Faraday effect.

In nonrelativistic quantum chemistry, quadratic response functions have been formulated and implemented at the electron uncorrelated level in the so-called time-dependent Hartree-Fock (HF) approximation[2–6]—this approximation is sometimes also referred to as the time-dependent coupled perturbed Hartree-Fock level or the random phase approximation—as well as at the electron correlated level employing second-order Møller-Plesset,[7] multiconfiguration self-consistent field (MCSCF),[2,6] and coupled cluster[8–10] reference states. More recently, the quadratic response function has also been formulated in the second-order polarization propagator approach[11] and formulated and implemented in Kohn-Sham density functional theory (DFT).[12,13] Successful use of these computational techniques has been demonstrated in numerous publications in the literature and, furthermore, it has been shown that a residue analysis of the response functions at the electronic transition frequencies of the system enables the calculation of observables in absorption spectroscopies and properties of electronically excited states.[2] At small frequency detunings of the perturbing fields, however, one must be cautious since the dispersion of the response functions is severely overestimated in this region due to the divergences at resonances. This issue has been considered in a series of publications by Norman *et al.*, and a *resonance convergent* formulation of response theory up to second order has been proposed and implemented at the HF, MCSCF, and DFT levels of theory.[14] It stands clear that, in the nonrelativistic realm, there exist sophisticated and highly accurate methodologies and program implementations for the determination of the linear and nonlinear responses in the electronic density to time-dependent electromagnetic field perturbations.

In photonics, it is well-known that the use of organometallic compounds can give unprecedented performance in certain applications,[15] but it is clear that, from a theoretical perspective, the inclusion of one or several heavy atoms calls for the treatment of relativistic effects in one way or another. It is possible to consider these effects by perturbation theory and, in the nonrelativistic framework, to add relativistic cor-

[a)]Electronic mail: panor@ifm.liu.se.

rections to the perturbation operator that describes the coupling to the external electromagnetic fields. This approach has been adopted to determine, e.g., phosphorescence,[16,17] electron spin resonance,[18] and nuclear magnetic resonance parameters[19] but, although these calculations employ quadratic response functions, they are all examples of second-order molecular properties since one of the perturbation operators in the response functions refers to an intrinsic field. In order to address a third-order molecular property in a relativistic-perturbational approach, one would need to evaluate a cubic response function which is computationally more complex, and we are not aware of such work. Apart from the increased computational complexity, a relativistic-perturbational approach is also limited by the fact that it is not applicable when relativistic effects are large and, therefore, must be included in the zeroth-order Hamiltonian.

There exist a number of ways to include relativistic effects in the zeroth-order molecular Hamiltonian. One can replace the core electron densities by effective potentials and include only the valence electrons in the parametrization of the wave function.[20] The parameters of the effective core potentials (ECPs) may be optimized against accurate relativistic atomic densities and later used in regular nonrelativistic calculations. The ECP approach indirectly accounts for scalar relativistic as well as spin-orbit effects in the atomic cores, and it can be applied to all elements of the Periodic Table while providing a reasonable accuracy (see Refs. 21–23 for evaluations of this method for third-order molecular properties). The obvious limitation is the neglect of direct (rather than indirect via the core potential) relativistic effects in the valence electron density. The severity of this approximation varies strongly for different molecular properties; not only does it vary with respect to the order of the molecular property but it also varies substantially for different properties of the same order. The most striking example when spin-orbit effects in the valence electron density are of prominent importance in the calculation of a quadratic response function is given by the two-photon absorption spectra (which relate to a first-order residue of the quadratic response function). It was demonstrated by Henriksson *et al.*[24] that even for a light element such as neon, the inclusion of spin-orbit interactions is necessary to obtain a qualitatively correct two-photon absorption spectrum.

At the all-electron level of theory, spin-free scalar relativistic corrections may be added to the one-electron Hamiltonian and, with the neglect of the picture change in the perturbation operators, response properties can be determined without further modifications of the nonrelativistic code. In this way, the hyperpolarizabilities of a series of group IIb sulfides were determined[25] in the spin-averaged Douglas-Kroll approximation, as introduced by Hess,[26,27] and the same approach has later been benchmarked against four-component calculations and then showing significant discrepancies for the hyperpolarizabilities of iodine and tellurium hydrides.[21] Full inclusion of scalar relativistic and spin-orbit effects in the calculation of third-order molecular properties was accomplished with the implementation of the quadratic response function (and its first- and second-order residues) in the time-dependent four-component Hartree-Fock approximation.[24,28,29] While accurate with respect to relativistic effects, it is expected that the applicability of this method is severely limited due to the large effects of electron correlation on nonlinear response properties and since it is inappropriate to treat relativity and electron correlation separately. In the present work, we therefore develop and implement the quadratic response function in the time-dependent four-component Kohn-Sham DFT approximation. Our work should be seen as an extension of the previous mentioned work in the HF approximation[24,28,29] as well as the work on the linear response function in the DFT approximation.[30]

In Sec. II A, we give a brief review of the four-component Kohn-Sham approximation and the derivation of the quadratic response function but, since these general aspects are largely covered in our previous work,[29,30] we focus primarily on a presentation of the details of the implementation that are unique to the extension made here (see Sec. II B). In Sec. III, we illustrate our implementation with an example calculation of the first-order electric-dipole hyperpolarizability for dibromo- and di-iodo-substituted benzene using a set of standard density functionals. We emphasize that although the implementation is completely general, we here present results for nonoscillating external perturbations which require functionals of the charge density only. For dynamic properties, we would like to perform a detailed investigation of also adding the induced noncollinear magnetization as a functional variable, and this work is in progress.

II. THEORY AND METHODOLOGY

A. Time-dependent four-component Kohn-Sham approximation

In the time-dependent four-component Kohn-Sham DFT approximation, the noninteracting reference system is described by a determinant of spinors $\phi_p(\mathbf{r})$. The time-reversal symmetric reference state of the isolated system $|0_s\rangle$ is variationally optimized with the use of an electronic Hamiltonian for the interacting system in which the kinetic energy is given by the free-particle Dirac Hamiltonian and the electron-electron repulsion is approximated by the instantaneous Coulomb interaction. This approximate form of the two-electron part of the relativistic Hamiltonian is improved on by the inclusion of the Gaunt term, or the full Breit interaction, but the introduction of current-current interactions in DFT requires a general consideration before introduced here.[31] Time-reversal symmetry of $|0_s\rangle$ is enforced by the occupation of Kramers pairs of spinors (corresponding to the closed-shell state in a nonrelativistic theory)—a pair of spinors are related by the time-reversal operator,

$$\Phi_{\bar{p}}(\mathbf{r}) = \hat{\mathcal{K}}\phi_p(\mathbf{r}), \quad \hat{\mathcal{K}} = \begin{bmatrix} 0_2 & -\mathbf{I}_2 \\ \mathbf{I}_2 & 0_2 \end{bmatrix} \hat{\mathcal{K}}_0, \tag{1}$$

where $\hat{\mathcal{K}}_0$ denotes the complex conjugation operator. The eigenvalues of the spinors are divided into two sets that are separated by *circa* twice the electron rest energy, and spinors corresponding to the upper and lower sets are sometimes referred to as electronic and positronic orbitals, respectively (although they all represent electron wave functions). The

reference state includes only electronic orbitals and is optimized in a minmax sense.[32]

When subjected to an external time-dependent electromagnetic field, the reference state becomes time dependent in a way that is not described by a trivial phase factor but involves electronic transitions to virtual orbitals. We parametrize this time dependence in a nonredundant and unitary way as follows:[2,31]

$$|\tilde{0}_s(t)\rangle = \exp[-\hat{\kappa}(t)]|0_s\rangle, \quad \hat{\kappa}(t) = \kappa_{ai}\hat{a}_a^\dagger\hat{a}_i - \kappa_{ai}^*\hat{a}_i^\dagger\hat{a}_a. \tag{2}$$

Here and in the following, we have made use of the Einstein summation convention for repeated indices and $a,b,\ldots,i,j,\ldots$, and $p,q,\ldots$ are indices of virtual, occupied, and general molecular orbitals, respectively. In general, the summation over virtual orbitals in Eq. (2) includes the positronic orbitals and the corresponding electron transfer amplitudes are at times denoted by κ_{ai}^- (to be distinguished from rotations among electronic orbitals with amplitudes κ_{ai}^+). In calculations of electric-field induced valence properties, such as the electric-dipole hyperpolarizability, the effect of redressing of the electronic states due to the inclusion of the κ_{ai}^- parameters in the propagator is small and can be ignored with the benefit of memory savings.[23]

For weak, periodic external fields, we can use the quasienergy formalism to determine the time dependence of the κ parameters[33]—a technique which was also used for the derivation and implementation of the linear response function at this level of theory[30] (see, however, Ref. 34 for a discussion about the validity of this approach). The relevant time-averaged Kohn-Sham quasienergy functional can be written as

$$Q[\rho] = T_s[\rho] + V[\rho] + J[\rho] + Q_{xc}[\rho] + S_s[\rho], \tag{3}$$

where the time-dependent electron density is introduced as ρ and depends implicitly on the κ parameters. The response functions are defined as derivatives of the quasienergy with respect to the Fourier amplitudes of the external electromagnetic field, and the third-order response, or the quadratic response function, is given by

$$\langle\langle \hat{A};\hat{B},\hat{C}\rangle\rangle_{\omega_B,\omega_C} = \left.\frac{d^3Q}{d\varepsilon_A(\omega_A)d\varepsilon_B(\omega_B)d\varepsilon_C(\omega_C)}\right|_{\varepsilon=0}. \tag{4}$$

In evaluating this derivative, we note that the sum of terms in Eq. (3) excluding Q_{xc} corresponds formally to Hartree-Fock theory without exchange interaction. We can, therefore, benefit from the implementation of the quadratic response function reported in Ref. 29 and use it with a mere turnoff of the exchange interaction (or partial turnoff for hybrid functionals) together with the addition of the contribution from Q_{xc}. We will adopt the adiabatic approximation and employ the time-dependent exchange-correlation functional as a substitute for Q_{xc},

$$Q_{xc}[\rho] \to E_{xc}[\rho] = \int e_{xc}(\rho,\zeta)d\tau. \tag{5}$$

The energy density is here assumed to be a function of ρ and the square norm of the electron density gradient $\zeta=\nabla\rho\cdot\nabla\rho$, and a time averaging is implied here as well. The time averaging will impose that the response function [Eq. (4)] is nonzero only when $\omega_A=-(\omega_B+\omega_C)$. In the next section, we will present the detailed expressions needed for the implementation of the part in Eq. (4) that is due to E_{xc}.

B. Implementation of the exchange-correlation contribution to the quadratic response function

In the evaluation of the third-order derivative of E_{xc} with respect to the amplitudes of the external fields, we will use chain rule differentiation of the energy density $e(\rho,\zeta)$. We will view the electron density as dependent on the κ parameters and determine the response of the latter to the external perturbation from the variational condition $\delta Q[\rho]=0$. Since the $2n+1$ rule applies in the present case, it will be sufficient to determine the first-order response in κ with respect to $\varepsilon(\omega)$ in order to determine the quadratic response function. We note that the details and code implementation concerned with the determination of this linear response have already been considered in Ref. 30. The structure of the implementation of the quadratic response function at the Hartree-Fock level is such that first, the formation of a generalized electronic gradient

$$\left.\frac{\partial}{\partial\kappa_{ai}}\frac{d^2E_{xc}}{d\varepsilon_B d\varepsilon_C}\right|_{\varepsilon=0} \tag{6}$$

is made and, thereafter, this gradient is contracted with the response of the κ_{ai} parameters with respect to the external field.[29] In order to comply with this structure, we therefore seek an explicit expression for the quantity in Eq. (6).

This exchange-correlation contribution will be added to the generalized gradient as due to the Coulomb interaction and which is denoted as $E^{[3]}N^BN^C$ in Ref. 29. Let us now turn to the differentiation of E_{xc} and first consider the partial derivatives that will appear. In doing so, we will make use of the fact that $\varepsilon\to 0$ implies that $\kappa\to 0$ and vice versa and, although partial differentiation is to be made independently for κ_{ai} and κ_{ai}^*, we restrict the presentation to include only one of them.

With the use of the density operator,

$$\hat{\rho} = \Omega_{pq}\hat{a}_p^\dagger\hat{a}_q, \quad \Omega_{pq} = \phi_p^\dagger(\mathbf{r})\phi_q(\mathbf{r}), \tag{7}$$

the electron density can be written as

$$\rho(\mathbf{r}) = \langle\tilde{0}_s|\hat{\rho}|\tilde{0}_s\rangle = \Omega_{pq}\langle 0_s|e^{\hat{\kappa}}\hat{a}_p^\dagger\hat{a}_q e^{-\hat{\kappa}}|0_s\rangle. \tag{8}$$

Expanding the density matrix elements with use of the Baker-Campbell-Hausdorff expansion yields

$$\rho = \sum_{n=0}^{\infty}\rho^{(n)}, \quad \rho^{(n)} = \frac{\Omega_{pq}}{n!}\langle 0_s|\hat{\boldsymbol{\kappa}}^n\hat{a}_p^\dagger\hat{a}_q|0_s\rangle, \tag{9}$$

where the action of the superoperator $\hat{\boldsymbol{\kappa}}$ is the formation of a commutator according to $\hat{\boldsymbol{\kappa}}\hat{A}=[\hat{\kappa},\hat{A}]$. The differentiation of the density with respect to the external fields gives

$$\rho^{ABC\cdots} := \left.\frac{\partial^n\rho}{\partial\varepsilon_A\partial\varepsilon_B\partial\varepsilon_C\cdots}\right|_{\varepsilon=0} = \Omega_{ai}^{BC\cdots}\frac{\partial\kappa_{ai}}{\partial\varepsilon_A}, \tag{10}$$

where we have introduced

$$\Omega_{ai}^{BC\cdots} := \frac{\partial^n \rho^{(n)}}{\partial\kappa_{ai}\partial\kappa_{bj}\partial\kappa_{ck}\cdots}\frac{\partial\kappa_{bj}}{\partial\varepsilon_B}\frac{\partial\kappa_{ck}}{\partial\varepsilon_C}\cdots . \tag{11}$$

In order to account for gradient-corrected density functionals, we also introduce the following partial derivatives of ζ with respect to the external field:

$$\zeta^B := \left.\frac{\partial\zeta}{\partial\varepsilon_B}\right|_{\varepsilon=0} = 2\nabla\rho\cdot\nabla\rho^B, \tag{12}$$

$$\zeta^{BC} := \left.\frac{\partial^2\zeta}{\partial\varepsilon_B\partial\varepsilon_C}\right|_{\varepsilon=0} = 2(\nabla\rho\cdot\nabla\rho^{BC} + \nabla\rho^B\cdot\nabla\rho^C). \tag{13}$$

The numerical grid-integration kernel in the program assumes the integrand to be written on the form

$$s\Omega_{pq} + \mathbf{v}\cdot\nabla\Omega_{pq},$$

where the scalar s and vectorial $\mathbf{v}$ functions as well as the atomic orbital density matrix corresponding to Ω_{pq} are to be specified for a given property integration. Let us illustrate how this works for the electronic gradient,

$$\left.\frac{\partial E_{\mathrm{xc}}}{\partial\overset{*}{\kappa}_{ai}}\right|_{\kappa=0} = \int\left[\frac{\partial e_{\mathrm{xc}}}{\partial\rho}\left.\frac{\partial\rho}{\partial\overset{*}{\kappa}_{ai}}\right|_{\kappa=0} + \frac{\partial e_{\mathrm{xc}}}{\partial\zeta}\left.\frac{\partial\zeta}{\partial\overset{*}{\kappa}_{ai}}\right|_{\kappa=0}\right]d\tau = -\int f_{\mathrm{xc};ai}\,d\tau, \tag{14}$$

in which appears the exchange-correlation part of the Kohn-Sham matrix,

$$f_{\mathrm{xc};pq} = s_f\Omega_{pq} + \mathbf{v}_f\cdot\nabla\Omega_{pq}, \qquad s_f = \frac{\partial e_{\mathrm{xc}}}{\partial\rho}, \quad \mathbf{v}_f = \frac{1}{|\nabla\rho|}\frac{\partial e_{\mathrm{xc}}}{\partial|\nabla\rho|}\nabla\rho. \tag{15}$$

Continuing to linear response, we get

$$\frac{\partial}{\partial\overset{*}{\kappa}_{ai}}\left.\frac{\partial E_{\mathrm{xc}}}{\partial\varepsilon_B}\right|_{\varepsilon=0} = -\int(f_{\mathrm{xc};ai}^B + g_{\mathrm{xc};ai}^{[B]})d\tau, \tag{16}$$

where the integrand consists of the exchange-correlation part of the one-index transformed Kohn-Sham matrix,

$$f_{\mathrm{xc};pq}^B = s_f\Omega_{pq}^B + \mathbf{v}_f\cdot\nabla\Omega_{pq}^B, \tag{17}$$

and a remainder that equals to

$$g_{\mathrm{xc};pq}^{[B]} = s_g\Omega_{pq} + \mathbf{v}_g\cdot\nabla\Omega_{pq},$$

$$s_g^{[B]} = \frac{\partial^2 e_{\mathrm{xc}}}{\partial\rho^2}\rho^B + \frac{\partial^2 e_{\mathrm{xc}}}{\partial\rho\partial\zeta}\cdot 2(\nabla\rho\cdot\nabla\rho^B),$$

$$\mathbf{v}_g^{[B]} = \left[\frac{\partial^2 e_{\mathrm{xc}}}{\partial\rho\partial\zeta}\rho^B + \frac{\partial^2 e_{\mathrm{xc}}}{\partial\zeta^2}\cdot 2(\nabla\rho\cdot\nabla\rho^B)\right]\cdot 2\nabla\rho + \frac{\partial e_{\mathrm{xc}}}{\partial\zeta}\cdot 2\nabla\rho^B. \tag{18}$$

We will reach our desired expression for the quadratic response by performing a differentiation of Eq. (16) with respect to the external field. We collect the final result of this derivation in the form

$$\frac{\partial}{\partial\overset{*}{\kappa}_{ai}}\left.\frac{d^2 E_{\mathrm{xc}}}{d\varepsilon_B d\varepsilon_C}\right|_{\varepsilon=0} = -\int(f_{\mathrm{xc};ai}^{BC} + g_{\mathrm{xc};ai}^{[C]B} + g_{\mathrm{xc};ai}^{[B]C} + h_{\mathrm{xc};ai}^{[BC]})d\tau, \tag{19}$$

where we recognize the doubly one-index transformed exchange-correlation part of the Kohn-Sham matrix $f_{\mathrm{xc};pq}^{BC}$ as well as matrices $g_{\mathrm{xc};ai}^{[C]B}$ and $g_{\mathrm{xc};ai}^{[B]C}$ which are one-index transformed versions of Eq. (18) with respect to B and C, respectively. The remainder is collected into

$$h_{\mathrm{xc};pq}^{[BC]} = s_h\Omega_{pq} + \mathbf{v}_h\cdot\nabla\Omega_{pq},$$

$$s_h = \sum\mathcal{P}_{B,C}\left\{\frac{\partial^3 e_{\mathrm{xc}}}{\partial\rho^3}\rho^B\rho^C + 2\frac{\partial^3 e_{\mathrm{xc}}}{\partial\rho^2\partial\zeta}\rho^B\cdot 2(\nabla\rho\cdot\nabla\rho^C) + \frac{\partial^3 e_{\mathrm{xc}}}{\partial\rho\partial\zeta^2}\cdot 2(\nabla\rho\cdot\nabla\rho^B)\cdot 2(\nabla\rho\cdot\nabla\rho^C) + \frac{\partial^2 e_{\mathrm{xc}}}{\partial\rho^2}\rho^{BC} + \frac{\partial^2 e_{\mathrm{xc}}}{\partial\rho\partial\zeta}\cdot 2[(\nabla\rho\cdot\nabla\rho^{BC}) + (\nabla\rho^B\cdot\nabla\rho^C)]\right\}, \tag{20}$$

$$\mathbf{v}_h = \sum\mathcal{P}_{B,C}\left\{\left[\frac{\partial^3 e_{\mathrm{xc}}}{\partial\zeta^3}\cdot 2(\nabla\rho\cdot\nabla\rho^B)\cdot 2(\nabla\rho\cdot\nabla\rho^C) + 2\frac{\partial^3 e_{\mathrm{xc}}}{\partial\rho\partial\zeta^2}\rho^B\cdot 2(\nabla\rho\cdot\nabla\rho^C) + \frac{\partial^3 e_{\mathrm{xc}}}{\partial\rho^2\partial\zeta}\rho^B\rho^C + \frac{\partial^2 e_{\mathrm{xc}}}{\partial\rho\partial\zeta}\rho^{BC} + \frac{\partial^2 e_{\mathrm{xc}}}{\partial\zeta^2}\cdot 2[(\nabla\rho\cdot\nabla\rho^{BC}) + (\nabla\rho^B\cdot\nabla\rho^C)]\right]\cdot 2\nabla\rho + \left[\frac{\partial^2 e_{\mathrm{xc}}}{\partial\rho\partial\zeta}\rho^C + \frac{\partial^2 e_{\mathrm{xc}}}{\partial\zeta^2}\cdot 2(\nabla\rho\cdot\nabla\rho^C)\right]\cdot 4\nabla\rho^B + \frac{\partial e_{\mathrm{xc}}}{\partial\zeta}\cdot 2\nabla\rho^{BC}\right\},$$

where the operator $\Sigma\mathcal{P}_{B,C}$ denotes the sum over permutations between B and C. An implementation of Eq. (19) has been added to the DIRAC program[35] and below, we will present an example calculation of the electric-dipole hyperpolarizability which corresponds to a quadratic response function [Eq. (4)] evaluated for electric-dipole operators. The implementation is general in the sense that it merely assumes the perturbations to be due to one-electron operators and our work is, therefore, in principle, applicable to a series of electromagnetic properties. However, the introduction of a magnetic perturbation breaks the time-reversal symmetry of the system and requires the consideration of spin polarization in the formalism. In fact, even the application of time-dependent electric fields will induce electronic currents and thereby magnetic fields, so also the evaluation of dynamic polarizabilities should take spin polarization into account. We will return to this topic in a future work.

III. EXAMPLE CALCULATIONS

A. Computational details

All calculations in the present work were performed for molecular structures that were optimized at the one-component Kohn-Sham DFT level of theory using the hybrid B3LYP exchange-correlation functional;[36] for H, C, and Br,

the 6-31G* basis set was used,[37,38] and for iodine, the Stuttgart ECP was used.[39] Structure optimizations were performed in the C_{2v} point group with the GAUSSIAN program.[40] The molecules are placed with the z axis as principle axis and in the yz plane with the heavy atoms along the negative z direction.

The all-electron property calculations were performed with a locally modified version of the DIRAC program,[35] and those where an ECP was used for Br or I were performed with a version of the DALTON program[41] to which an implementation of the Coulomb attenuated B3LYP (Ref. 42) (CAM-B3LYP) has been added.[43] The property calculations based on single determinant reference states (all-electron as well as ECP based) were performed with fully uncontracted basis sets that are based on the exponents from Sadlej's polarization basis set[44] with further addition of polarization and diffuse functions. The basis sets were augmented using the formula

$$\zeta_{N+j} = \left[\frac{\zeta_N}{\zeta_{N-1}}\right]^j \zeta_N, \quad j \in [1, N_{\text{aug}}], \tag{21}$$

where N_{aug} is the number of augmentation functions added and ζ_N and ζ_{N-1} refer to the two most diffuse exponents in the original basis sets. The only exception to this rule is the f shell of the iodine basis set, which was not augmented. To the basis set of bromine, we added four f functions based on the four most diffuse p exponents in the original basis set. The sizes of the singly augmented large component basis sets used in the property calculations were $[7s5p]$, $[11s7p5d]$, $[16s13p10d4f]$, and $[20s16p13d4f]$ for H, C, Br, and I, respectively, and the small-component basis functions were generated from those of the large component with the use of the restricted kinetic-balance condition. In all four-component calculations, we have ignored the interactions between the small component densities, i.e., the $(SS|SS)$ integrals. This approximation has virtually no influence on the presented results, as demonstrated in Ref. 23, and will not be further discussed here. All DFT functionals were employed self-consistently and with their proper derivatives to the required orders in the perturbations.

For comparison, wave function correlated results were obtained at the coupled cluster level with inclusion of single and double electron excited configurations (CCSD). For these calculations, we adopted the contracted Sadlej basis set[44] for hydrogen and carbon but augmented with the same diffuse functions as described above. For bromine and iodine, we employed the valence basis set of the Stuttgart ECPs (Ref. 39) but augmented and polarized using the functions from the Sadlej basis set and Eq. (21). The sizes of the heavy atom basis sets in the CCSD calculations were $[6s6p5d4f]/[4s4p3d2f]$ (bromine) and $[6s6p8d2f]/[4s4p3d1f]$ (iodine).

B. Results and discussion

With a molecular dipole moment aligned with the z axis, the relevant experimental observable for second-harmonic generation is $\mu\bar{\beta}$,[45] where

$$\bar{\beta}(-2\omega;\omega,\omega) = \frac{1}{5}\sum_{\alpha=x,y,z}(\beta_{z\alpha\alpha} + 2\beta_{\alpha z\alpha}). \tag{22}$$

In previous studies, we have shown that relativistic effects in heavy atom substituted π-conjugated systems are pronounced for the dipole moment as well as the first-order hyperpolarizability (but not for the linear polarizability);[22,23] for bromobenzene, the effects are predominantly scalar relativistic in nature but for iodobenzene, scalar relativistic and spin-orbit effects are about equally important.[23] Whereas changes due to relativity in the dipole moment can be attributed to changes in the chemical bond polarities, the effects on the hyperpolarizabilities are not as easily interpreted. The sum-over-states expression for β, which reads as

$$\beta_{\alpha\beta\gamma}(-\omega_\sigma;\omega_1,\omega_2) = \hbar^{-2}\sum \mathcal{P}_{-\sigma,1,2}\sum_{k,l}{}' \frac{\langle 0|\hat{\mu}_\alpha|k\rangle\langle k|\bar{\hat{\mu}}_\beta|l\rangle\langle l|\hat{\mu}_\gamma|0\rangle}{(\omega_k-\omega_\sigma)(\omega_l-\omega_2)}, \tag{23}$$

reveals an intricate dependence of the hyperpolarizability on interexcited state transition moments and excited-to-ground state dipole moment differences, in addition to a dependence on the linear absorption spectrum via the ground-to-excited state transition dipole moments and excitation energies. The permutation operator introduced in Eq. (23) permutes the pairs of dipole moment operators and optical frequencies $(\hat{\mu}_\alpha,-\omega_\sigma)$, $(\hat{\mu}_\beta,\omega_1)$, and $(\hat{\mu}_\gamma,\omega_2)$, and $\bar{\hat{\mu}}$ denotes the electric-dipole fluctuation operator. One thing that becomes clear from the sum-over-states expression is the separation between scalar relativistic and spin-orbit effects, since the latter can be attributed to the coupling between states in the singlet and triplet manifolds. The nonrelativistic and relativistic linear absorption spectra presented in Ref. 23 show significant spin-forbidden absorption only for the iodobenzenes, and scalar relativistic and spin-orbit effects on β are also of comparable magnitude in this case, whereas the spin-orbit effects are small on the same property for the bromobenzenes.

The same argumentation can be made for the linear polarizability. In fact, α depends only on the observables in the linear absorption spectrum, namely, transition energies and intensities. The absence of relativistic effects that are seen in Tables I and II for this property is, therefore, puzzling but has been previously noted also for the thiophene homologs which serve as important building blocks in optical materials.[22]

In the present work, we focus at a formulation of the quadratic response function at the electron correlated four-component level of theory. We give here a presentation of the response function which is quite different from the sum-over-states expression in Eq. (23) but is rather seen as energy derivatives. Since the correlation energy depends on the electron density, its value per electron will basically be larger, the heavier the atom. What makes property calculations at the Hartree-Fock level at all reasonable for heavy atoms are the facts that the molecular property is a measure of the energy difference with respect to external fields and that the induced fluctuations in the core electron densities are very small—in the valence region, where density fluctuations are larger, the

TABLE I. Optical properties for disubstituted bromobenzenes at the Hartree-Fock, Kohn-Sham, and post-HF levels of theory. Different exchange-correlation functionals are considered for the inclusion of electron correlation effects. All quantities are given in a.u.

Method		μ_z	α_{xx}	α_{yy}	α_{zz}	β_{zxx}	β_{zyy}	β_{zzz}
				meta-dibromobenzene				
LDA	NR	0.6149	72.79	166.1	124.2	26.13	−168.8	32.79
	ECP	0.5728	73.93	168.2	125.5	32.10	−167.4	44.76
	4C	0.5903	73.00	166.5	124.5	29.04	−163.4	41.00
BLYP	NR	0.6105	73.62	167.2	125.1	29.96	−155.6	44.22
	ECP	0.5902	73.60	167.0	125.0	30.82	−147.1	47.97
	4C	0.5864	73.85	167.6	125.3	33.13	−149.8	53.01
B3LYP	NR	0.6435	71.86	161.2	121.7	21.16	−117.7	36.31
	ECP	0.6203	72.01	161.4	121.8	22.92	−112.6	40.95
	4C	0.6186	72.03	161.5	121.9	23.63	−112.6	43.41
CAM-B3LYP	NR	0.6626	70.85	156.5	119.4	17.76	−88.99	34.92
	ECP	0.6333	71.22	157.1	119.7	20.07	−85.60	40.32
	4C	0.6361	71.00	156.8	119.6	19.81	−84.30	41.08
HF	NR	0.7482	69.78	150.5	115.8	3.57	−48.97	27.85
	ECP	0.7291	69.9	150.8	116.0	4.91	−47.30	31.27
	4C	0.7218	69.81	150.8	115.9	4.55	−45.50	31.64
CCSD	ECP	0.6344	72.18	156.6	120.3	12.87	−82.70	33.06
				ortho-dibromobenzene				
LDA	NR	0.8925	71.93	131.4	150.9	41.73	−62.10	−164.4
	ECP	0.8208	73.00	132.9	152.3	50.83	−55.44	−152.1
	4C	0.8513	72.14	131.6	151.0	46.44	−56.28	−152.8
BLYP	NR	0.8814	72.71	132.1	151.6	47.09	−52.58	−148.8
	ECP	0.8479	72.70	132.0	151.5	48.14	−46.90	−138.6
	4C	0.8409	72.94	132.4	151.9	52.40	−46.22	−136.6
B3LYP	NR	0.9395	71.01	128.3	147.1	33.37	−39.78	−113.5
	ECP	0.9008	71.16	128.4	147.2	35.71	−35.25	−105.3
	4C	0.8977	71.18	128.5	147.2	37.29	−34.45	−103.3
CAM-B3LYP	NR	0.9739	70.03	125.5	143.5	27.66	−28.81	−80.26
	ECP	0.9248	70.37	125.9	143.9	30.96	−24.62	−72.58
	4C	0.9296	70.17	125.7	143.7	31.01	−23.97	−71.05
HF	NR	1.1147	69.10	121.4	138.8	6.72	−9.99	−35.62
	ECP	1.0826	69.21	121.6	138.9	8.45	−7.56	−31.41
	4C	1.0709	69.13	121.5	138.9	8.30	−6.61	−29.79
CCSD	ECP	0.9310	71.34	126.5	144.1	20.50	−28.65	−82.57

effects of electron correlation are smaller. As a rule of thumb for the polarizability of molecules containing first- and second-row elements, the isotropic value is typically underestimated by some 5% at the Hartree-Fock level of theory, whereas anisotropies suffer from larger errors.[46] For the hyperpolarizabilities, on the other hand, the effects of electron correlation are known to be both large and unsystematic.

In Tables I and II, we present the optical properties of disubstituted bromobenzene and iodobenzene, respectively, in their *meta* and *ortho* conformations. We employ a series of four standard density functionals in the correlated four-component calculations, namely, local-density approximation (LDA), BLYP, B3LYP, and CAM-B3LYP, and the ordering of functionals in the tables reflects the consensus of increasing accuracy as due to gradient and exact exchange corrections. An apparent consequence of the use of the more sophisticated density functionals is the improved quality of the orbital energies and, since the difference in orbital energies between virtual and occupied orbitals appears on the diagonal of the electronic Hessian, it will correspond to improved excitation energies in the response function approach as well. In Ref. 47, it was also well illustrated how the inclusion of exact exchange in the density functional affects linear response calculation of excitation energies. It is the exact exchange that provides the Coulomb attraction between the hole and the electron in these calculations, and the more spatially separated the hole and electron orbitals are, the greater the need for exact exchange in the functional is. The present systems are by no means extreme charge-transfer systems but, at the same time, it is clear that the halogen

TABLE II. Optical properties for disubstituted iodobenzenes at the Hartree-Fock, Kohn-Sham, and post-hF levels of theory. Different exchange-correlation functionals are considered for the inclusion of electron correlation effects. All quantities are given in a.u.

Method		μ_z	α_{xx}	α_{yy}	α_{zz}	β_{zxx}	β_{zyy}	β_{zzz}
				meta-di-iodobenzene				
LDA	NR	0.6337	94.24	214.0	149.1	85.17	−175.1	140.6
	ECP	0.5674	95.86	216.1	150.6	96.74	−166.0	167.0
	4C	0.5661	94.61	215.1	149.5	96.78	−151.2	171.4
BLYP	NR	0.6240	95.86	216.0	150.5	95.56	−150.4	166.4
	ECP	0.5885	95.16	214.3	149.7	96.71	−128.2	174.8
	4C	0.5575	96.32	217.4	151.1	108.7	−125.6	200.3
B3LYP	NR	0.6501	93.55	208.1	146.5	79.16	−88.74	151.1
	ECP	0.6076	93.30	207.4	146.2	82.61	−73.72	162.0
	4C	0.5806	93.79	209.9	146.9	89.19	−64.85	179.0
CAM-B3LYP	NR	0.6618	91.88	201.2	143.4	68.39	−37.66	141.1
	ECP	0.6057	92.17	201.6	143.7	73.46	−25.95	155.5
	4C	0.5867	91.99	202.2	143.7	76.96	−15.23	165.7
HF	NR	0.7537	91.23	196.1	140.5	56.17	12.08	140.0
	ECP	0.7074	91.14	196.5	140.5	59.36	22.27	150.5
	4C	0.6793	90.91	197.2	140.5	61.26	31.21	157.2
CCSD	ECP	0.5822	96.54	205.1	147.6	80.97	−46.26	180.7
				ortho-di-iodobenzene				
LDA	NR	0.8877	92.07	166.3	182.7	125.0	−42.42	−46.42
	ECP	0.7777	93.59	167.9	184.0	142.3	−26.39	−16.02
	4C	0.7766	92.45	166.6	182.9	143.9	−19.06	−2.32
BLYP	NR	0.8639	93.49	167.7	183.9	136.7	−24.59	−16.73
	ECP	0.8071	92.87	166.1	182.7	138.2	−8.59	5.99
	4C	0.7544	93.94	168.1	184.2	157.9	1.05	29.70
B3LYP	NR	0.9103	91.31	162.4	178.6	113.4	1.21	25.32
	ECP	0.8411	91.11	161.6	178.0	118.1	14.86	45.94
	4C	0.7962	91.57	162.7	178.8	129.7	25.04	67.06
CAM-B3LYP	NR	0.9336	89.74	158.1	174.1	97.05	22.97	66.22
	ECP	0.8415	90.03	158.2	174.2	104.6	36.07	86.91
	4C	0.8105	89.88	158.3	174.3	110.4	45.22	104.3
HF	NR	1.0740	89.19	154.3	170.2	78.37	53.66	123.4
	ECP	0.9973	89.13	154.2	170.1	82.94	65.23	139.0
	4C	0.9519	88.93	154.3	170.4	86.26	72.80	151.2
CCSD	ECP	0.8023	94.14	162.7	177.7	117.3	23.97	89.22

atoms will play the role of donors in excitations to the π^* orbitals. We, therefore, anticipate that the use of the CAM-B3LYP can have an impact on results, and we would argue that these results are the best ones at the four-component level of theory. We would also like to draw attention to the systematic decrease in α when comparing results obtained with the series of functionals BLYP, B3LYP, and CAM-B3LYP. This trend is directly coupled to an increasing portion of exact exchange and thereby increased excitation energies of the system.

When measured against the four-component CAM-B3LYP results, the correlation contributions to β_{zxx}, β_{zyy}, and β_{zzz} of *meta*-bromobenzene amount to 15.3, −38.8, and 9.4 a.u., respectively, and for *meta*-iodobenzene, the corresponding values are 15.7, −46.4, and 8.5 a.u. In both cases, there is thus a strong error cancellation for the Hartree-Fock values of the observable $\bar{\beta}$ since electron correlation lowers the value of the *zyy* component but increases the values of the other two components. This illustrates how unsystematic correlation effects can be for the first-order hyperpolarizability. On the other hand, we note that the correlation effects on the hyperpolarizabilities of the two *meta* systems are close in magnitude. That again indicates that it is the correlation energy in the valence region that matters for this property, and that this energy is almost the same in the two systems. If we make the same comparison for the two *ortho* systems, we see correlation contributions of 22.7, −17.4, and −41.3 a.u. for the three nonzero β components of bromobenzene and 24.1, −27.6, −46.9 a.u. for the three components of iodobenzene.

We have argued that the ordering of DFT results in the tables reflects the quality. In order to get a more objective measure of the performance of the various functionals, we have also determined the optical properties using a nonrelativistic wave function correlated approach in conjunction with the Stuttgart relativistic ECPs. Due to the computational cost associated with the CCSD method, we are forced to employ a reduced basis set and, given the fact that the basis set requirements are stronger in wave function than in density functional approaches, we cannot use the CCSD results as benchmarks. Furthermore, the lack of inclusion of relativistic effects in the valence region will make the results based on ECPs error prone for the iodobenzenes. For the β-tensor elements of bromobenzenes, the largest discrepancy between ECP and four-component results at the CAM-B3LYP level is as small as 1.5 a.u. (or 2%), whereas for the iodobenzenes, this error bar is 17.4 a.u. It is, therefore, reasonable to use the bromobenzene CCSD results for the evaluation of the various density functionals. For each individual β component of the bromobenzenes, the best agreement with the CCSD results is obtained with use of the CAM-B3LYP functional but, at the same time, it is clear that discrepancies between the correlated results can be as large as 10 a.u. (see the *zzz* component of *ortho*-bromobenzene).

The calculations of the hyperpolarizabilities of the halobenzenes amply demonstrate that electron correlation effects can be very large for this property. Of greater concern to the present work, however, is the fact that relativistic effects on the hyperpolarizability are substantial for the bromobenzenes and large for the iodobenzenes. The development of electron correlated propagator methods with proper inclusion of relativity is particular important since the two effects are not additive. Without exception for the β tensor, the relativistic effects at the correlated level of theory exceed those at the uncorrelated level of theory, e.g., the relativistic effects for β_{zxx}, β_{zyy}, and β_{zzz} at the CAM-B3LYP level amount to 13.3, 22.2, and 38.1 a.u., respectively, whereas at the Hartree-Fock level, the corresponding values are 7.9, 19.2, and 27.8 a.u. The relativistic corrections are without exception positive, thereby increasing the value of $\bar{\beta}$.

IV. CONCLUSIONS

A derivation and implementation of the quadratic response function at the four-component density functional level of theory has been presented. The adiabatic, Kramers-restricted Kohn-Sham approximation has been adopted with consideration made of gradient-corrected functionals. We exemplify the significance of this work with calculations of the optical properties of disubstituted halobenzenes and thereby illustrate internal heavy atom effects on the hyperpolarizabilities in π-conjugated systems. Our best results are obtained with the use of the Coulomb attenuated B3LYP functional,[42] which here provides notably different hyperpolarizability values from B3LYP. It is shown that correlation as well as relativistic effects on β are large for the systems under investigation. Relativity alone reduces the $\mu\bar{\beta}$-response signals by 62% and 75% for *meta*- and *ortho*-bromobenzene, respectively, and enhances the same response by 17% and 21% for *meta*- and *ortho*-iodobenzene, respectively (these values are based on the CAM-B3LYP results). The results in the present work also demonstrates the well-known fact that correlation and relativistic effects are not additive and that our work is called for.

ACKNOWLEDGMENTS

We acknowledge the use of computational resources at the National Supercomputer Centre (NSC) in Linköping, Sweden.

[1] R. W. Boyd, *Nonlinear Optics*, 2nd ed. (Academic, New York, 2003).
[2] J. Olsen and P. Jørgensen, J. Chem. Phys. **82**, 3235 (1985).
[3] H. Sekino and R. Bartlett, J. Chem. Phys. **85**, 976 (1986).
[4] S. Karna and M. Dupuis, J. Comput. Chem. **12**, 487 (1991).
[5] J. Rice, R. Amos, S. Colwell, N. Handy, and J. Sanz, J. Chem. Phys. **93**, 8828 (1990).
[6] H. Hettema, H. Jensen, P. Jørgensen, and J. Olsen, J. Chem. Phys. **97**, 1174 (1992).
[7] J. Rice and N. Handy, Int. J. Quantum Chem. **43**, 91 (1992).
[8] C. Hättig, O. Christiansen, H. Koch, and P. Jørgensen, Chem. Phys. Lett. **269**, 428 (1997).
[9] J. Gauss, O. Christiansen, and J. Stanton, Chem. Phys. Lett. **296**, 117 (1998).
[10] P. Rozyczko and R. Bartlett, J. Chem. Phys. **107**, 10823 (1997).
[11] J. Olsen, P. Jørgensen, T. Helgaker, and J. Oddershede, J. Phys. Chem. A **109**, 11618 (2005).
[12] S. van Gisbergen, J. Snijders, and E. Baerends, J. Chem. Phys. **109**, 10644 (1998); **111**, 6652(E) (1999).
[13] P. Salek, O. Vahtras, T. Helgaker, and H. Ågren, J. Chem. Phys. **117**, 9630 (2002).
[14] P. Norman, D. M. Bishop, H. J. Aa. Jensen, and J. Oddershede, J. Chem. Phys. **123**, 194103 (2005).
[15] D. Roberto, R. Ugo, E. Tessore, F. Lucenti, S. Quici, S. Vezza, P. Fantucci, I. Invernizzi, S. Bruni, I. Ledoux-Rak, and J. Zyss, Organometallics **21**, 161 (2002).
[16] O. Vahtras, H. Ågren, P. Jørgensen, H. J. Aa. Jensen, T. Helgaker, and J. Olsen, J. Chem. Phys. **97**, 9178 (1992).
[17] I. Tunell, Z. Rinkevicius, O. Vahtras, P. Salek, T. Helgaker, and H. Ågren, J. Chem. Phys. **119**, 11024 (2003).
[18] M. Engström, O. Vahtras, and H. Ågren, Chem. Phys. Lett. **328**, 483 (2000).
[19] P. Manninen, K. Ruud, P. Lantto, and J. Vaara, J. Chem. Phys. **122**, 114107 (2005).
[20] L. R. Kahn, P. Baybutt, and D. G. Truhlar, J. Chem. Phys. **65**, 3826 (1976).
[21] P. Norman, B. Schimmelpfennig, K. Ruud, H. J. Aa. Jensen, and H. Ågren, J. Chem. Phys. **116**, 6914 (2002).
[22] B. Jansik, B. Schimmelpfennig, P. Norman, H. Ågren, and K. Ohta, J. Mol. Struct.: THEOCHEM **633**, 237 (2003).
[23] J. Henriksson, U. Ekström, and P. Norman, J. Chem. Phys. **124**, 214311 (2006).
[24] J. Henriksson, P. Norman, and H. J. Aa. Jensen, J. Chem. Phys. **122**, 114106 (2005).
[25] S. Raptis, M. Papadopoulos, and A. Sadlej, J. Chem. Phys. **111**, 7904 (1999).
[26] M. Douglas and N. Kroll, Ann. Phys. (N.Y.) **82**, 89 (1974).
[27] G. Jansen and B. Hess, Phys. Rev. A **39**, 6016 (1989).
[28] E. Tellgren, J. Henriksson, and P. Norman, J. Chem. Phys. **126**, 064313 (2007).
[29] P. Norman and H. J. Aa. Jensen, J. Chem. Phys. **121**, 6145 (2004).
[30] P. Salek, T. Helgaker, and T. Saue, Chem. Phys. **311**, 187 (2005).
[31] T. Saue and T. Helgaker, J. Comput. Chem. **23**, 814 (2002).
[32] T. Saue, K. Fægri, T. Helgaker, and O. Gropen, Mol. Phys. **91**, 937 (1997).
[33] O. Christiansen, P. Jørgensen, and C. Hättig, Int. J. Quantum Chem. **68**, 1 (1998).
[34] N. T. Maitra and K. Burke, Chem. Phys. Lett. **441**, 167 (2007).
[35] H. J. Aa. Jensen, T. Saue, L. Visscher, V. Bakken, E. Eliav, T. Enevoldsen, T. Fleig, O. Fossgaard, T. Helgaker, J. Laerdahl *et al.*, DIRAC, a relativistic *ab initio* electronic structure program, release as DIRAC4.0,

2004.
[36] A. D. Becke, J. Chem. Phys. **98**, 5648 (1993).
[37] W. J. Hehre, R. Ditchfield, and J. A. Pople, J. Chem. Phys. **56**, 2257 (1972).
[38] V. A. Rassolov, J. A. Pople, M. A. Ratner, and T. L. Windus, J. Chem. Phys. **109**, 1223 (1998).
[39] M. Kaupp, P. Schleyer, H. Stoll, and H. Preuss, J. Am. Chem. Soc. **113**, 6012 (1991).
[40] M. J. Frisch, G. W. Trucks, H. B. Schlegel *et al.*, GAUSSIAN 03, revision B05, Gaussian, Inc., Pittsburgh, PA, 2003.
[41] DALTON, a molecular electronic structure program, release 2.0, 2005 (see http://www.kjemi.uio.no/software/dalton/dalton.html).
[42] T. Yanai, D. P. Tew, and N. C. Handy, Chem. Phys. Lett. **393**, 51 (2004).
[43] M. J. G. Peach, T. Helgaker, P. Salek, T. W. Keal, O. B. Lutnæs, D. J. Tozer, and N. C. Handy, Phys. Chem. Chem. Phys. **8**, 558 (2006).
[44] A. J. Sadlej, Collect. Czech. Chem. Commun. **53**, 1995 (1988).
[45] D. Shelton and J. Rice, Chem. Rev. (Washington, D.C.) **94**, 3 (1994).
[46] S. A. C. McDowell, R. D. Amos, and N. C. Handy, Chem. Phys. Lett. **235**, 1 (1995).
[47] A. Dreuw and M. Head-Gordon, J. Am. Chem. Soc. **126**, 4007 (2004).

Paper III

III

Two-photon absorption in the relativistic four-component Hartree–Fock approximation

Johan Henriksson
Patrick Norman
Hans Jørgen Aa. Jensen

The Journal of Chemical Physics **122**, 114106 (2005)

THE JOURNAL OF CHEMICAL PHYSICS **122**, 114106 (2005)

Two-photon absorption in the relativistic four-component Hartree–Fock approximation

Johan Henriksson[a] and Patrick Norman[b]
Department of Physics and Measurement Technology, Linköping University, SE-581 83 Linköping, Sweden

Hans Jørgen Aa. Jensen[c]
Department of Chemistry, University of Southern Denmark, DK-5230 Odense M, Denmark

(Received 21 December 2004; accepted 19 January 2005; published online 21 March 2005)

A first implementation of the single residue of the quadratic response function in the four-component Hartree–Fock approximation is presented. The implementation is based on a Kramers paired molecular orbital basis and takes full advantage of time and spatial symmetry reductions in a quaternion formulation—in analogy with the previous work on the quadratic response function [J. Chem. Phys. **121**, 6145 (2004)]. Sample calculations are given in terms of the monochromatic and coherent two-photon absorption cross sections in the noble gases. The relativistic two-photon selection rule $\Delta J=\{0,\pm 2\}$ allows for nonrelativistically spin-forbidden transitions, and, even in neon, strong two-photon absorption is shown to occur for the $X\,^1S_0 \rightarrow 2\,^3P_2$ transition. It is argued that relevant comparisons between nonrelativistic and relativistic calculations must be performed at the level of integrated absorption cross sections. © *2005 American Institute of Physics*. [DOI: 10.1063/1.1869469]

I. INTRODUCTION

Two-photon absorption (TPA) was predicted already in 1931 by Göppert-Mayer[1] but not observed in experiment until the advent of the laser. We here refer to the instantaneous optical process in which two light quanta are annihilated under resonant conditions in the transition between two states in a quantum mechanical system. The main features of this process is that it occurs with a probability depending quadratically on the incident light intensity, and that it allows for low-energy induced optical transitions. For these and other, more technical, reasons, two-photon absorption is today used in a variety of applications, e.g., spectroscopy, up-conversion of lasers, optical power limiting, and microscopy.[2]

The energy absorbed from the radiation field due to two-photon absorption is proportional to the imaginary part of the intensity-dependent refractive index, or, in other words, the third-order polarization $\gamma(-\omega;\omega,-\omega,\omega)$. However, under resonant conditions it has proven effective to express the TPA cross section in terms of the so-called two-photon matrix elements, which can be considered as real and obtained from the second-order response of the reference state wave function. This technique has been used by several authors in order to calculate TPA cross sections by means of standard electronic structure theory in quantum chemistry, and implementations include the Hartree–Fock,[3] multiconfigurational self-consistent field,[3] coupled cluster,[4] and density functional theory[5] methods.

Over the past several years, we have been involved in the development of optical power limiting materials.[6] The performance of these materials is analyzed in terms of the Jablonski diagram in which TPA is used to overcome the band gap, and the long-gained experience by us and others shows that organometallic compounds are particularly suitable to provide broadband protection against laser damage. It is clear that the triplet manifold of states plays a crucial role in this success and that spin-forbidden transitions are induced by the heavy atoms in the organic network. With this background as main motivation, it is our intention here to extend the list of quantum chemical methods given above to include fully relativistic four-component methods. In doing so, we correctly account for the coupling of non-relativistic singlet and triplet states, and the absorption is governed by the change in the total angular momentum. We will develop the two-photon matrix element at the four-component, Kramers-restricted, Hartree–Fock level of theory, and the uncorrelated treatment is expected to be reasonable because of the closed-shell (and large band gap) character of the target compounds in the optical power limiting applications. We do by no means, however, exclude ourselves from a future extension to include electron correlation but rather see the present work as a first step on the way.

Our implementation will be illustrated by sample calculations on the noble gas atoms rather than complex organometallic molecules. This is partly a matter of computational size, but, more importantly, the choice of spherically symmetric systems illustrates the relativistic selection rules for two-photon absorption well and will furnish a general discussion on the inclusion of relativity for this property.

[a]Electronic mail: johhe@ifm.liu.se
[b]Electronic mail: panor@ifm.liu.se
[c]Electronic mail: hjj@chem.sdu.dk

II. THEORY AND METHODOLOGY

A. One- and two-photon absorption

When subjected to periodic electromagnetic radiation with period time T, the average rate of energy absorbance per unit time by a material is given by

$$\langle R_{\mathrm{abs}}\rangle_T = \int_V \langle \mathbf{j}\cdot\mathbf{E}\rangle_T d\mathbf{r}, \tag{1}$$

where $\mathbf{j}$ is the current density in the material and $\mathbf{E}$ is the applied electric field.[7] The current density is proportional to the time derivative of the induced polarization, and the imaginary parts of the linear and nonlinear polarizations therefore correspond to one- and multiphoton absorption, respectively. Even orders of the polarization will vanish in the integration over one period of time—here denoted by $\langle\ldots\rangle_T$—and, hence, we need to be concerned with the linear polarizability and the second-order hyperpolarizability in order to address one- and two-photon absorption. As far as linear absorption is concerned, we adopt the custom to present results for the oscillator strength,

$$\delta_{\mathrm{OPA}} = \frac{2\omega_f}{3}\sum_\alpha |\langle 0|\hat{\mu}_\alpha|f\rangle|^2, \tag{2}$$

where ω_f is the transition frequency and $\hat{\mu}_\alpha$ is the electric dipole operator along the molecular axis α. However, in the infinite excited-state lifetime approximation, the oscillator strength is closely related to the imaginary part of the linear polarizability that accounts for the linear loss of radiation energy in Eq. (1), see Ref. 8 for details. Correspondingly, the two-photon absorption cross section is proportional to the imaginary part of the hyperpolarizability $\gamma(-\omega;\omega,-\omega,\omega)$, which, assuming that only one two-photon (TP) resonant state contributes significantly, can be written as[9]

$$\mathrm{Im}[\gamma_{\alpha\beta\gamma\delta}(-\omega;\omega,-\omega,\omega)] = \frac{\hbar}{\Gamma_f/2} S^{0\to f}_{\alpha\gamma}(\omega)[S^{0\to f}_{\delta\beta}(\omega)]^*, \tag{3}$$

where Γ_f is the lifetime broadening of the TP state and the so-called two-photon absorption matrix element is written as

$$S^{0\to f}_{\alpha\beta}(\omega) = \hbar^{-2}\sum_k \left[\frac{\langle 0|\hat{\mu}_\alpha|k\rangle\langle k|\hat{\mu}_\beta|f\rangle}{\omega_k-\omega} + \frac{\langle 0|\hat{\mu}_\beta|k\rangle\langle k|\hat{\mu}_\alpha|f\rangle}{\omega_k-\omega}\right]. \tag{4}$$

From a computational point of view, it is easier to compute the TPA matrix element rather than the second-order hyperpolarizability since the TPA matrix element is also a residue of the first-order hyperpolarizability,

$$\lim_{\omega_2\to\omega_f}(\omega_f-\omega_2)\beta_{\alpha\beta\gamma}(-\omega_\sigma;\omega_1,\omega_2) = S^{0\to f}_{\alpha\beta}\left(\frac{\omega_f}{2}\right)\langle f|\hat{\mu}_\gamma|0\rangle, \tag{5}$$

where, in the left-hand side of Eq. (5), we have $\omega_\sigma=\omega_1+\omega_2$ and $\omega_1=-\omega_f/2$. Considering randomly oriented samples as gases and liquids, the relevant orientationally averaged two-photon absorption cross section is determined from the expression[10]

$$\delta_{\mathrm{TPA}} = \frac{1}{15}\sum_{\alpha,\beta}\left\{FS^{0\to f}_{\alpha\alpha}\left(\frac{\omega_f}{2}\right)\left[S^{0\to f}_{\beta\beta}\left(\frac{\omega_f}{2}\right)\right]^* + GS^{0\to f}_{\alpha\beta}\left(\frac{\omega_f}{2}\right)\times\left[S^{0\to f}_{\alpha\beta}\left(\frac{\omega_f}{2}\right)\right]^* + HS^{0\to f}_{\alpha\beta}\left(\frac{\omega_f}{2}\right)\left[S^{0\to f}_{\beta\alpha}\left(\frac{\omega_f}{2}\right)\right]^*\right\}, \tag{6}$$

where F, G, and H are factors that depend on the polarization of the incident light. In this work the implementation of the equivalences of Eqs. (4) and (6) in the relativistic four-component Hartree–Fock approximation is presented.

B. Two-photon absorption in the four-component Hartree–Fock approximation

In the four-component Hartree–Fock approximation the reference state is represented by a single Slater determinant with one-electron four-spinors as elements. The eigenvalues of the canonical Hartree–Fock orbitals fall into two sets that are separated by twice the rest energy of the electron, and the reference state is optimized with a restriction of only occupying orbitals with positive energy—one refers to these orbitals as electronic, whereas the others are referred to as positronic. Time-reversal symmetry in the reference state is enforced by occupation of Kramers pair orbitals,

$$\psi_i(\mathbf{r}) = \begin{pmatrix}\psi_i^{L\alpha}\\ \psi_i^{S\alpha}\\ \psi_i^{L\beta}\\ \psi_i^{S\beta}\end{pmatrix}, \quad \psi_{\bar{i}}(\mathbf{r}) = \hat{\mathcal{K}}\psi_i(\mathbf{r}) = \begin{pmatrix}-\psi_i^{L\beta^*}\\ -\psi_i^{S\beta^*}\\ \psi_i^{L\alpha^*}\\ \psi_i^{S\alpha^*}\end{pmatrix}, \tag{7}$$

and these orbitals are related by the time-reversal operator $\hat{\mathcal{K}}=-i[I_2\otimes\sigma_y]\hat{\mathcal{K}}_0$, where $\hat{\mathcal{K}}_0$ is the complex conjugation operator.

The time dependence of the reference state is parametrized by a unitary exponential operator according to[11]

$$|\psi(t)\rangle = e^{i\hat{\kappa}(t)}|0\rangle, \quad \hat{\kappa}(t) = \sum_{i,s}(\kappa_{is}a_s^\dagger a_i + \kappa_{is}^* a_i^\dagger a_s), \tag{8}$$

where a nonredundant parametrization includes electron transfer from occupied electronic orbitals i to unoccupied electronic and positronic orbitals s—the corresponding transfer amplitudes are here denoted by κ^{e-e} and κ^{e-p}, respectively. We use time-dependent perturbation theory to obtain corrections to the molecular polarization that are induced by the external electric fields:

$$\langle\psi(t)|\hat{\mu}|\psi(t)\rangle = \langle 0|\hat{\mu}|0\rangle + \int_{-\infty}^{\infty} d\omega_1\langle\langle\hat{\mu};\hat{V}_\alpha\rangle\rangle_{\omega_1}F_\alpha^{\omega_1}e^{-i\omega_1 t} + \frac{1}{2}\int_{-\infty}^{\infty}d\omega_1\int_{-\infty}^{\infty}d\omega_2\langle\langle\hat{\mu};\hat{V}_\alpha,\hat{V}_\beta\rangle\rangle_{\omega_1,\omega_2}\times F_\alpha^{\omega_1}F_\beta^{\omega_2}e^{-i(\omega_1+\omega_2)t}+\cdots, \tag{9}$$

where the Fourier coefficients define the linear and quadratic response functions, F^ω is the amplitude of the external field, and the electric-dipole coupling operator is given by $\hat{V}_\alpha = e(\hat{r}_\alpha\otimes I_4)$. Implementations of the linear and quadratic response functions in the four-component Hartree–Fock approximation are described in Refs. 12 and 13, respectively,

and, at the nonrelativistic Hartree–Fock level, the first-order residue of the quadratic response function has been presented by Hettema *et al.*[3] The TPA matrix element in the Hartree–Fock approximation can be written as[3]

$$S^{0\to f}_{\alpha\beta}(\omega_\sigma) = N^{\alpha}_{j}(-\omega_\sigma)\beta^{[2]}_{jk}N^{f}_{k}(\omega_f) + N^{\beta}_{j}(\omega_1)[\alpha^{[2]}_{jk} + \alpha^{[2]}_{kj}]N^{f}_{k}(\omega_f) + N^{\alpha}_{j}(-\omega_\sigma)[E^{[3]}_{jkl} + E^{[3]}_{jlk} - \omega_1 S^{[3]}_{jkl} - \omega_f S^{[3]}_{jlk}]N^{\beta}_{k}(\omega_1)N^{f}_{l}(\omega_f), \quad (10)$$

where the linear response vectors are given by

$$N^{X}_{j}(\omega) = [E^{[2]} - \hbar\omega S^{[2]}]^{-1}_{jk}X^{[1]}_{k}, \quad X \in \{\alpha,\beta\}, \quad (11a)$$

$$[E^{[2]} - \hbar\omega S^{[2]}]_{jk}N^{f}_{k}(\omega) = 0, \quad (11b)$$

and $E^{[i]}$, $S^{[i]}$, and $\alpha^{[i]}$ and $\beta^{[i]}$ are generalized Hessian, overlap, and property matrices, respectively. In this work, we have implemented Eq. (10) in the Kramers restricted four-component Hartree–Fock approximation. We fully exploit computational cost reductions involved with spatial molecular symmetries of point group D_{2h} and subgroups, and the time-reversal symmetry of the wave function is exploited in a quaternion formalism.[14] Our work is integrated in the DIRAC program.[15]

III. COMPUTATIONAL DETAILS

All calculations in the present work were performed at the Hartree–Fock level of theory using uncontracted basis sets of spherical Gaussian functions—with use of five and seven components of the *d* and *f* functions, respectively. The results from four-component relativistic calculations include all large- and small-component integrals (*LL*, *LS*, and *SS*) as well as all orbital rotations ($e\to e$ and $e\to p$). In the calculations on He, Ne, and Ar, the exponents of the basis sets were taken from Dunning's quadruply augmented, correlation-consistent, triple zeta basis sets (qaug-cc-pVTZ).[16–18] For Kr, Xe, and Rn, the corresponding basis sets were not available, and exponents were instead taken from the well-tempered basis sets of Huzinaga and Klobukowski.[19] In the notation of Huzinaga and Klobukowski, *f* functions were added to the original basis sets for Kr, Xe, and Rn in accordance with $n_f \in [15,22]$, $n_f \in [13,24]$, and $n_f \in [11,24]$, respectively. Furthermore, the well-tempered basis sets were quadruply augmented using the formula

$$\zeta_{N+j} = \left[\frac{\zeta_N}{\zeta_{N-1}}\right]^{j}\zeta_N, \quad j \in [1,N_{\text{aug}}], \quad (12)$$

where N_{aug} is the number of augmentation functions added and ζ_N and ζ_{N-1} refer to the two most diffuse exponents in the original basis sets. The sizes of the large component basis sets used in the property calculations were $[10s4p5d]$, $[14s9p6d5f]$, $[19s13p6d5f]$, $[30s24p18d12f]$, $[32s27p21d16f]$, and $[32s28p22d18f]$ for He, Ne, Ar, Kr, Xe, and Rn, respectively, and the small-component basis functions were generated from those of the large component with use of the restricted kinetic-balance condition.

All calculations were performed with a locally modified version of the DIRAC program.[15]

IV. RESULTS AND DISCUSSION

The one- and two-photon absorption (OPA and TPA) cross sections have been calculated for the low-lying valence transitions in the noble gases. The effects of relativity on the absorption spectra are estimated by a comparison of results obtained in the nonrelativistic time-dependent Hartree–Fock (TDHF) approximation with those obtained in the relativistic time-dependent four-component Hartree–Fock (TDDHF) approximation. Our results presented below for one- and two-photon absorption cross sections correspond to the summed absorption to the degenerate M_J components of the excited states. We expect relativistic effects to come into play in different ways depending on the size of the atom. For the heavy elements the inner-core density is composed of electrons with high kinetic energies and the density will thus be strongly altered by relativity. In an indirect manner this will generate a potential for the valence electrons which is quite different from the nonrelativistic one. However, the direct effects of relativity on the low kinetic-energy, valence, electrons need not be that large. These arguments form the foundation for the use of so-called effective-core potentials in quantum chemical calculations, and we have made frequent use of this technique in past calculations of linear and nonlinear absorption spectra without having had the opportunity to benchmark against results from four-component methods.[6] Therefore, the present work is important in that it addresses also the direct relativistic effects in the valence electron density for light as well as heavy elements. We will demonstrate how relativity alters the one- and two-photon absorption spectra. To begin with, it is clear that the nonrelativistic atomic selection rules on orbital and spin angular momentum (OPA, $\Delta L = \pm 1$ and $\Delta S = 0$; TPA, $\Delta L = \{0,\pm 2\}$ and $\Delta S = 0$) are to be replaced by the relativistic atomic selection rules on total angular momentum (OPA, $\Delta J = \pm 1$ and TPA, $\Delta J = \{0,\pm 2\}$).

Regarding basis sets, the made choice is based on TDDHF calculations of excitation energies and cross sections for helium, neon, and argon using uncontracted basis sets with exponents from triply and quadruply augmented cc-pVXZ, $X \in \{T,Q,5\}$.[16–18] Excitation energies are seen to be quite insensitive to the choice of basis set, whereas changes are noticeable in the two-photon absorption cross sections. For the $X\,^1S_0 \to 1\,^1S_0$ transition in helium, the difference between cross sections obtained with qaug-cc-pVTZ (which is the basis set used in later calculations) and qaug-cc-pV5Z are within 1%, while for the $X\,^1S_0 \to 2\,^1S_0$ transition, the value changes from $\delta = 1.6002$ a.u. (see Table I) to $\delta = 1.4737$ a.u. using qaug-cc-pV5Z. For neon and argon, the two-photon absorption cross sections as obtained with the two different basis sets are within 4% and 1%, respectively. So, apart from the single transition in helium, the results presented here for helium, neon, and argon should be within 5% of the Hartree–Fock limiting values.

A. One-photon absorption

Results for the linear absorption spectra of helium, neon, argon, krypton, xenon, and radon are presented in Tables I–VI, respectively. For helium we cover one-photon transi-

TABLE I. Nonrelativistic TDHF and relativistic TDDHF excitation energies, ΔE (eV), and one- and two-photon absorption cross sections (a.u.), δ, for helium.

			TDHF			TDDHF	
Configuration	Desig.	Expt.[a]	ΔE	δ^{b}	J	ΔE	δ^{b}
$1s2s$	$^3S_1$	19.819	19.694	0	1	19.694	0
	$^1S_0$	20.615	21.125	10.426	0	21.126	10.424
$1s2p$	$^3P_2^o$	20.963	21.220	0	2	21.221	0
	$^3P_1^o$	20.963	21.220	0	1	21.221	0.000 00
	$^3P_0^o$	20.964	21.220	0	0	21.221	0
	$^1P_1^o$	21.217	21.694	0.253 52	1	21.695	0.253 50
$1s3s$	$^3S_1$	22.718	23.043	0	1	23.044	0
	$^1S_0$	22.920	23.405	1.600 6	0	23.405	1.600 2
$1s3p$	$^3P_2^o$	23.006	23.381	0	2	23.382	0
	$^3P_1^o$	23.006	23.381	0	1	23.382	0.000 00
	$^3P_0^o$	23.006	23.381	0	0	23.382	0
	$^1P_1^o$	23.086	23.537	0.078 248	1	23.538	0.078 242

[a]Experimental excitation energies are taken from Ref. 20.
[b]Whether we refer to δ_{OPA} or δ_{TPA} is clear from the atomic selections rules.

tions from the $1s$ shell to the $2p$ and $3p$ shells. At the nonrelativistic level the one-photon excited states are triply orbital degenerate, and, being a first-row element, there are no significant differences in the linear absorption spectra of helium at the relativistic level.

For neon we include one-photon induced transitions from the $2p$ shell to the $3s$ and $4s$ shells, and for the remaining elements we have restricted results to include only $np \rightarrow (n+1)s$ transitions. Starting with neon there is a noticeable absorption at the relativistic level to the nonrelativistically spin-forbidden states, e.g., the oscillator strength for the $X\,^1S_0 \rightarrow 1\,^3P_1^o$ transition is 0.0043. It is clear that this intensity has "leaked" over from the allowed $X\,^1S_0 \rightarrow 1\,^1P_1^o$ transition with $\delta_{\mathrm{OPA}} = 0.1608$, and it is the integrated linear absorption cross section that should be compared to the nonrelativistic value of $\delta_{\mathrm{OPA}} = 0.1645$, see Table II and Fig. 1.

The discussion on absorption leakage becomes more apparent for argon where, for the corresponding transitions, it amounts to 9%, see Table III. Even if the relativistic effects

TABLE II. Nonrelativistic TDHF and relativistic TDDHF excitation energies, ΔE (eV), and one- and two-photon absorption cross sections (a.u.), δ, for neon.

			TDHF			TDDHF	
Configuration	Desig.	Expt.[a]	ΔE	δ^{b}	J	ΔE	δ^{b}
$2p^5 3s$	$^3P_2^o$	16.619	17.990	0	2	17.927	0
	$^3P_1^o$	16.671	17.990	0	1	17.997	0.004 329
	$^3P_0^o$	16.716	17.990	0	0	18.045	0
	$^1P_1^o$	16.848	18.363	0.164 47	1	18.349	0.160 81
$2p^5 3p$	$^3S_1$	18.382	19.532	0	1	19.510	0
	$^3D_3$	18.555	19.967	0	3	19.910	0
	$^3D_2$	18.576	19.967	0	2	19.950	0.819 4
	$^3D_1$	18.613	19.967	0	1	19.993	0
	$^1D_2$	18.637	20.129	11.060	2	20.090	5.608 6
	$^1P_1$	18.694	20.159	0	1	20.137	0
	$^3P_2$	18.704	20.159	0	2	20.164	4.712 6
	$^3P_0$	18.712	20.159	0	0	20.173	0.3097
	$^3P_1$	18.727	20.159	0	1	20.186	0
	$^1S_0$	18.966	20.564	12.850	0	20.554	12.591
$2p^5 4s$	$^3P_2^o$	19.664	21.215	0	2	21.156	0
	$^3P_1^o$	19.688	21.215	0	1	21.197	0.009 680
	$^3P_0^o$	16.761	21.215	0	0	21.276	0
	$^1P_1^o$	19.780	21.295	0.028 633	1	21.316	0.018974

[a]Experimental excitation energies are taken from Ref. 20.
[b]Whether we refer to δ_{OPA} or δ_{TPA} is clear from the atomic selections rules.

TABLE III. Nonrelativistic TDHF and relativistic TDDHF excitation energies, ΔE (eV), and one and two-photon absorption cross sections (a.u.), δ, for argon.

			TDHF			TDDHF	
Configuration	Desig.	Expt.[a]	ΔE	δ^{b}	J	ΔE	δ^{b}
$3p^5 4s$	$^3P_2^o$	11.548	11.860	0	2	11.759	0
	$^3P_1^o$	11.624	11.860	0	1	11.864	0.025 829
	$^3P_0^o$	11.723	11.860	0	0	11.957	0
	$^1P_1^o$	11.828	12.209	0.315 06	1	12.206	0.291 28
$3p^5 4p$	$^3S_1$	12.907	12.976	0	1	12.945	0
	$^3D_3$	13.076	13.372	0	3	13.287	0
	$^3D_2$	13.095	13.372	0	2	13.332	24.234
	$^3D_1$	13.153	13.372	0	1	13.404	0
	$^1D_2$	13.273	13.501	113.40	2	13.459	52.543
	$^3P_0$	13.282	13.572	0	0	13.575	34.635
	$^1P_1$	13.302	13.572	0	1	13.567	0
	$^3P_2$	13.328	13.572	0	2	13.598	38.244
	$^3P_1$	13.480	13.572	0	1	13.634	0
	$^1S_0$	13.845	13.781	161.45	0	13.806	127.76

[a]Experimental excitation energies are taken from Ref. 20.
[b]Whether we refer to δ_{OPA} or δ_{TPA} is clear from the atomic selections rules.

on the integrated absorption are small for argon, the absorption spectra will be quite different due to the two peaks separated by 0.14 eV in the relativistic case as compared to the one single peak in the nonrelativistic case.

In the linear absorption spectrum of krypton and xenon, the corresponding two peaks are separated by 0.68 and 1.0 eV, respectively, and they are more or less equally intense. We note that the experimental energy separations of the one-photon states with $J=1$ are 0.20, 0.61, and 1.13 eV for argon,[20] krypton,[21] and xenon,[22] respectively, and a comparison to the corresponding TDDHF values given above show that the theoretical values are in error with about 0.1 eV. Considering the inherent weakness in the Hartree–Fock approach when it comes to the description of triplet states, this agreement is noteworthy.

In the radon spectrum, the experimental energy separation of the two one-photon states with $J=1$ is as large as 3.9 eV,[22] and, since we adopt a bottom-up algorithm in solving the generalized eigenvalue equation [Eq. (11b)], we were not able to resolve the $1\ ^1P_1^0$ state in the calculation.

A general remark to be made is that, although the agreement between experimental and theoretical excitation energies are good for the low-lying states in the noble gases, it is clear that electron correlation plays a significantly more important role for neon. Here, discrepancies as large as 10% are seen for the transition energies.

B. Two-photon absorption

Turning attention to the TPA cross sections, there appear striking differences between nonrelativistic and relativistic

TABLE IV. Nonrelativistic TDHF and relativistic TDDHF excitation energies, ΔE (eV), and one- and two-photon absorption cross sections (a.u.), δ, for krypton.

			TDHF			TDDHF	
Configuration	Desig.	Expt.[a]	ΔE	δ^{b}	J	ΔE	δ^{b}
$4p^5 5s$	$^3P_2^o$	9.915	10.254	0	2	9.931	0
	$^3P_1^o$	10.033	10.254	0	1	10.125	0.151 56
	$^3P_0^o$	10.563	10.254	0	0	10.619	0
	$^1P_1^o$	10.644	10.609	0.375 60	1	10.800	0.233 79
$4p^5 5p$	$^3S_1$	11.304	11.319	0	1	11.176	0
	$^3D_3$	11.443	11.689	0	3	11.427	0
	$^3D_2$	11.445	11.689	0	2	11.471	120.33
	$^3D_1$	11.526	11.689	0	1	11.580	0
	$^1D_2$	11.546	11.811	257.18	2	11.609	70.920
	$^3P_0$	11.666	11.897	0	0	11.736	242.85
	$^1P_1$	12.101	11.897	0	1	12.183	0
	$^3P_1$	12.144	11.897	0	1	12.229	0
	$^3P_2$	12.141	11.897	0	2	12.240	77.215
	$^1S_0$	12.257	12.048	359.24	0	12.395	112.71

[a]Experimental excitation energies are taken from Ref. 21.
[b]Whether we refer to δ_{OPA} or δ_{TPA} is clear from the atomic selections rules.

TABLE V. Nonrelativistic TDHF and relativistic TDDHF excitation energies, ΔE (eV), and one- and two-photon absorption cross sections (a.u.), δ, for xenon.

			TDHF			TDDHF	
Configuration	Desig.	Expt.[a]	ΔE	δ^{b}	J	ΔE	δ^{b}
$5p^5 6s$	$^3P_2^o$	8.315	8.792	0	2	8.217	0
	$^3P_1^o$	8.437	8.792	0	1	8.422	0.213 68
	$^3P_0^o$	9.447	8.792	0	0	9.193	0
	$^1P_1^o$	9.570	9.149	0.430 90	1	9.420	0.188 16
$5p^5 6p$	$^3S_1$	9.580	9.669	0	1	9.352	0
	$^3D_3$	9.686	10.039	0	3	9.577	0
	$^3D_2$	9.721	10.039	0	2	9.594	348.05
	$^3D_1$	9.789	10.039	0	1	9.723	0
	$^1D_2$	9.821	10.151	579.80	2	9.758	168.27
	$^3P_0$	9.934	10.251	0	0	9.858	752.12
	$^1P_1$	10.956	10.251	0	1	10.720	0
	$^3P_1$	11.055	10.251	0	2	10.812	21.308
	$^3P_2$	11.069	10.251	0	3	10.814	0
	$^1S_0$	11.141	10.343	876.75	1	10.845	0
$5p^5 7p$	$^3S_1$	10.902	11.187	0	2	10.866	45.309
	$^3D_2$	10.954	11.285	0	0	10.901	103.69
	$^3D_3$	10.969	11.285	0	1	10.997	0
	$^1D_2$	10.996	11.319	88.328	2	11.072	148.79
	$^3D_1$	11.001	11.285	0	1	11.074	0
	$^3P_0$	11.015	11.348	0	0	11.187	206.29

[a]Experimental excitation energies are taken from Ref. 22.
[b]Whether we refer to δ_{OPA} or δ_{TPA} is clear from the atomic selection rules.

results already for neon, see Table II. The $1\,^3D_2$, $1\,^1D_2$, and $1\,^3P_2$ states are split in energy by no more than 0.21 eV, and, due to the electron spin-orbit coupling, the states therefore mix effectively. A relativistic configuration interaction calculation on neon confirmed that there is strong mixing, and, thus, it is not an artifact of the Hartree–Fock approximation. As a consequence, the TPA cross sections are split over the different states of equal J value, and the two triplet states acquire about half of the total intensity for $J=2$. Considering that neon is a second-row element, it is a surprising fact that nonrelativistic calculations do not even provide a qualitatively correct description of the two-photon absorption, and, in comparing intensities obtained with nonrelativistic and relativistic methods, it is therefore necessary to use the integrated TPA cross sections as reference values, e.g., two-photon transition amplitudes will not be useful in this respect. From Figs. 2 and 3 it is apparent that the integrated two-photon intensities to states with both $J=2$ and $J=0$ in neon are virtually the same at the relativistic and nonrelativistic levels of theory—as we expect them to be.

The energy splitting of the $1\,^3D_2$, $1\,^1D_2$, and $1\,^3P_2$ states in argon amounts to 0.27 eV at the TDDHF level (to be compared with 0.24 eV in experiment[20]) and, in this case, the main part of the two-photon absorption intensity is attributed to the nonrelativistically spin-forbidden states. Also for argon, it is clear from Fig. 4 that the relativistic effects on the total cross sections for $J=2$ and $J=0$ states are very small. Therefore, as far as the two-photon absorption spectrum is concerned, the same quantum yield is predicted at the nonrelativistic and relativistic levels of theory, but there is a significant relativistic broadening due to the large triplet intensities. With respect to applications for optical power limiting, this will be important since dynamic simulations of laser pulse propagation in two-photon active materials are strongly dependent on broadening of excited states.[6]

Beginning with krypton, there are strong relativistic effects also on the integrated TPA cross sections; the relative differences between nonrelativistic and relativistic results for δ_{TPA} are shown in Fig. 4. The theoretical and experimental[21] energy splittings between the $1\,^3D_2$, $1\,^1D_2$, and $1\,^3P_2$ states in krypton are as large as 0.77 and 0.70 eV, respectively. Since the states with identical total angular momentum become so spread in energy, it is increasingly difficult to compare the nonrelativistic absorption cross sections to the relativistic ones. It is only when there is a clear separation in energy between manifolds of excited states that we can make a fair comparison with partially integrated absorption cross sections. For krypton we believe the $4p^5 5p$ manifold of states to be sufficiently separated from other TP states in the spectrum in order to make this comparison, but for xenon (Table V) and, in particular, radon (Table VI) it is less meaningful. Figures 2 and 3 do, however, report a comparison of partially integrated TPA cross sections at the non-relativistic and relativistic levels of theory with inclusion of as many states that we were able to resolve in the calculations. We believe that Fig. 4 provides a reasonable estimate of the relativistic effects for linear and nonlinear absorption.

As far as earlier theoretical work on two-photon absorption in the noble gases is concerned, we note that the first *ab initio* calculations of the two-photon transition probabilities for neon and argon were performed by Moccia and Rizzo in 1984.[23] Using a sum-over-states approach and the random

TABLE VI. Nonrelativistic TDHF and relativistic TDDHF excitation energies, ΔE (eV), and one- and two-photon absorption cross sections (a.u.), δ, for radon.

			TDHF			TDDHF	
Configuration	Desig.	Expt.[a]	ΔE	δ[b]	J	ΔE	δ[b]
$6p^5 7s$	$^3P_2^o$	6.772	8.117	0	2	6.552	0
	$^3P_1^o$	6.942	8.117	0	1	6.822	0.290 43
	$^3P_0^o$	10.660	8.117	0		[c]	[c]
	$^1P_1^o$	10.793	[c]	[c]		[c]	[c]
$6p^5 7p$	$^3S_1$	8.213	8.960	0	1	7.924	0
	$^1D_2$	8.271	9.432	869.51	2	8.084	927.00
	$^3D_3$	8.436	9.325	0	3	8.158	0
	$^3D_1$	8.472	9.325	0	1	8.268	0
	$^3D_2$	8.529	9.325	0	2	8.333	502.53
	$^3P_0$	8.647	9.536	0	0	8.441	1868.1
	$^1P_1$	[d]	9.536	0			
	$^3P_2$	[d]	9.536	0			
	$^3P_1$	[d]	9.536	0			
	$^1S_0$	[d]	9.602	1348.5			
$6p^5 8p$	$^3S_1$	9.552	10.420	0	1	9.258	0
	$^1D_2$	9.567	10.550	131.87	2	9.300	82.208
	$^3D_3$	9.622	10.517	0	3	9.333	0
	$^3D_1$	9.631	10.517	0	1	9.361	0
	$^3D_2$	9.649	10.517	0	2	9.384	91.767
	$^3P_0$	9.691	10.580	0	1	9.384	0
	$^1P_1$	[d]	10.580	0	0	9.425	384.64
	$^3P_2$	[d]	10.580	0	2	9.879	39.218
	$^3P_1$	[d]	10.580	0	3	9.915	0
	$^1S_0$	[d]	10.614	287.59	1	9.940	0
					2	9.968	79.222
					0	10.024	360.21

[a]Experimental excitation energies are taken from Ref. 22.
[b]Whether we refer to δ_{OPA} or δ_{TPA} is clear from the atomic selections rules.
[c]Could not be resolved in the calculations.
[d]Was not presented in the tables used, Ref. 22.

phase approximation, they considered the $^1S_0$ and $^1D_0$ states in neon and argon corresponding to the electronic transitions $2p \rightarrow 3p$ and $2p \rightarrow 4f$ (neon) and $3p \rightarrow 4p$ and $3p \rightarrow 4f$ (argon).

More recently, Hettema *et al.*[3] performed response theory calculations of the off-diagonal elements in the TP transition matrix tensor ($S_{xy}^{0 \rightarrow f}$) for the $^1D_2$ state in neon (corresponding to the $2p \rightarrow 3p$ electronic transition). Using the Hartree–Fock (HF) and the singles-and-doubles restricted active space (SD RAS) methods, they reported excitation energies to be 20.106 eV and 19.170 eV, respectively, whereas the corresponding TP transition matrix elements were re-

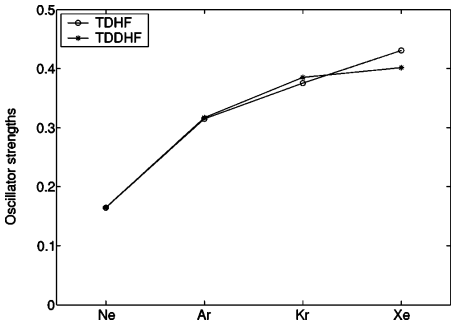

FIG. 1. The TDHF and integrated TDDHF oscillator strengths.

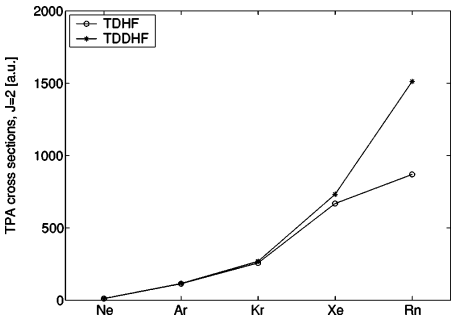

FIG. 2. The TDHF and integrated TDDHF two-photon absorption cross sections for states with $J=2$.

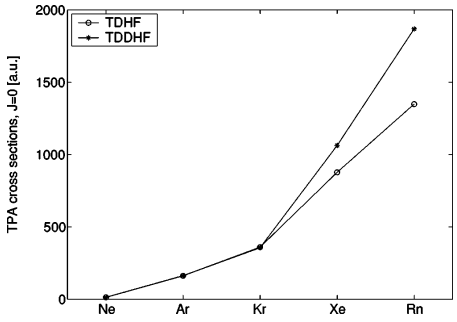

FIG. 3. The TDHF and integrated TDDHF two-photon absorption cross sections for states with $J=0$.

ported to be 2.9663 a.u. and 3.3450 a.u. The calculations of Hettema *et al.* do not refer to monochromatic TPA. Instead, the energy of one of the two incident photons was held fixed at 9.320 eV, which corresponds to 46.4% and 48.6% of the HF and SD RAS excitation energy, respectively. Disregarding this lack of monochromaticity, it is concluded that our nonrelativistic results of 20.129 eV and 2.8801 a.u. for the transition energy and TP matrix element, respectively, are in good agreement with the reference data. Our relativistic values for the same properties are 20.090 eV and 2.0510 a.u., respectively, which, at sight, may appear conspicuous. However, this discrepancy between relativistic and nonrelativistic values is entirely due to the leakage of intensity discussed above. As mentioned above, it is not appropriate to add the contribution to $S^{0\to f}$ from the other states with identical J values, since this comparison must instead be performed for the cross sections that correspond to the physical observable in this case.

For the corresponding $^1D_2$ state in argon, the monochromatic TP matrix element $S_{xy}^{0\to f}$ has been calculated by Sundholm *et al.*[24] with means of HF and complete active space (CAS) response theory. Excitation energies and tensor elements were reported to be 13.485 and 13.185 eV and 9.499 and 10.424 a.u. at the HF and CAS levels, respectively. In the present work, the corresponding nonrelativistic results amount to 13.501 eV and 9.222 a.u. and again we conclude a good agreement with previous literature values.[24]

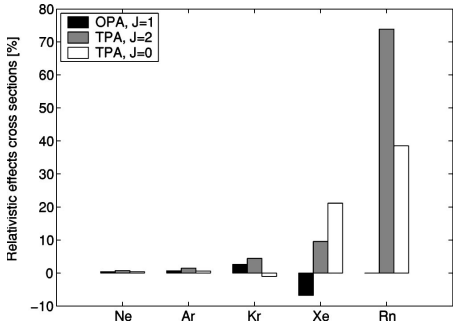

FIG. 4. The relativistic effects on the oscillator strengths and the two different two-photon absorption cross sections. (Note that the oscillator strengths has not been calculated for radon.)

To date, the most accurate nonrelativistic results for the monochromatic two-photon absorption cross sections in the noble gases are those of Hättig and co-workers.[4] They have applied a hierarchical set of coupled cluster response methods, using the taug-cc-pV5Z basis set,[16–18] in order to study the lowest two-photon transitions in helium, neon, and argon. Their best values correspond to coupled cluster calculations with inclusion of single and double excited configurations (CCSD). For the $^1S_0$ state in helium an excitation energy of 20.615 eV and a cross section of 12.306 a.u. are reported.[4] Our uncorrelated result for the cross section is 10.426 a.u., which agrees well with the correlated result. On the one hand, we expect the description of TP states that are spectroscopically separated from the linear absorption spectrum to be influenced by two electron excited configurations, and the random phase approximation may in such cases not be accurate. One example of this situation is given by the $X\,^1A_g \to 2\,^1A_g$ transition in *trans*-butadiene. But, on the other hand, for the noble gases the very large band gap prohibits the coupling to the doubly electron excited configurations, and our one-electron propagator approximation is therefore warranted in this case.

As mentioned above with respect to excitation energies, the effects of electron correlation are larger in neon than for any of the other atoms. In comparing our nonrelativistic uncorrelated results with the CCSD values of Hättig and co-workers,[4] it becomes clear that also the two-photon absorption cross sections in neon are strongly affected by electron correlation. For example, the TPA cross section of the $^1D_2$ state in neon is underestimated by almost 50% at the Hartree–Fock level of theory [CCSD results are $\Delta E = 18.532$ eV and $\delta_{\mathrm{TPA}} = 19.915$ a.u. (Ref. 4)], and the close agreement between uncorrelated and correlated results that we observe for the $^1S_0$ state is regarded as fortuitous [CCSD results are $\Delta E = 18.855$ eV and $\delta_{\mathrm{TPA}} = 12.559$ a.u. (Ref. 4)]. So electron correlation does play a significant role in calculations of the two-photon spectrum of neon when quantitative values for transition energies and intensities are desired, but the nonrelativistic approaches will inevitably fail at providing the leakage of intensity into the triplet manifold of states that we discussed earlier. We are not aware of any experimental two-photon spectra for neon, but, if measured, we predict a splitting of the absorption lines in accordance with the cross sections reported in Table II.

Finally, in comparison with the CCSD reference data of Hättig and co-workers,[4] we note that the quality of the Hartree–Fock results for the TPA cross sections in argon is relatively high. The CCSD results for the $^1D_2$ state are $\Delta E = 13.218$ eV and $\delta_{\mathrm{TPA}} = 104.59$ a.u., and, for the $^1S_0$ state, results are $\Delta E = 13.487$ eV and $\delta_{\mathrm{TPA}} = 197.71$ a.u.[4] The nonrelativistic Hartree–Fock results for the TPA cross sections given in Table III are in good agreement with the electron correlated results, and, in addition with the favorable comparison between experimental and Hartree–Fock values of

the excitation energies, we conclude that we account for a relatively accurate description of the electronic structure of ground and excited states in argon. We therefore argue that the strong two-photon absorption intensities of the triplet states shown in Table III at the relativistic level of theory should not be an artifact and due to lack of electron correlation in our treatment.

V. CONCLUSIONS

We report a first implementation of the response theory expression for the two-photon absorption matrix element at the four-component level of theory. We employ the Kramers restricted Hartree–Fock approximation with a direct atomic orbital driven construction of the Fock-type matrices needed in the evaluation of the response functions. The computational strategies and formulations parallel those for the quadratic response function at the same level of theory.[13]

A sample application in terms of the monochromatic two-photon absorption cross sections in the noble gases is presented. The calculations show enhanced relativistic effects on the property with the atomic number. A more conspicuous observation is the strong leakage of two-photon absorption cross section into the triplet manifold of states that occur for light as well as heavy elements. This effect, which is due to the electronic spin-orbit coupling, will provide splittings of absorption lines in the two-photon spectra. The present work underlines the need for inclusion of relativistic effects in two-photon absorption calculations in general.

ACKNOWLEDGMENTS

The authors thank Timo Fleig for helping them with relativistic configuration interaction results for neon. This work received financial support from Nordisk Forskerakademi (NorFA network Grant No. 030262) and the Danish Natural Science Research Council (Grant No. 21-02-0467). We acknowledge the use of computational resources at the National Supercomputer Centre (NSC) in Linköping, Sweden.

[1] M. Göppert-Mayer, Ann. Phys. **9**, 273 (1931).
[2] B. A. Reinhardt, Photonics Sci. News **4**, 21 (1998).
[3] H. Hettema, H. J. Aa. Jensen, P. Jørgensen, and J. Olsen, J. Chem. Phys. **97**, 1174 (1992).
[4] C. Hättig, O. Christiansen, and P. Jørgensen, J. Chem. Phys. **108**, 8355 (1998).
[5] P. Sałek, O. Vahtras, J. Guo, Y. Luo, T. Helgaker, and H. Ågren, Chem. Phys. Lett. **374**, 446 (2003).
[6] P. Norman and H. Ågren, J. Comp. Theoretical Nanoscience (to be published).
[7] J. D. Jackson, *Classical Electrodynamics*, 3rd ed. (Wiley, New York, 1999).
[8] P. Norman, D. M. Bishop, H. J. Aa. Jensen, and J. Oddershede, J. Chem. Phys. **115**, 10322 (2001).
[9] P. Macak, P. Cronstrand, A. Baev, P. Norman, F. Gel'mukhanov, Y. Luo, and H. Ågren, in *Nonlinear Optical Responses of Molecules, Solids and Liquids: Methods and Applications*, edited by M. G. Papadopoulos (Plenum, New York, 2003).
[10] W. M. McClain, J. Chem. Phys. **55**, 2789 (1971).
[11] J. Olsen and P. Jørgensen, J. Chem. Phys. **82**, 3235 (1985).
[12] T. Saue and H. J. Aa. Jensen, J. Chem. Phys. **118**, 522 (2003).
[13] P. Norman and H. J. Aa. Jensen, J. Chem. Phys. **121**, 6145 (2004).
[14] T. Saue and H. J. Aa. Jensen, J. Chem. Phys. **111**, 6211 (1999).
[15] H. J. Aa. Jensen, T. Saue, and L. Visscher with contributions from V. Bakken, E. Eliav, T. Enevoldsen *et al.*, DIRAC, a relativistic *ab initio* electronic structure program, Release DIRAC04.0 (2004), see http://dirac.chem.sdu.dk
[16] T. H. Dunning, Jr., J. Chem. Phys. **90**, 1007 (1989).
[17] D. E. Woon and T. H. Dunning, Jr., J. Chem. Phys. **98**, 1358 (1993).
[18] D. E. Woon and T. H. Dunning, Jr., J. Chem. Phys. **100**, 2975 (1994).
[19] S. Huzinaga and M. Klobukowski, Chem. Phys. Lett. **212**, 260 (1993).
[20] C. E. Moore, *Atomic Energy Levels: As Derived From the Analyses of Optical Spectra*, Natl. Bur. Stand. (U.S.) Circ. No. 467 (U.S. GPO, Washington, D.C., 1949), Vol. 1.
[21] C. E. Moore, *Atomic Energy Levels: As Derived From the Analyses of Optical Spectra*, Natl. Bur. Stand. (U.S.) Circ. No. 467 (U.S. GPO, Washington, D.C., 1958), Vol. 2.
[22] C. E. Moore, *Atomic Energy Levels: As Derived From the Analyses of Optical Spectra*, Natl. Bur. Stand. (U.S.) Circ. No. 467 (U.S. GPO, Washington, D.C., 1958), Vol. 3.
[23] R. Moccia and A. Rizzo, Mol. Phys. **51**, 1095 (1984).
[24] D. Sundholm, A. Rizzo, and P. Jørgensen, J. Chem. Phys. **101**, 4931 (1994).

Paper IV

First order excited state properties in the four-component Hartree–Fock approximation; the excited state electric dipole moments in CsAg and CsAu

IV

Erik Tellgren
Johan Henriksson
Patrick Norman

The Journal of Chemical Physics **126**, 064313 (2007)

THE JOURNAL OF CHEMICAL PHYSICS **126**, 064313 (2007)

First-order excited state properties in the four-component Hartree-Fock approximation: The excited state electric dipole moments in CsAg and CsAu

Erik Tellgren
Department of Chemistry, University of Oslo, P.O. Box 1033 Blindern, N-0315 Oslo, Norway

Johan Henriksson and Patrick Norman[a)]
Department of Physics, Chemistry and Biology, Linköping University, SE-581 83 Linköping, Sweden

(Received 22 November 2006; accepted 3 January 2007; published online 13 February 2007)

An implementation of the second-order residue of the quadratic response function is presented in the four-component Hartree-Fock approximation, and the calculation of first-order properties of electronically excited states can thereby be achieved. Results are presented for the excited state electric dipole moments of the valence excited states in CsAg and CsAu. For CsAg, and even more so for CsAu, nonscalar relativistic effects on this property may be substantial, e.g., at the four-component level of theory, the excited-to-ground state dipole moment difference $\Delta\mu$ ranges from 1.994 to 4.110 a.u. for the six components of the $1\ ^3\Pi$ state in CsAg, whereas, at the scalar relativistic level of theory, the common value of $\Delta\mu$ is 2.494 a.u. © *2007 American Institute of Physics*. [DOI: 10.1063/1.2436877]

I. INTRODUCTION

First-order molecular properties provide the linear correction to the molecular energy in the presence of a perturbing external or internal electromagnetic field and it also governs the linear absorption of radiation or, equivalently, the one-photon absorption. Whereas the determination of first-order properties of electronic ground states can be done to a high accuracy both in experiment and theory, the contrary is often true for excited states which is a fact that is prohibitive for the understanding of the photophysics of chromophores. For example, the electric dipole moment is a property that provides information about the molecular and electronic structure of short-lived electronically excited states. It determines the course of a photochemical transformation as well as the tunability in the emission energy as a function of the solvent polarity. In addition, the difference in dipole moment between the excited and the ground state ($\Delta\mu=\mu_e-\mu_g$) is a key parameter in the understanding and design of nonlinear optical materials.[1–5] In connection with the design of nonlinear optical materials, it is also important to address the excited state absorption and to understand the interplay between coherent nonlinear absorption in the ground state and the linear absorption in the excited state.[6–8]

There are several experimental techniques for determining the electric dipole moment of excited states, but a common denominator is that they measure the dependence of a transition energy with respect to an external electric field (either applied or from a polar solvent). Techniques based on solvent induced absorption or emission shifts for the determination of $\Delta\mu$ are time-resolved microwave dielectric absorption measurements,[9] solvatochromatic absorption and fluorescence shifts,[10,11] and thermochromic shifts of the solvent polarity.[12] An alternative to the solvent based approaches is offered by high-resolution optical Stark measurements on molecular beams.[13]

As far as the development of quantum chemical methods for the calculations of excited state properties is concerned, there are two main routes to follow. The first, and most straightforward, alternative is based on the optimization of the electronic density of the excited state, or states if it is a transition process, with a subsequent evaluation of the property of interest.[14] Such an approach does not maintain orthogonality among states and is limited to electronic structure methods that do provide an accurate description of the often complex, open-shell, nature of the excited states. The second alternative is based on a residue analysis of the nonlinear response functions of the ground state;[15] it avoids the explicit reference to the excited states and only the ground state wave function needs to be optimized. The method is gauge invariant in its exact as well as approximate state formulations, and it enables the determination of excited state properties also in the single determinant approximation (such as Hartree-Fock and Kohn-Sham theories). In approximate molecular electronic structure theory, we refer to the general formulation of time-dependent perturbation theory by Olsen and Jørgensen as *response theory*.[16]

In 1992, Hettema *et al.*[17] presented an implementation of the first-order nonlinear response function in the multiconfiguration self-consistent field approximation, and since then it has been implemented for most standard electronic structure methods including the nonrelativistic second-order Møller-Plesset,[18] coupled cluster,[19–22] and density functional theory[23] methods and the relativistic four-component Hartree-Fock method.[24,25] The present work continues this line of development with an implementation of the second-order residue of the quadratic response function at the four-component Hartree-Fock level of theory. The motivation for our work is that it enables the determination of first-order

a)Electronic mail: panor@ifm.liu.se

properties of electronically excited states for molecules that include heavy elements, such as, for instance, inorganic or organometallic compounds. Four-component approaches provide accurate treatment of relativistic effects. The results in the present work are adopting the instantaneous Coulombic electron-electron interaction but the theory and implementation is open-ended towards improvements, such as the Breit interaction, in the Hamiltonian. With the present Hamiltonian we take full account of the spin-own-orbit interaction, and we expect that corrections due to the spin-other-orbit interactions will be small for the properties of interest. The main uncertainty in the presented four-component results will be due to the neglect of electron correlation, and we see our work as the basis for future developments of the quadratic response function at various electron correlated levels of theory.

In the next section, we will make a brief presentation of the theory and point out the key points that distinguish it from its nonrelativistic counterpart in Ref. 17. We will then illustrate our work by determining the electric dipole moment of the valence excited states of CsAg and CsAu.

II. THEORY AND METHODOLOGY

The DIRAC program[26] includes modules for the calculation of linear[27] and quadratic[24,25] response functions at the relativistic four-component Hartree-Fock level of theory, and, in this work, we extend these functionalities to include first-order properties and transition moments of excited states. Our formulation follows that of the previous work and the implementation has been integrated with the existing modules of the program.

Our starting point is the Hartree-Fock ground state $|0\rangle$ of an unperturbed Hamiltonian $\hat{H}_0$. The time-dependent perturbed state is expressed using the exponential parametrization

$$|\psi(t)\rangle = e^{i\hat{\kappa}(t)}|0\rangle, \quad \hat{\kappa}(t) = \sum_n \kappa_n(t)\hat{q}_n^\dagger, \tag{1}$$

where the operator $\hat{\kappa}(t)$ is a Hermitian linear combination of excitation $(\hat{q}_{+|n|}^\dagger = \hat{a}_a^\dagger \hat{a}_i)$ and deexcitation operators $(\hat{q}_{-|n|}^\dagger = \hat{a}_i^\dagger \hat{a}_a)$ that transfer electrons from occupied i to virtual orbitals a. Hermiticity imposes the constraint $\kappa_{-n}(t) = \kappa_n^*(t)$ on the orbital transfer amplitudes.

The main difference compared to the nonrelativistic case is that one-particle states $\phi(\mathbf{r})$ in the four-component formalism take the form of complex bispinors

$$\phi(\mathbf{r}) = (\phi^{L\alpha}(\mathbf{r}), \phi^{L\beta}(\mathbf{r}), \phi^{S\alpha}(\mathbf{r}), \phi^{S\beta}(\mathbf{r}))^T, \tag{2}$$

and the one-electron part of the Hamiltonian is given by

$$\hat{h}_D = c\hat{\boldsymbol{\alpha}} \cdot \hat{\mathbf{p}} + \hat{\beta}mc^2 + \hat{V}_{\text{en}}, \tag{3}$$

where the Dirac-Pauli representation is chosen for the Dirac matrices ($\hat{\beta}$, $\hat{\alpha}^1$, $\hat{\alpha}^2$, and $\hat{\alpha}^3$) and $\hat{V}_{\text{en}}$ denotes the Coulomb potential from the nuclei multiplied with the electronic charge. To a first approximation, the two-electron part is formed from the instantaneous Coulomb interactions but additional terms such as the Gaunt or full Breit corrections may well be included. The perturbation added to the Hamiltonian is taken to be of the form

$$\hat{V}(t) = \sum_\alpha \varepsilon_\alpha(t)\hat{X}_\alpha, \tag{4}$$

where $\varepsilon_\alpha(t)$ is the time-dependent strength of the perturbing field and $\hat{X}_\alpha$ is the coupling operator between the field and the quantum mechanical system along the molecular axis α. The eigenvalues of the one-particle Hamiltonian in Eq. (3) (or Fock operator in the many-electron case) are split into two groups separated by twice the electron rest energy and the corresponding states are referred to as "electronic" and "positronic" in the respective groups. The excitation operators $\hat{q}_n^\dagger$ can excite the electrons from the occupied to virtual electronic orbitals as well as to the manifold of positronic orbitals. In a matrix representation one can, by exploiting the time reversal and quaternion symmetry of bispinors, reduce the dimension of operator matrices that need to be stored and diagonalized by a factor of 2, as explained by Saue *et al.*[28,29] and in the context of quadratic response by Norman and Jensen.[24]

The time dependence of the orbital transfer amplitudes $\kappa_n(t)$ is determined by perturbation theory, and the resulting equations of motion for the amplitudes are in general approximate state theory coupled and therefore solved in the frequency domain, rather than in the time domain. To linear order in the perturbation field strengths ε_α, one arrives at a matrix equation that reads as[21]

$$(\mathbf{E}^{[2]} - \omega\mathbf{S}^{[2]})\boldsymbol{\kappa}^\alpha(\omega) = \mathbf{g}^\alpha. \tag{5}$$

The frequency independent matrices are obtained from the expressions

$$E_{nm}^{[2]} = -\langle 0|[\hat{q}_{-n}^\dagger, [\hat{q}_m^\dagger, \hat{H}_0]]|0\rangle, \quad S_{nm}^{[2]} = \langle 0|[\hat{q}_{-n}^\dagger, \hat{q}_m^\dagger]|0\rangle,$$
$$g_n^\alpha = \langle 0|[\hat{q}_{-n}^\dagger, \hat{X}_\alpha]|0\rangle. \tag{6}$$

Because of Wigner's $2n+1$ rule, the linear response of the wave function is sufficient to determine the quadratic response functions and, in particular, their residues. For our purposes it is therefore sufficient to determine the linear response in the orbital transfer amplitudes [Eq. (5)].

Although the exact many-body energy eigenstates $|k\rangle$ and excitation energies ω_k are not available, it is instructive to consider the sum-over-state expression for the quadratic response function, i.e.,

$$\langle\langle \hat{X}_\alpha; \hat{X}_\beta, \hat{X}_\gamma \rangle\rangle_{\omega_\beta, \omega_\gamma} = -\sum_{\mathcal{P}} \sum_{k,l>0} \frac{\langle 0|\hat{X}_\alpha|k\rangle\langle k|\bar{X}_\beta|l\rangle\langle l|\hat{X}_\gamma|0\rangle}{(\omega_\alpha + \omega_k)(\omega_\gamma - \omega_l)}, \tag{7}$$

where $\bar{X}_\beta = \hat{X}_\beta - \langle 0|\hat{X}_\beta|0\rangle$ and $\Sigma_{\mathcal{P}}$ generates the sum of terms obtained from permutations of the indices α, β, and γ. Excited state properties and transition moments appear in the numerators and may be obtained as residues of the exact quadratic response functions. Response theory therefore constitutes a natural framework for calculating excited state transition moments. Moreover, the formalism is sufficiently ge-

neric to be directly applicable at the four-component relativistic level of theory.

Returning to the Hartree-Fock approximation, we obtain representations of the excited states by solving the generalized eigenvalue equation

$$\mathbf{E}^{[2]}\mathbf{U} = \mathbf{S}^{[2]}\mathbf{U}\boldsymbol{\Omega}, \tag{8}$$

where $\Omega_{kl}=\mathrm{sgn}(k)\omega_{|k|}\delta_{kl}$ is a diagonal matrix containing the excitation energies. The kth column $U^{(k)}$ of $\mathbf{U}$ represents the kth excited state. Within the Hartree-Fock approximation, an excited state transition moment may be obtained, in analogy with the exact case, as a residue of a quadratic response function[21]

$$\langle k|\hat{X}_\alpha|l\rangle - \delta_{kl}\langle 0|\hat{X}_\alpha|0\rangle = [\mathbf{F}^\alpha + \mathbf{G}(-\omega_k,\omega_f)\boldsymbol{\kappa}^\alpha(\omega_k-\omega_f)]U^{(-k)}U^{(f)}, \tag{9}$$

where

$$F^\alpha_{kl} = \tfrac{1}{2}\sum_{\mathcal{P}}\langle 0|[[\hat{X}_\alpha,\hat{q}^\dagger_k],\hat{q}^\dagger_l]|0\rangle \tag{10}$$

and

$$G_{klm}(\omega_\beta,\omega_\gamma) = \tfrac{1}{6}\sum_{\mathcal{P}}(\langle 0|[[[\hat{H}_0,\hat{q}^\dagger_k],\hat{q}^\dagger_l],\hat{q}^\dagger_m]|0\rangle + (\omega_\beta+\omega_\gamma)\langle 0|[[\hat{q}^\dagger_k,\hat{q}^\dagger_l],\hat{q}^\dagger_m]|0\rangle). \tag{11}$$

Our implementation is Kramers restricted and handles the spatial D_{2h} point group and subgroups thereof and it exploits the quaternion symmetry of four-component wave functions.[28,29] Furthermore, since we employ the first-order polarization propagator approach, or random phase approximation, we can provide an accurate description only for excited states that are dominated by single excitations.

The perturbation operator [Eq. (4)] is assumed to be a one-electron operator and the two-electron Hamiltonian operator is handled by constructions of modified Fock matrices but with the generic routines in the program. That means that the computational scaling of the implementation of first-order excited state properties parallels that of other parts of the program, such as the self-consistent field optimization of the electron density. A discussion on the computational scaling of the evaluation of the quadratic response function at the four-component Hartree-Fock level of theory is found in Ref. 30.

The program flow in the excited state property module is such that, for each irreducible representation, Eq. (8) is solved to obtain the requested number of excited states and transition frequencies, and then Eq. (5) is solved for all requested operators $\hat{X}_\alpha$ and frequencies corresponding to the excitation energies. Finally, the excited state properties and moments are assembled according to Eq. (9).

III. SAMPLE CALCULATIONS

We illustrate our implementation with calculations of the electric dipole moment of the lowest valence excited states of CsAg and CsAu. These systems have been the subject for previous studies concerned with spectroscopic constants, dissociation energies, and ground state dipole moments[31,32] as well as excitation energies, polarizabilities, and hyperpolarizabilities.[24] CsAu (but not CsAg) has been observed experimentally in solid, liquid, and gas phases.

A. Computational details

We have used the bond lengths of 3.316 and 3.263 Å for CsAg and CsAu, respectively, which correspond to the optimized structures at the relativistic coupled cluster singles and doubles (CCSD) with perturbative triples level of theory.[31] The molecules are placed with the coinage metal atoms at the origin and Cs pointing along the positive z axis, a direction which thereby coincides with that of the ground state dipole moment.

For the all-electron calculations, we have employed the uncontracted dual family Gaussian basis sets from the work of Fossgaard *et al.*[31] and augmented these with diffuse functions. The exponents added were determined from a geometric series based on the two smallest exponents in each shell of the original basis sets, and the sizes of the final basis sets were $[23s19p13d4f]$, $[23s18p11d2f]$, and $[24s19p15d9f]$ for Ag, Cs, and Au, respectively. For the calculations using relativistic effective-core potentials (ECPs), we have used the Stuttgart ECPs (Ref. 33) together with the valence parts of the basis sets described above. The sizes of the employed valence basis sets were $[11s10p8d4f]$, $[10s9p6d2f]$, and $[10s8p8d3f]$ for Ag, Cs, and Au, respectively, and the number of electrons included in our wave function parametrization with ECPs were 19, 9, and 19 for Ag, Cs, and Au, respectively.

In the four-component calculations we represented the nuclei with Gaussian charge distributions with exponents of 2.0389×10^8, 1.7951×10^8, and 1.4223×10^8 a.u. for silver, cesium, and gold nuclei, respectively. The small component basis sets were generated from the large component ones by adopting the condition of restricted kinetic balance. The four-component calculations make full account for polarization of the electronic states due to the positronic states, i.e., all e-p rotations are included in the response calculations, and the purely small component integrals $(SS|SS)$ are included in the calculations. Approximations in the calculations of quadratic response functions can be made without significant loss in accuracy[30] but, due to the modest size of the systems in the present work, such approximations have not been called for.

The nonrelativistic as well as the ECP calculations have been performed with a version of the DALTON program[34] that has been extended to include the Coulomb attenuated exchange-correlation functional CAM-B3LYP by Peach *et al.*,[35] whereas the four-component calculations have been performed with a locally modified version of the DIRAC program.[26]

B. Results and discussion

The chemical bonds between the coinage metal atoms and cesium are strongly polar and the ionicity is to a large extent attributed to the relativistic contractions of the 5s and 6s orbitals of silver and gold, respectively.[31] We have determined the electronic properties of the ground and valence excited states at the ground state equilibrium geometry, and

TABLE I. Excitation energies (eV), dipole moments (a.u.), and oscillator strengths for the low-lying states of nonrelativistic Σ^+ and Π symmetries in CsAg. The total angular momentum M_J labels the states in the relativistic calculations. The superscript on states with $M_J=0$ indicates the symmetry under σ_v reflections.

	Nonrelativistic			Spin-free				Four component		
Sym	ΔE	$\Delta\mu$	f	ΔE	$\Delta\mu$	f	$\lvert M_J\rvert$	ΔE	$\Delta\mu$	f
$^3\Pi$	[a]	[a]	[a]	0.381	2.494	0	0^-	0.215	4.110	0
							0^+	0.234	3.959	0.0000
							1	0.373	2.427	0.0000
							2	0.489	1.994	0
$^3\Sigma^+$	0.534	−4.714	0	0.694	−4.226	0	0^-	0.701	−4.085	0
							1	0.699	−4.099	0.0000
$^3\Sigma^+$	1.526	1.258	0	1.810	1.096	0	0^-	1.809	1.065	0
							1	1.810	1.068	0.0000
$^1\Sigma^+$	1.746	−3.480	0.3377	1.918	−3.573	0.3438	0^+	1.919	−3.572	0.3427
$^1\Pi$	2.107	−1.324	0.3859	2.347	−1.456	0.3631	1	2.348	−1.475	0.3608
$^3\Sigma^+$	2.265	−6.137	0	2.551	−6.168	0	0^-	2.544	−5.665	0
							1	2.550	−5.944	0.0020
$^3\Pi$	2.292	−4.814	0	2.574	−4.877	0	0^+	2.563	−4.841	0.0019
							0^-	2.574	−5.348	0
							1	2.580	−5.059	0.0001
							2	2.588	−4.886	0
$^1\Sigma^+$	2.495	−4.159	0.0220	2.774	−3.848	0.0185	0^+	2.776	−3.840	0.0188
$^1\Sigma^+$	2.680	1.279	0.1070	2.905	0.368	0.1005	0^+	2.907	0.342	0.0997
$^1\Pi$	2.670	−2.488	0.0468	2.960	−2.443	0.0510	1	2.962	−2.450	0.0506
$^3\Sigma^+$	2.874	−3.615	0	3.131	−5.270	0	0^-	3.133	−5.261	0
							1	3.133	−5.261	0.0000
$^1\Sigma^+$	3.001	−2.942	0.0042	3.254	−2.952	0.0017	0^+	3.256	−2.909	0.0018
$^3\Sigma^+$	2.996	2.184	0	3.267	4.456	0	0^-	3.269	4.437	0
							1	3.269	4.441	0.0000

[a]The states are triplet instable and therefore not reported.

our results are therefore mainly pertinent to absorption spectroscopy since in emission spectroscopy nuclear relaxation in the excited state is an issue. An extension of response theory to include nuclear dynamics in the excited state has been done in the nonrelativistic realm (see, e.g., Ref. 36) but such a consideration is beyond the scope of the present work.

1. Absorption spectra

The vertical electronic absorption spectra of CsAg and CsAu as given in the four-component Hartree-Fock approximation have been presented and discussed by Norman and Jensen.[24] Excitation energies and oscillator strengths of the low-lying states are reported also in this work and differ slightly from those in Ref. 24 due to inclusion of diffuse functions to the basis sets. In the nonrelativistic (and spin-free) calculations, the states are characterized by their total separate spin and orbital angular momentum projection on the bond axis, whereas, in the relativistic calculations, the generator of rotations about the internuclear axis is the total angular momentum operator $\hat{J}_z$ and the states are characterized by the corresponding quantum number M_J. The relativistic selection rule for one-photon absorption is $\Delta M_J=\pm 1$ or $\Delta M_J=0$ with maintained symmetry with respect to σ_v reflections.

In Tables I and II we present results from Hartree-Fock calculations at the nonrelativistic (NR), the spin-free (SF),[37] and the fully relativistic four-component (4C) levels of theory. The SF calculations include scalar relativistic effects only, and by comparing SF and 4C results it is thus possible to quantify the importance of spin-orbit interactions. The lowest state in CsAg is the $1\ ^3\Pi$ state (the state is not resolved in the nonrelativistic calculation due to the problem of triplet instability), which in the four-component calculations corresponds to the set of states $\{0^-,0^+,\pm 1,\pm 2\}$ that are spin orbit splitted by 0.27 eV. Next follows two states of $^3\Sigma^+$ symmetry with nonrelativistic transition energies of 0.534 and 1.526 eV, respectively. The spin-orbit splittings in these states are less than 0.01 eV and the relativistic corrections to the excitation energies are almost fully retrieved at the scalar relativistic level of theory. The optical characteristics of CsAg in the visible region are governed by the $1\ ^1\Sigma^+$ and $1\ ^1\Pi$ states with NR values for ΔE that equal to 1.746 and 2.107 eV, respectively. For the valence transitions within the singlet manifold in CsAg, it is in general seen that the spin-orbit effects are negligible.

If we turn attention to CsAu (see Table II), it is clear that nonscalar relativistic effects become more prominent and a nonrelativistic labeling of states is less meaningful. In this case the optically most active states are the 0^+ state with $\Delta E=2.551$ eV and the twofold degenerate $\lvert M_J\rvert=1$ state with $\Delta E=3.129$ eV. As a consequence of the large relativistic contraction of the gold 6*s* orbital, the discrepancies in the nonrelativistic spectrum are substantial, both with respect to transition energies and intensities (as governed by the oscillator strengths). The nonrelativistic excitation energies severely underestimate the relativistic ones (e.g., the NR tran-

TABLE II. Excitation energies (eV), dipole moments (a.u.), and oscillator strengths for the low-lying states of nonrelativistic Σ^+ and Π symmetries in CsAu. The total angular momentum M_J labels the states in the relativistic calculations. The superscript on states with $M_J=0$ indicates the symmetry under σ_v reflections.

	Nonrelativistic			Spin-free				Four component		
Sym	ΔE	$\Delta\mu$	f	ΔE	$\Delta\mu$	f	$\lvert M_J\rvert$	ΔE	$\Delta\mu$	f
$^3\Pi$	[a]	[a]	[a]	1.545	0.337	0	0^-	1.261	0.442	0
							1	1.454	0.218	0.0005
							0^+	1.347	0.446	0.0007
							2	1.670	0.316	0
$^3\Sigma^+$	0.669	−4.040	0	1.722	−2.694	0	1	1.765	−2.263	0.0000
							0^-	1.775	−2.444	0
$^3\Sigma^+$	1.694	1.123	0	2.674	−0.577	0	1	2.664	−0.923	0.0011
							0^-	2.668	−0.880	0
$^1\Sigma^+$	1.804	−3.743	0.3392	2.531	−5.069	0.2067	0^+	2.551	−5.073	0.2030
$^1\Pi$	2.173	−1.385	0.4071	3.107	−2.228	0.2647	1	3.129	−2.205	0.2599
$^3\Sigma^+$	2.371	−5.565	0	3.419	−6.334	0	0^-	3.434	−5.821	0
							1	3.440	−6.079	0.0005
$^3\Pi$	2.442	−4.243	0	3.470	−5.156	0	0^+	3.461	−5.093	0.0059
							0^-	3.477	−5.554	0
							1	3.490	−5.253	0.0001
							2	3.504	−5.054	0
$^1\Sigma^+$	2.633	−2.726	0.0160	3.573	−2.899	0.0319	0^+	3.598	−2.888	0.0319
$^1\Sigma^+$	2.755	0.071	0.1126	3.730	−2.041	0.1055	0^+	3.752	−2.146	0.1000
$^1\Pi$	2.793	−1.112	0.0351	3.818	−1.898	0.0499	1	3.838	−1.995	0.0457
$^3\Sigma^+$	2.960	−4.940	0	3.975	−5.721	0	0^-	3.992	−5.211	0
							1	3.994	−5.291	0.0004
$^3\Pi$	2.974	1.701	0	4.074	1.138	0	1	4.100	1.128	0.0000
							2	4.100	1.129	0
							0^+	4.134	−3.703	0.0048

[a]The states are triplet instable and therefore not reported.

sition energy of the $1\,^1\Pi$ state is 0.96 eV below its relativistic counterpart for the $|M_J|=1$ state), whereas the situation is reversed for the oscillator strengths (e.g., the oscillator strength of the nonrelativistic $1\,^1\Pi$ state is exceeding that of the relativistic $|M_J|=1$ state by 57%). In a.u., the expression for the oscillator strength is

$$f^{0n} = \frac{2\Delta E}{3}\sum_{\alpha} |\langle 0|\hat{\mu}_\alpha|n\rangle|^2, \tag{12}$$

where $\hat{\mu}_\alpha$ is the electric dipole moment operator along the molecular axis α. It is therefore clear that the reason for the overestimated oscillator strengths in the nonrelativistic limit is due to severely overestimated transition dipole moments, as also shown in Ref. 24.

2. Excited state dipole moments

From the double residue of the quadratic response function, which forms the basis for our implementation, the emerging quantity is the excited-to-ground state *difference* in properties. The excited state property is retained only after adding the ground state property obtained at the same level of theory. But, as mentioned in Sec. I, measurements of excited state dipole moments are based on chromatic shifts which are also dependent on $\Delta\mu=\mu_e-\mu_g$, so, in the tables, we have chosen to present $\Delta\mu$ and μ_g rather than μ_e. The excited-to-ground state difference in dipole moments is a direct reflection of the electronic charge flow in the absorption process. The ground state dipole moments at the four-component Hartree-Fock level are 3.612 and 4.261 a.u. for CsAg and CsAu, respectively, which, considering the bond lengths, correspond to effective charges of $-0.58e$ and $-0.69e$ on silver and gold in the respective compounds. Our act of expressing the dipole moments in this work as atomic charge shifts is of course not to be taken literally but as a convenient measure of dipole moments and dipole moment fluctuations.

The results for $\Delta\mu$ in CsAg are presented in Table I. In connection with the lowest transition, i.e., $1\,^3\Pi \leftarrow X\,^1\Sigma^+$, there is an electron charge flow from cesium to silver that is increasingly pronounced with diminishing projection of the angular momentum along the bond axis. For the $|M_J|=2$ and 0^- states the effective charges on silver are reduced from $-0.57e$ by another $-0.32e$ and $-0.67e$, respectively. The difference in charge flow between the different components of the $1\,^3\Pi$ state is a pure effect of spin-orbit coupling, and the nonrelativistic and scalar relativistic calculations therefore predict intermediate values for the charge flows but identical for all six state components. In contrast we note that, in the $1\,^3\Sigma^+ \leftarrow X\,^1\Sigma^+$ transition, electron charge flows from silver to cesium and the effective charges of silver in the $|M_J|=1$ and 0^- states are almost identical and equal to about $+0.08e$. In other words, in this transition silver returns more electron charge than it retrieved in the formation of the ionic bond in the ground state. The optically active states ($1\,^1\Sigma^+$ and $1\,^1\Pi$) both have a reduced dipole moment as compared to the

TABLE III. Excitation energies (eV) and dipole moments (a.u.) of the lowest nonrelativistically dipole allowed states in CsAg and CsAu.

			$1\,^1\Sigma^+$		$1\,^1\Pi$	
Method		μ_g	ΔE	$\Delta\mu$	ΔE	$\Delta\mu$
			CsAg			
HF	NR	3.540	1.746	−3.480	2.107	−1.324
	ECP	3.531	1.936	−3.366	2.373	−1.308
	SF	3.615	1.918	−3.573	2.347	−1.456
	4C	3.612	1.919	−3.572	2.348	−1.475
DFT[a]	NR	3.646	1.913	−3.879	2.254	−2.590
	ECP	3.704	2.131	−3.718	2.866	−2.568
CCSD	ECP	3.983	2.290	−4.724	3.093	−2.682
			CsAu			
HF	NR	3.576	1.804	−3.743	2.173	−1.385
	ECP	4.210	2.533	−4.897	3.127	−2.145
	SF	4.261	2.531	−5.069	3.107	−2.228
	4C	4.261	2.551	−5.073	3.129	−2.205
DFT[a]	NR	3.690	2.004	−4.182	2.625	−2.417
	ECP	4.228	2.740	−5.039	3.673	−2.713
CCSD	ECP	4.440	3.057	−5.596	3.993	−2.956

[a]Refers to calculations with the CAM-B3LYP exchange-correlation functional.

ground state; in the former state the effective charge on silver is $-0.006e$ and in the latter it is $-0.34e$. Spin-orbit effects are of course insignificant for the properties of the $1\,^1\Sigma^+$ state due to the zero spin and orbital angular momentum in this state and since it is a case of *L-S* coupling; the scalar relativistic effects on $\Delta\mu$ amount to less than 3%. In the $1\,^1\Pi$ state, relativistic effects on $\Delta\mu$ amount to 10%, out of which 1.3% is attributed to spin-orbit coupling.

The results for $\Delta\mu$ in CsAu are presented in Table II. Whereas the $1\,^3\Pi \leftarrow X\,^1\Sigma^+$ transition in CsAg was accompanied by large flow of electron charge from Cs to the coinage metal atom, this is not the case in CsAu where the charge transport amounts to $0.04e-0.07e$ for the different state components. In the lowest nonrelativistically dipole allowed transition ($1\,^1\Sigma^+ \leftarrow X\,\Sigma^{+1}$), there is a large change in the dipole moment ($\Delta\mu=-5.073$ a.u.) which corresponds to a charge transfer of $0.82e$ from gold to cesium. Charge flows in the same direction but to a lesser extent in the $1\,^1\Pi \leftarrow X\,^1\Sigma^+$ transition; the change in dipole moment equals −2.205 a.u., which corresponds to a charge transfer of $0.36e$.

3. Effects of electron correlation

So far, we have made accurate account of relativistic effects in the calculation of excited state dipole moments, but made no estimate of errors concerned with the neglect of electron correlation. We mentioned in the Introduction that our development of the double residue of the quadratic response function in this work is to be seen as a first step towards future implementations for electron correlated four-component methods. Nevertheless, we can already, at this point, estimate the quality of our results for $\Delta\mu$ of CsAg and CsAu with respect to electron correlation by employing implementations made for nonrelativistic electronic structure methods in conjunction with the use of relativistic effective-core potentials. We will focus our attention at the lowest optically active states which are referred to as $1\,^1\Sigma^+$ and $1\,^1\Pi$ in a nonrelativistic framework. In doing so we avoid the $^3\Pi$ states, where valence spin-orbit effects proved large already for the lighter CsAg compound and where the ECP approach as well as scalar relativistic methods are bound to fail.

Before turning to the question of electron correlation, let us start by evaluating the potential accuracy of the ECP approach in the favorable cases of the optically active states. The four-component Hartree-Fock results for ΔE of the $1\,^1\Sigma^+$ and $1\,^1\Pi$ states of CsAg and CsAu are 1.919, 2.348, 2.551, and 3.129 eV, respectively, and the errors in the corresponding nonrelativistic calculations are −0.17, −0.24, −0.75, and −0.96 eV (see Table III). With the use of small-core ECPs the errors are reduced to +0.02, +0.02, −0.02, and 0.00 eV. The accuracy of the ECP calculations are not quite as high for the quadratic response property $\Delta\mu$. With maintained ordering of states and molecules, we note discrepancies for the $\Delta\mu$ results of 3%, 10%, 26%, and 37% in the nonrelativistic calculations and 6%, 11%, 3%, and 3% in the ECP calculations. For $\Delta\mu$ in CsAu the relativistic effects are well reproduced in the ECP calculations, whereas in the case of $\Delta\mu$ in CsAg the relativistic effects are quite small and thereby error sensitive for that reason. We estimate the error bar in the uncorrelated ECP calculations of $\Delta\mu$ to be 0.20 a.u. and expect that error bar to give a fair indication of the accuracy also in the correlated ECP calculations on the optically active states.

The inclusion of electron correlation strengthens the bonds in the compounds,[31] which is accompanied by enhanced ground state dipole moments, see Table III. At the relativistic CCSD(T) level of theory, the ground state dipole moments were reported by Fossgaard *et al.*[31] to be equal to 4.206 and 4.615 a.u. for CsAg and CsAu, respectively. Using ECPs, our CCSD results for μ_g of CsAg and CsAu are 3.983

and 4.440 a.u., respectively, which indicate that the ground state ionicity is slightly underestimated at the CCSD/ECP level of theory. For the excited-to-ground state dipole moment differences the CCSD/ECP results are the best reference values that we can produce at this time.

We have also reported results obtained at the density functional theory (DFT) level using the Coulomb attenuated hybrid exchange-correlation functional CAM-B3LYP (Ref. 38) and ECPs. We are primarily interested in these results in order to get an indication of the performance that one can expect from a future implementation of the quadratic response function at the four-component DFT level of theory. It has been noted above that the valence transitions of interest are associated with large reorganization of electron charge, and it therefore becomes important to have an appropriate long-range Coulomb interaction to describe the electron-hole interaction correctly. For that reason we have utilized the Coulomb attenuated functional proposed by Yanai *et al.*[38] Using the CCSD results as reference, we see that the DFT calculations of $\Delta\mu$ in the $1\,^1\Pi$ state of CsAg and CsAu capture 92% and 70% of the correlation effects. This is a very promising performance for such a sensitive property as the second-order residue of the quadratic response functions in a system with large redistribution of electron charge at the resonances of interest. However, turning to the calculations of the dipole moment of the $1\,^1\Sigma^+$ states in the two molecules, the DFT results are far from convincing—as little as 26% and 20% of the correlation effects are accounted for in the DFT calculations. We are inclined to believe that the difficulties for DFT to correctly describe the change in dipole moment in the $1\,^1\Sigma^+ \leftarrow X\,^1\Sigma^+$ transition are attributed to the very large reorganization of charge that takes place and which makes the calculation extraordinarily sensitive to the description of the long-range Coulomb interactions: the charge transfers of this transition are $0.57e$ and $0.82e$ in CsAg and CsAu, respectively. In the $1\,^1\Pi \leftarrow X\,^1\Sigma^+$ transition the charge transfers are much less; they amount to $0.23e$ and $0.36e$ for CsAg and CsAu, respectively. The larger flow of charge in the latter case correlates very well with the reduced performance of DFT (capturing only 70% of the correlation effects), and there seems to be a limit of charge transfer somewhere around $0.25e$ beyond which the use of the current functional is not reliable for calculations of excited state dipole moments.

IV. CONCLUSIONS

We have presented an implementation of the second-order residue of the quadratic response function in the four-component Hartree-Fock approximation and can thereby determine first-order properties of electronically excited state. Apart from being restricted to one-electron properties, the implementation is general and in the present work illustrated by the calculation of the dipole moment of the valence excited states in CsAg and CsAu. The accuracy of results with respect to relativistic effects is set by the representation of the relativistic electron-electron interaction operator in the zeroth-order Hamiltonian. Since our implementation of the excited state property is based on the construction of Fock matrices from modified density matrices, the computational scaling and handling of two-electron integrals parallel that of other modules in the program such as the self-consistent field optimization of the reference state.

The electron correlation effects are in most cases substantial in the evaluation of the quadratic response function, e.g., the correlation effects on the excited-to-ground state dipole moment difference ($\Delta\mu=\mu_e-\mu_g$) for the $1\,^1\Sigma^+$ and $1\,^1\Pi$ states amount, respectively, to 40% and 105% for CsAg and 14% and 38% for CsAu. We were not able to draw firm conclusions about the ability to retrieve the correlation contribution to $\Delta\mu$ from density functional theory methods. The results indicate that density functional theory in combination with the Coulomb attenuated functional of Yanai *et al.*[38] performs well for calculations of $\Delta\mu$ in cases where the charge transfer between the two atoms is less than $0.25e$ but performs poorly when the charge transfer exceeds $0.50e$.

ACKNOWLEDGMENTS

The authors acknowledge financial support from the European Marie Curie Research and Training Network NANOQUANT (Grant No. MCRTN-CT-2003-506842) and from Nord-Forsk (Grant No. 030262). A grant for computing time at the National Supercomputer Centre (NSC), Sweden is also gratefully acknowledged.

[1] J. Abe, Y. Shirai, N. Nemoto, F. Miyata, and Y. Nagase, J. Phys. Chem. B **101**, 576 (1997).
[2] F. W. Vance, L. Karki, J. K. Reigle, J. T. Hupp, and M. A. Ratner, J. Phys. Chem. A **102**, 8320 (1998).
[3] L. Karki, F. W. Vance, J. T. Hupp, S. M. LeCours, and M. J. Therien, J. Am. Chem. Soc. **120**, 2606 (1998).
[4] M. Yamashita, S. Kikuma, Y. Yamaoka, H. Murakami, R. Morita, and H. Shigekawa, Appl. Phys. Lett. **75**, 28 (1999).
[5] P. Cronstrand, P. Norman, Y. Luo, and H. Ågren, J. Chem. Phys. **121**, 2020 (2004).
[6] J. Rogers, J. Slagle, D. McLean, R. Sutherland, B. Sankaran, R. Kannan, L.-S. Tan, and P. Fleitz, J. Phys. Chem. A **108**, 5514 (2004).
[7] P. Foggi, F. V. R. Neuwahl, L. Moroni, and P. R. Salvi, J. Phys. Chem. A **107**, 1689 (2003).
[8] P. Norman and H. Ågren, J. Comput. Theor. Nanosci. **1**, 343 (2004).
[9] A. Samanta, S. Saha, and R. W. Fessenden, J. Phys. Chem. A **105**, 5438 (2001).
[10] J. Kabatc, B. Osmialowski, and J. Paczkowski, Spectrochim. Acta, Part A **63**, 524 (2006).
[11] A. M. Wiosetek-Reske, S. Wysocki, and G. W. Bak, Spectrochim. Acta, Part A **62**, 1172 (2005).
[12] A. Kawski, B. Kuklinski, and P. Bojarski, Chem. Phys. Lett. **425**, 257 (2006).
[13] C. Kang, J. T. Yi, and D. W. Pratt, Chem. Phys. Lett. **423**, 7 (2006).
[14] M. Merchán, L. Serrano-Andrés, M. P. Fülscher, and B. O. Roos, in *Recent Advances in Multireference Theory*, edited by K. Hirao (World Scientific, Singapore, 1999), Vol. 4, p. 161.
[15] P. Norman and K. Ruud, in *Nonlinear Optical Properties of Matter: From Molecules to Condensed Phases*, edited by M. G. Papadopoulos, A. J. Sadlej, and J. Leszczynski (Springer, New York, 2006), Chap. 1.
[16] J. Olsen and P. Jørgensen, J. Chem. Phys. **82**, 3235 (1985).
[17] H. Hettema, H. J. Aa. Jensen, P. Jørgensen, and J. Olsen, J. Chem. Phys. **97**, 1174 (1992).
[18] J. Rice and N. Handy, Int. J. Quantum Chem. **43**, 91 (1992).
[19] C. Hättig, O. Christiansen, H. Koch, and P. Jørgensen, Chem. Phys. Lett. **269**, 428 (1997).
[20] O. Christiansen, A. Halkier, H. Koch, P. Jørgensen, and T. Helgaker, J. Chem. Phys. **108**, 2801 (1998).
[21] O. Christiansen, P. Jørgensen, and C. Hättig, Int. J. Quantum Chem. **68**, 1 (1998).
[22] J. Gauss, O. Christiansen, and J. Stanton, Chem. Phys. Lett. **296**, 117

(1998).
[23] P. Salek, O. Vahtras, T. Helgaker, and H. Ågren, J. Chem. Phys. **117**, 9630 (2002).
[24] P. Norman and H. J. Aa. Jensen, J. Chem. Phys. **121**, 6145 (2004).
[25] J. Henriksson, P. Norman, and H. J. Aa. Jensen, J. Chem. Phys. **122**, 114106 (2005).
[26] H. J. Aa. Jensen, T. Saue, L. Visscher *et al.* DIRAC, a relativistic *ab initio* electronic structure program, Release DIRAC04.0, 2004.
[27] T. Saue and H. J. Aa. Jensen, J. Chem. Phys. **118**, 522 (2003).
[28] T. Saue, K. Fægri, T. Helgaker, and O. Gropen, Mol. Phys. **91**, 937 (1997).
[29] T. Saue and H. J. Aa. Jensen, J. Chem. Phys. **111**, 6211 (1999).
[30] J. Henriksson, U. Ekström, and P. Norman, J. Chem. Phys. **124**, 214311 (2006).
[31] O. Fossgaard, O. Gropen, E. Eliav, and T. Saue, J. Chem. Phys. **119**, 9355 (2003).
[32] L. Belpassi, F. Tarantelli, A. Sgamellotti, and H. M. Quiney, J. Chem. Phys. **122**, 184109 (2005).
[33] D. Andrae, U. Haussermann, M. Dolg, H. Stoll, and H. Preuss, Theor. Chim. Acta **77**, 123 (1990).
[34] DALTON, a molecular electronic structure program, Release 2.0, 2005 (see http://www.kjemi.uio.no/software/dalton/dalton.html).
[35] M. J. G. Peach, T. Helgaker, P. Salek, T. W. Keal, O. B. Lutnæs, D. J. Tozer, and N. C. Handy, Phys. Chem. Chem. Phys. **8**, 558 (2006).
[36] A. Köhn and C. Hättig, J. Chem. Phys. **119**, 5021 (2003).
[37] L. Visscher and T. Saue, J. Chem. Phys. **113**, 3996 (2000).
[38] T. Yanai, D. P. Tew, and N. C. Handy, Chem. Phys. Lett. **393**, 51 (2004).

Paper V

On the evaluation of quadratic response functions at the four-component Hartree–Fock level: Nonlinear polarization and two-photon absorption in bromo- and iodobenzene

Johan Henriksson
Ulf Ekström
Patrick Norman

V

The Journal of Chemical Physics **124**, 214311 (2006)

THE JOURNAL OF CHEMICAL PHYSICS **124**, 214311 (2006)

On the evaluation of quadratic response functions at the four-component Hartree-Fock level: Nonlinear polarization and two-photon absorption in bromo- and iodobenzene

Johan Henriksson, Ulf Ekström, and Patrick Norman[a)]
Department of Physics, Chemistry, and Biology, Linköping University, SE-581 83 Linköping, Sweden

(Received 28 March 2006; accepted 19 April 2006; published online 7 June 2006)

The nonlinear polarization and two-photon absorption parameters have been determined for dibromo- and di-iodobenzene in their *meta*- and *ortho*-conformations and with relativistic effects accounted for to a varying degree. By exclusion of small component integrals in the calculations of the first-order hyperpolarizability, results within 1% of fully relativistic four-component Hartree-Fock values are obtained at a cost of 8.7 times the corresponding nonrelativistic calculations. It is shown that the nonlinear absorption in bromobenzene (and even more so in iodobenzene) is broad banded due to spin-orbit interactions among the excited states, and nonrelativistic and scalar relativistic calculations are not to be used in this case. © *2006 American Institute of Physics*. [DOI: 10.1063/1.2204604]

I. INTRODUCTION

The design of molecular materials with large and specific nonlinear optical responses has attracted a wide-spread experimental as well as theoretical interest, see for instance the book edited by Papadopoulos *et al.*[1] for a recent account. Among the first principles approaches in quantum chemistry a formulation of time-dependent perturbation theory known as *response theory* has proven to be a most successful platform for the design of efficient computational schemes, and the work of Olsen and Jørgensen[2] from 1985 is considered by many to be a starting point in this development. A more modern formulation of response theory that incorporates variational and nonvariational electronic structure methods on the same footing is provided by Christiansen *et al.*,[3] and recently the theory has also been extended by Norman *et al.*[4] to include near-resonant and resonant regions of the spectra.

The general response theory is formulated in such a way that explicit formulas for the response functions that collect orders in the responses to the perturbing fields can be derived. As far as nonlinear response functions are concerned there exist today implementations for virtually all standard nonrelativistic electronic structure methods,[5–12] and these are typically also supplemented with the possibility to incorporate scalar relativistic effects by use of the second-order, spin-free, Douglas-Kroll-Hess transformation[13,14] or relativistic effective-core potentials.[15] Full account for relativistic effects, on the other hand, requires a four-component approach, and the development of analytic nonlinear response functions corresponding to the nonrelativistic ones given above is yet largely unexplored; apart from the quadratic response function that has been presented in the four-component Hartree-Fock approximation.[16,17]

The use of fully relativistic response functions in real applications is undisputed and from the technological side it is largely driven by the design of organometallic molecular compounds with specific nonlinear optical properties, see for instance the review on optical power limiting by Norman and Ågren.[18] There are a few factors, however, that slow down both the development and the application of response functions at the fully relativistic level of theory, among which the most noteworthy are as follows: (i) the coupling of spin and orbital degrees of freedoms enforces use of double groups in the classification of the one-electron wave functions, (ii) the inclusion of magnetic interactions in the zeroth-order Hamiltonian implies use of complex wave functions, and (iii) the inclusion of small components in the spinors inflicts the use of large basis sets in the calculations. One way to address the third issue is to use a two-component formalism such as the zeroth-order regular approximation.[19,20] In the present work we will compare this approach with the integral approximations made during the calculation of the four-component wave function and its responses.

It is well known that the small component electron density is strongly localized to the regions of nuclei and that it has only minor effects on the valence electron density. On the other hand, it is also well known that third-order properties such as the electric dipole hyperpolarizability and the closely related two-photon absorption transition matrix element are very sensitive to the diffuse tail in the molecular electron density and therefore suffer a strong dependence on basically all wave function parameters in practical calculations. It is the purpose of the present work to investigate to what extent the quality of hyperpolarizability and two-photon absorption calculations at the four-component level of theory can be maintained as integral and spinor approximations are introduced. The investigation is carried out at the electron uncorrelated Hartree-Fock level, but we expect that the conclusions drawn here with respect to small component integrals and positronic polarizations are generally valid for the two molecular properties under study. This work will serve as benchmark for future calculations of two-photon

[a)]Electronic mail: panor@ifm.liu.se

induced optical properties in applications where valence electron spin-orbit interactions need to be included. Of immediate concern for us will be the molecular property parameters in the Jablonski diagram that govern optical power limiting in organometallic chromophores,[18] and the mere size of the systems of interest is such that the approximations and reduced computational costs considered in the present work do become important.

We will base our study on disubstituted bromo- and iodobenzene in the *meta*- and *ortho*-conformations, and will thus be concerned with *internal* heavy atom effects on conjugated π-electron systems.

II. METHODOLOGY

The present work is concerned with the calculation of first-order electric dipole hyperpolarizability $\beta_{\alpha\beta\gamma}$ as well as transition matrix element $S_{\alpha\beta}^{0\to f}$ and cross section $\delta^{0\to n}$ for two-photon absorption at the four-component Hartree-Fock level of theory, and to investigate their sensitivity towards various approximations. We will compare this sensitivity against that found for first- and second-order properties, in this case electric dipole moment μ_α, electric dipole polarizability $\alpha_{\alpha\beta}$, and transition matrix elements $M_\alpha^{0\to f}$ and oscillator strengths $f^{0\to f}$ for one-photon absorptions. The individual transition matrix elements for one- and two-photon absorptions will not be tabulated so the comparison is, in this case, made for the cross sections. The connections between the ground state molecular properties and the linear, $\langle\langle\hat{\mu}_\alpha;\hat{\mu}_\beta\rangle\rangle_\omega$, and nonlinear, $\langle\langle\hat{\mu}_\alpha;\hat{\mu}_\beta,\hat{\mu}_\gamma\rangle\rangle_{\omega_1,\omega_2}$, response functions are as follows:

$$\mu_\alpha = \langle 0|\hat{\mu}_\alpha|0\rangle, \tag{1}$$

$$\begin{aligned}\alpha_{\alpha\beta}(-\omega;\omega) &= -\langle\langle\hat{\mu}_\alpha;\hat{\mu}_\beta\rangle\rangle_\omega \\ &= \hbar^{-1}\sum \mathcal{P}_{-\sigma,1}\sum_{n>0}\frac{\langle 0|\mu_\alpha|n\rangle\langle n|\mu_\beta|0\rangle}{\omega_n-\omega},\end{aligned} \tag{2}$$

$$\begin{aligned}\beta_{\alpha\beta\gamma}(-\omega_\sigma;\omega_1,\omega_2) &= \langle\langle\hat{\mu}_\alpha;\hat{\mu}_\beta,\hat{\mu}_\gamma\rangle\rangle_{\omega_1,\omega_2} \\ &= \hbar^{-2}\sum \mathcal{P}_{-\sigma,1,2} \\ &\quad\times\sum_{n,k>0}\frac{\langle 0|\hat{\mu}_\alpha|n\rangle\langle n|\overline{\hat{\mu}_\beta}|k\rangle\langle k|\hat{\mu}_\gamma|0\rangle}{(\omega_n-\omega_\sigma)(\omega_k-\omega_2)},\end{aligned} \tag{3}$$

where ω_n is the transition frequency of excited state $|n\rangle$, and $\hat{\mu}_\alpha$ is the electric dipole operator along the molecular axis α. For convenience we have also included the expressions for the response functions in the spectral representation, but it is clear that, when orbital variations are included in the wave function model, the explicit sum-over-states expressions will turn into nondiagonal matrix equations instead, see Ref. 2 for general details and Refs. 16, 17, and 21 for explicit details in the four-component Hartree-Fock approximation.

For the one- and two-photon absorption matrix elements we have

$$M_\alpha^{0\to f} = \langle 0|\hat{\mu}_\alpha|f\rangle, \tag{4}$$

$$S_{\alpha\beta}^{0\to f}(\omega) = \hbar^{-2}\sum_k\left[\frac{\langle 0|\hat{\mu}_\alpha|k\rangle\langle k|\hat{\mu}_\beta|f\rangle}{\omega_k-\omega}+\frac{\langle 0|\hat{\mu}_\beta|k\rangle\langle k|\hat{\mu}_\alpha|f\rangle}{\omega_k-\omega}\right], \tag{5}$$

and we see that these absorption matrix elements are directly connected to the first-order residues of the linear [Eq. (2)] and first-order nonlinear [Eq. (3)] response functions, respectively. The reader may consult Ref. 17 for the corresponding and explicit matrix formula for two-photon absorption in the four-component Hartree-Fock approximation.

III. COMPUTATIONAL DETAILS

All calculations in the present work were performed for molecular structures that were optimized with the Kohn-Sham density functional theory method using the hybrid B3LYP exchange correlation functional;[22] for H, C, and Br the 6−31G* basis set was used[23,24] and for iodine the Stuttgart effective-core potential (ECP) was used.[25] Structure optimizations were performed in the C_{2v} point group with the GAUSSIAN program.[26] The molecules are placed, with the z axis as principle axis, in the yz plane with the heavy atoms along the negative z direction.

The all-electron property calculations were performed with a locally modified version of the DIRAC program[27] that includes a two-photon absorption module,[17] and those where an ECP was used for Br or I were performed with the DALTON program.[28] The property calculations were performed at the uncorrelated Hartree-Fock level of theory with fully uncontracted basis sets that are based on the exponents from Sadlej's polarization basis set[29] with further addition of polarization and diffuse functions. The basis sets were augmented using the formula

$$\zeta_{N+j} = \left[\frac{\zeta_N}{\zeta_{N-1}}\right]^j\zeta_N, \quad j\in[1,N_{\text{aug}}], \tag{6}$$

where N_{aug} is the number of augmentation functions added, and ζ_N and ζ_{N-1} refer to the two most diffuse exponents in the original basis sets. The only exception to this rule is the f shell of the iodine basis set, which was not augmented. To the basis set of bromine we added four f functions based on the four most diffuse p exponents in the original basis set. The sizes of the singly augmented large component basis sets used in the property calculations were $[7s5p]$, $[11s7p5d]$, $[16s13p10d4f]$, and $[20s16p13d4f]$ for H, C, Br, and I, respectively, and the small component basis functions were generated from those of the large component with the use of the restricted kinetic-balance condition.

For the calculations based on the zeroth-order regular approximation (ZORA) we employed the unscaled four-component ZORA as implemented in the DIRAC program.[30] This formulation is equivalent to the two-component ZORA described in Refs. 19 and 20, but since it is implemented in a four-component framework we will not compare the computational cost in this case.

TABLE I. Optical properties for disubstituted halobenzenes at the nonrelativistic Hartree-Fock level of theory. All quantities are given in atomic units.

Basis set	μ_z	α_{xx}	α_{yy}	α_{zz}	β_{zxx}	β_{zyy}	β_{zzz}
			meta-dibromobenzene				
SAD	0.7549	69.80	150.4	115.7	3.57	−47.95	27.16
aug-SAD	0.7551	69.80	150.4	115.7	2.63	−48.30	25.96
daug-SAD	0.7550	69.80	150.4	115.7	2.58	−48.48	25.97
aug-p-SAD	0.7482	69.78	150.5	115.8	3.57	−48.97	27.85
daug-p-SAD	0.7480	69.79	150.5	115.8	3.86	−49.05	28.04
			meta-di-iodobenzene				
SAD	0.7537	91.21	196.1	140.5	56.75	12.72	139.4
aug-SAD	0.7537	91.23	196.1	140.5	56.17	12.08	140.0
daug-SAD	0.7536	91.23	196.1	140.5	56.14	12.09	140.2

IV. RESULTS

It is our intention in the present work to discuss the evaluation of quadratic response functions at the four-component Hartree-Fock level of theory, and we use disubstituted halobenzenes to exemplify some approximations that can be made in order to reduce the computational cost. This study will be concerned with the valence electron polarization and absorption as induced by an electric field in the electric dipole approximation. We will label four-component calculations as models A1-A4 and nonrelativistic calculations as models B1 and B2. The A1 model includes all large and small component integrals as well as full polarization of the electronic states due to the positronic states; the A2 model neglects interactions between small component densities, i.e., it ignores $(SS|SS)$ integrals; the A3 model, in addition to the approximations made in A2, ignores the redressing of the electronic states, i.e., ignores $(e\text{-}p)$ rotations in the propagator; the A4 model includes only scalar relativistic effects. The Z model is the unscaled four-component ZORA approach, including both scalar and nonscalar relativistic effects. The B1 model refers to regular all-electron nonrelativistic Hartree-Fock calculations; the B2 model includes the use of the effective-core potential Hamiltonian.

A. Basis set considerations

The basis set requirement for the large components of the spinors in a four-component calculation parallels that of the corresponding nonrelativistic calculation. In the evaluation of the first-order hyperpolarizability tensor and the two-photon absorption matrix elements we thus need to include polarization as well as diffuse functions in the one-particle basis set. In Table I we report a basis set investigation for the first-second-, and third-order electric dipole properties at the nonrelativistic Hartree-Fock level of theory. Our uncontracted basis set (SAD) is based on the exponents from Sadlej's polarization basis set which is optimized with respect to calculations of the molecular polarizability. Among the elements of interest, the original SAD basis set lacks polarization functions only for bromine (polarization of the 3*d* shell), so for other elements we will only add diffuse functions to the basis set. From Table I it is clear that the values of the linear polarizabilities are stable towards the addition of polarization and diffuse basis functions, but the first-order hyperpolarizability results are not. We conclude that the polarization functions on bromine are important and that, in terms of diffuse functions, single augmentation is adequate. Subsequent results reported in this work will be based on those basis sets.

B. Polarizabilities

The molecular in-plane components dominate the linear polarizability tensor due to the mobility of the π electrons in the yz plane, see Tables II and III. The out-of-plane component α_{xx} differs by 1%-2% for the *meta*- and *ortho*-conformations of bromo- and iodobenzene. The in-plane components (α_{yy} and α_{zz}), on the other hand, differ substantially due to the anisotropy induced by the electron rich at-

TABLE II. Optical properties for disubstituted bromobenzene at the Hartree-Fock level of theory. Different models are considered for the inclusion of relativistic effects. All quantities are given in atomic units.

Model	μ_z	α_{xx}	α_{yy}	α_{zz}	β_{zxx}	β_{zyy}	β_{zzz}
			meta-dibromobenzene				
A1	0.7218	69.81	150.8	115.9	4.55	−45.49	31.65
A2	0.7218	69.81	150.8	115.9	4.55	−45.50	31.64
A3	0.7218	69.81	150.8	115.9	4.54	−45.54	31.61
A4	0.7241	69.79	150.7	115.9	4.25	−45.48	30.88
Z	0.7223	69.81	150.8	115.9	4.54	−45.60	31.57
B1	0.7482	69.78	150.5	115.8	3.57	−48.97	27.85
B2	0.7291	69.90	150.8	116.0	4.91	−47.30	31.27
			ortho-dibromobenzene				
A1	1.0709	69.13	121.5	138.9	8.34	−6.65	−29.73
A2	1.0709	69.13	121.5	138.9	8.30	−6.61	−29.79
A3	1.0709	69.13	121.5	138.9	8.30	−6.61	−29.79
A4	1.0748	69.11	121.5	138.8	7.88	−6.94	−30.38
Z	1.0716	69.13	121.5	138.9	8.28	−6.75	−29.86
B1	1.1147	69.10	121.4	138.8	6.72	−9.99	−35.62
B2	1.0826	69.21	121.6	138.9	8.45	−7.56	−31.41

TABLE III. Optical properties for disubstituted iodobenzene at the Hartree-Fock level of theory. Different models are considered for the inclusion of relativistic effects. All quantities are given in atomic units.

Model	μ_z	α_{xx}	α_{yy}	α_{zz}	β_{zxx}	β_{zyy}	β_{zzz}
			meta-di-iodobenzene				
A1	0.6793	90.91	197.2	140.5	61.30	31.14	157.2
A2	0.6793	90.91	197.2	140.5	61.26	31.21	157.2
A3	0.6793	90.91	197.2	140.5	61.26	31.21	157.2
A4	0.6963	90.73	196.3	140.2	58.41	29.21	149.9
Z	0.6800	90.92	197.2	140.5	61.26	30.86	157.1
B1	0.7537	91.23	196.1	140.5	56.17	12.08	140.0
B2	0.7074	91.14	196.5	140.5	59.36	22.27	150.5
			ortho-di-iodobenzene				
A1	0.9519	88.93	154.3	170.4	86.23	72.81	151.3
A2	0.9519	88.93	154.3	170.4	86.26	72.80	151.2
A3	0.9519	88.93	154.3	170.4	86.26	72.80	151.2
A4	0.9804	88.77	153.8	169.9	82.07	69.15	143.2
Z	0.9531	88.94	154.3	170.4	86.24	72.52	150.9
B1	1.0740	89.19	154.3	170.2	78.37	53.66	123.4
B2	0.9973	89.13	154.2	170.1	82.94	65.23	139.0

oms; for the *ortho*-conformations, with the heavy atoms closer to the principle axis, the α_{zz} component is the dominating tensor element whereas the α_{yy} component dominates for the *meta*-conformations when the heavy atoms are more separated. The average in-plane polarizabilities $\alpha_{\parallel}=(\alpha_{yy}+\alpha_{zz})/2$ are only 2%-4% larger for the *meta*-compounds.

Effects of relativity on the static polarizabilities are virtually absent for bromo- as well as iodobenzene. Since the polarizability is closely related to the oscillator strength distribution according to

$$\alpha_{\alpha\alpha}(0;0)=3\sum_{n>0}\frac{f^n}{\omega_n^2};\quad f^n=\frac{2\omega_n}{3}|\langle 0|\mu_\alpha|n\rangle|^2, \tag{7}$$

there is a reason to believe that the linear absorption spectra of the compounds in the present study are equally unaffected by relativity. The oscillator strengths for the lowest valence excited states of bromo- and iodobenzene are presented in Tables IV and V. The states that contribute most significantly to the polarizabilities are relatively high in energy and not resolved in the relativistic calculation due to the large number of low-lying triplet states. However, we note that for iodobenzene there are several triplet states in the molecular "band gap" region that acquire significant oscillator strengths. By molecular band gap region we refer to energies smaller than the lowest spin- and dipole-allowed transition energies. However, it is clear that this is a case of *j*-*j* coupling, and a nonrelativistic notation of states becomes less meaningful, and, throughout, we therefore choose to label the three components of given triplet states according to the boson irreducible representation spanned by the respective four-component wave functions [e.g., the three components of a $^3A_1$ state span irreducible representations (irreps) B_1, B_2, and A_2]. The triplet states in the band gap of *ortho*-di-iodobenzene with largest oscillator strengths are the A_1 state at 4.34 eV ($f=0.51\times10^{-2}$) and the B_2 state at 4.58 eV ($f=0.65\times10^{-2}$), which correspond to contributions of 0.60 and 0.69 a.u. to α_{zz} and α_{yy}, respectively. In Table V we have chosen to include only states with significant two-photon absorption cross section, and neither of these two states are therefore reported in the table. We note, however, that these single contributions to the respective tensor components exceed the overall relativistic effects which amount to 0.2 and

TABLE IV. Excitation energies ΔE (eV), linear oscillator strengths f, and two-photon absorption cross sections δ_{TPA} (a.u.) for *ortho*-dibromobenzene using the nonrelativistic B1 method and the four-component relativistic A2 method.

B1				A2			
State	ΔE	f	δ_{TPA}	State	ΔE	f	δ_{TPA}
$^3A_1$	4.55	0	0	$1B_1$	4.55	0.0000	0.0004
				$1B_2$	4.55	0.0000	0.0000
				$1A_2$	4.55	0	0.0022
$^3B_2$	4.57	0	0	$1A_1$	4.57	0.0000	0.0001
				$2B_1$	4.57	0.0000	0.0003
				$2A_2$	4.57	0	0.0001
$^3A_1$	4.93	0	0	$3B_1$	4.93	0.0000	0.0001
				$2B_2$	4.93	0.0000	0.0002
				$3A_2$	4.93	0	0.0001
$^3B_1$	5.15	0	0	$2A_1$	5.10	0.0001	0.0611
				$3B_2$	5.11	0.0000	0.0678
				$4A_2$	5.10	0	0.0032
$^3A_2$	5.61	0	0	$3A_1$	5.55	0.0000	0.2331
				$4B_1$	5.53	0.0000	0.0510
				$4B_2$	5.55	0.0001	0.0103
$^1A_1$	5.64	0.0001	30.12	$4A_1$	5.64	0.0003	29.82
$^1B_2$	5.66	0.0218	2.700	$5B_2$	5.66	0.0214	2.763
$^3B_2$	5.81	0	0	$5B_1$	5.72	0.0001	5.676
				$5A_2$	5.79	0.0000	0.1969
				$5A_1$	5.83	0.0000	0.0007
$^1B_1$	5.88	0.0000	11.70	$6B_1$	5.90	0.0001	7.231

TABLE V. Excitation energies ΔE (eV), linear oscillator strengths f, and two-photon absorption cross sections δ_{TPA} (a.u.) for *ortho*-diiodobenzene using the nonrelativistic B1 method and the four-component relativistic A2 method. States with $\delta_{\mathrm{TPA}}<0.1$ a.u. are left out in the presentation.

Nonrelativistic (B1 method)				Relativistic (A2 method)			
State	ΔE	f	δ_{TPA}	State	ΔE	f	δ_{TPA}
				$1A_1$	3.68	0.0000	0.2162
				$1B_2$	3.77	0.0000	0.3138
				$1B_1$	3.82	0.0000	0.3795
				$2A_1$	3.92	0.0001	0.5631
				$2B_1$	4.02	0.0000	0.5888
				$2A_2$	4.03	0	0.2078
				$3A_2$	4.24	0	0.2020
				$4B_1$	4.45	0.0000	2.586
				$4A_2$	4.50	0	0.6356
				$4A_1$	4.53	0.0000	0.2947
				$5B_1$	4.57	0.0000	0.1060
$^1B_1$	4.68	0.0005	5.304	$6B_1$	4.65	0.0000	3.001
$^1A_2$	5.00	0	5.234	$6A_2$	4.77	0	2.835
$^1B_2$	5.09	0.0062	1.772	$5B_2$	4.86	0.0016	1.089
				$5A_1$	4.89	0.0000	3.471
				$8B_1$	5.30	0.0000	0.4545
				$8A_2$	5.31	0	0.2294
				$7B_2$	5.52	0.0003	0.3875
$^1B_2$	5.59	0.0533	2.726	$8B_2$	5.60	0.0505	2.963
$^1A_1$	5.59	0.0000	10.23	$6A_1$	5.62	0.0004	37.46
$^1A_1$	5.61	0.0013	44.38	$7A_1$	5.71	0.0010	14.90

0.0 a.u. for α_{zz} and α_{yy}, respectively. From the results in Table III it is also clear that there does not exist a cancellation of scalar relativistic and spin-orbit effects for the polarizability, and given the spin-forbidden absorption reported above, the reason for the lack of relativistic effects on the polarizability of iodobenzene is less than clear. The ZORA approximation gives polarizabilities in almost exact agreement with the full four-component results, both for the bromo- and iodobenzenes.

With respect to the linear polarizability we also note that calculations performed with the effective-core potential Hamiltonian are in excellent agreement with the corresponding all-electron results. This shows that the core polarization is negligible in the present case.

C. Hyperpolarizabilities

While relativistic effects on the polarizabilities of the halobenzenes are negligible this is not the case for the hyperpolarizabilities. Due to symmetry, the only unique and nonzero tensor elements are $\beta_{z\alpha\alpha}$ $(\alpha\in\{x,y,z\})$ and the orientational averaged hyperpolarizability is defined as

$$\bar{\beta}=\frac{3}{5}(\beta_{zzz}+\beta_{zyy}+\beta_{zxx}). \tag{8}$$

It is reasonable that the first-order hyperpolarizability decreases from the *ortho*- to the *meta*-conformation in order to finally vanish in the *para*-conformation. The values of $\bar{\beta}$ for *ortho*- and *meta*-bromobenzene are −16.82 and −5.57 a.u., respectively, and those for *ortho*- and *meta*-iodobenzene are 186.2 and 149.8 a.u., respectively. On a wave function level this decrease is associated with a reduced ground-to-excited state transition moment along the z axis. In this sense, the most important transitions among the lower valence states are the $|nA_1\rangle$ states at 6.99 eV (f=0.848), 6.99 eV (f=0.442), 6.80 eV (f=0.838), and 6.85 eV (f=0.279) for *o*-$C_6H_4Br_2$, *m*-$C_6H_4Br_2$, *o*-$C_6H_4I_2$, and *m*-$C_6H_4I_2$, respectively. These results are obtained at the nonrelativistic level of theory and the states fall outside the energy region that is reported in Tables IV and V.

One reason for us to choose these systems is an interest to see how relativistic effects differ between *meta*- and *ortho*-conformations. In the latter conformation we would expect two-center relativistic effects to be larger due to spatial closeness of the two heavy atoms.

For *m*-bromobenzene the relativistic effects on the β_{zzz}, β_{zyy}, and β_{zxx} components are 14%, 7%, and 27%, respectively, and for *o*-bromobenzene the corresponding values are 17%, 33%, and 24%, respectively. The triplet states in the band gap of *o*-bromobenzene with largest oscillator strengths are the A_1 state at 5.10 eV ($f=0.11\times10^{-3}$) and the B_2 state at 5.55 eV ($f=0.10\times10^{-3}$). These values of oscillator strengths are some 50 times smaller compared to the most intensive spin-forbidden transitions in *o*-iodobenzene that were discussed above, and spin-orbit coupling is therefore not likely to be main responsible for the large relativistic effects on the hyperpolarizabilities of the bromobenzenes. In Table III we also include results obtained with model A4 which is based on the spin-free Hamiltonian and which therefore include only scalar relativistic effects. For the hyperpolarizability of the bromobenzenes, the discrepancies in the scalar relativistic model as compared to the fully relativistic model A1 amount to no more than 2.5% for the domi-

nant tensor elements. Accuracies within 1% are obtained only by inclusion of spin-orbit coupling (models A2, A3, and Z).

For *m*-iodobenzene the relativistic effects on the β_{zzz}, β_{zyy}, and β_{zxx} components are 12%, 258%, and 9%, respectively, and for *o*-iodobenzene the corresponding values are 23%, 36%, and 10%, respectively. So, apart from β_{zyy} of *m*-iodobenzene the relativistic effects are of similar magnitude for iodobenzenes as for bromobenzenes. However, the nature of the effects are different as can be understood from the more intensive spin-forbidden transitions. The scalar relativistic model (model A4) is in error by 5%–7% when compared to the fully relativistic values. Addition of spin-orbit coupling brings the accuracy well within 1% regardless of whether or not we include small component integrals or positronic polarization of the electron states (models A2 and A3, respectively). Also the approximate ZORA method gives results well within 1% of the A1 values, supporting the conclusion that, for the hyperpolarizabilities of the molecules under study, the scalar and nonscalar relativistic effects are of comparable importance.

On the calculation of hyperpolarizablities of halobenzenes, we finally note that the effective-core potential results (model B2) are in all cases superior to the nonrelativistic counterparts. Such a consistent performance for a sensitive high-order molecular property such as the hyperpolarizability is noteworthy and has been recognized before.[31] In these calculations there are no explicit internal magnetic interactions incorporated, but the ECPs are parameterized against accurate relativistic atomic densities.

D. Two-photon absorption

We have demonstrated above that the ground state nonlinear polarization can be determined accurately with neglect made of small component integrals and electron-positron orbital rotations. With bromine as the heavy atom one can even reduce the relativistic treatment to only include scalar relativistic effects and still maintain high accuracy in the calculation. For two-photon absorption it was demonstrated by Henriksson *et al.*[17] that a scalar relativistic treatment is inappropriate for the calculation of the spectra of the noble gases, and in the present work we extend this investigation to include π-conjugated systems for which the interest lies also in technological applications. The two-photon cross section for the absorption of linearly or circularly polarized light by a randomly oriented sample is given by[32]

$$\delta_{\mathrm{TPA}} = \frac{1}{15}\sum_{\alpha,\beta}\left\{ FS^{0\to f}_{\alpha\alpha}\left(\frac{\omega_f}{2}\right)\left[S^{0\to f}_{\beta\beta}\left(\frac{\omega_f}{2}\right)\right]^* + GS^{0\to f}_{\alpha\beta}\left(\frac{\omega_f}{2}\right) \times\left[S^{0\to f}_{\alpha\beta}\left(\frac{\omega_f}{2}\right)\right]^* + HS^{0\to f}_{\alpha\beta}\left(\frac{\omega_f}{2}\right)\left[S^{0\to f}_{\beta\alpha}\left(\frac{\omega_f}{2}\right)\right]^*\right\}, \quad (9)$$

where F, G, and H are factors that depend on the polarization of the incident light and the two-photon matrix elements S are those defined in Eq. (5). We will restrict our report to include only absorption for circularly polarized light in which case $F=-1$ and $G=H=3/2$.

In Table IV we present the two-photon absorption cross sections for the *o*-dibromobenzenes. We note a spin-allowed two-photon transition to a state of A_1 symmetry at 5.64 eV with a nonrelativistic cross section of 30.12 a.u. The corresponding relativistic calculation with the A2 model gives an energy of 5.64 eV but a cross section of 29.82 a.u. However, we stress that the relativistic effect on the integrated cross sections is even less because in the relativistic calculation there are also A_1 states at energies 5.10 and 5.55 eV that acquire cross sections of 0.06 and 0.23 a.u. The integrated cross section in the relativistic case is therefore 30.11 a.u., which is virtually identical to that obtained in the nonrelativistic case.

An even more striking example of this smearing out of the two-photon absorption intensity is given among the B_1 states in *o*-dibromobenzene. The two states at energies 5.71 and 5.90 eV in the relativistic calculation interact strongly due to spin-orbit interaction (the corresponding nonrelativistic singlet state is at 5.88 eV) and the intensity is almost spread equal on the two states. In this case there is a relativistic enhancement of the integrated cross section which amounts to 5.68 and 7.23 a.u. for the two individual states to be compared with the singlet absorption cross section in the nonrelativistic case of 11.70 a.u.

In Table V the two-photon absorption cross sections for the *o*-di-iodobenzenes are presented. At the nonrelativistic level of theory the two singlet states, lowest in energy and of A_1 symmetry, are positioned at 5.59 and 5.61 eV and then there is a gap of 1.2 eV to the third singlet state in this symmetry. The integrated cross section of these two singlet states amounts to 54.6 a.u. In the relativistic calculation there are seven states of A_1 symmetry in the energy interval 3.68–5.71 eV but only a gap of 0.3 eV to the eighth state in this symmetry, so a division is not as clear as in the nonrelativistic case. Nevertheless, if we sum up the cross sections for the first seven states of A_1 symmetry we obtain an integrated cross section of 57.0 a.u., which again demonstrates that the integrated cross sections may be fairly reasonable in a nonrelativistic treatment but that the absorption is far too narrow banded as compared to a correct relativistic treatment.

In contrast to linear absorption spectroscopy, two-photon absorption spectroscopy is dependent on the polarization of the electric field, which thus provides a further possibility to characterize the two-photon active excited states. For irreducible representations B_1, B_2, and A_2 in the C_{2v} point group, only the off-diagonal elements of the two-photon absorption amplitude tensor $S_{\alpha\beta}$ [Eq. (5)] are nonzero. This will inflict that the ratio of the two-photon absorption cross section for circularly and linearly polarized light is equal to 1.5 for all states in these symmetries (the absorption for circularly polarized light is stronger). On the other hand the corresponding ratio R for absorption to states of A_1 symmetry is not constant, and while $R=1.28$ for the two A_1 states of *o*-di-iodobenzenes at 5.62 and 5.71 eV we find that $R=1.43$ for the state at 4.89 eV. This polarization dependence should make it possible to identify the triplet states for which we predict a strong spin-forbidden two-photon absorption.

TABLE VI. Wall times for the evaluation of the quadratic response function at the four-component Hatree-Fock (4C-HF) level relative to the wall time of the corresponding nonrelativistic Hartree-Fock (HF) calculation.

		Wave function parameterization				
Model		$(LL\|LL)$	$(LL\|SS)$	$(SS\|SS)$	$(e\text{-}p)$	Wall time
4C-HF	A1	×	×	×	×	25.9
	A2	×	×		×	8.7
	A3	×	×			8.7
HF	B1	×				1

V. SUMMARY AND DISCUSSION

The perhaps single-most important disadvantage of four-component methods in quantum chemistry is the high computational cost due to the description of the small component in the spinors. Other issues, such as the inclusion of magnetic fields and magnetic field interactions, are, on the other hand, much simpler in a fully relativistic framework. In this paper we are concerned with the evaluation of the quadratic response function at the four-component Hartree-Fock level of theory, and we have demonstrated that, with neglect of small component $(SS|SS)$ integrals, results for the hyperpolarizabilities of halobenzenes are accurate to within 1%. From Table VI we note that the overall wall time, as measured in units of the wall time for the corresponding nonrelativistic Hartree-Fock calculation, is reduced from 25.9 with inclusion of $(SS|SS)$ integrals to 8.7 when they are left out. We expect these observations to be generally valid for the calculation of hyperpolarizabilities of organic based heavy atom compounds, and we thus recommend the use of this approximation on more general terms.

We have demonstrated that for calculations of nonlinear electric properties in the dipole approximation the electron-positron orbital rotations can be left out in the calculation of the propagator, but this amounts only to memory savings. The results calculated using the zeroth-order regular approximation are highly accurate (within 1% of fully relativistic results), and since, in a two-component implementation, the method is expected to have a computational scaling in between a nonrelativistic treatment and a relativistic treatment without $(SS|SS)$ integrals, it is a cost effective yet accurate approach to treat nonscalar relativistic effects for the systems and properties studied here.

We have also shown that the scalar relativistic corrections are accurate to within 2.5% for the calculations of the hyperpolarizabilities of bromobenzenes, but that discrepancies of 5%–7% are obtained when spin-orbit interactions are left out in iodobenzenes. From the quadratic response function we can determine two-photon absorption matrix elements (and thereby also cross sections). For the bromine compounds, and even more so for the iodine compounds, nonrelativistic as well as scalar relativistic calculations of the two-photon absorption spectra are qualitatively incorrect. The integrated two-photon absorption cross sections may be comparable to the fully relativistic ones, but spin-orbit interactions cause the absorption to be broad banded, i.e., the absorption intensity is most effectively spread out over electronically excited states of nonrelativistic triplet spin symmetry in a broad energy range. In any application that involve coherent two-photon absorption this will be important, and nonscalar relativistic effects should be considered for compounds that include third (and lower) row elements. We note that this result is particular to the nonlinear absorption process and is not significant in the linear absorption spectra.

The current work also presents results obtained with the effective-core Hamiltonian without explicit inclusion of magnetic interactions. It is shown that even a sensitive property such as the hyperpolarizability is quite well described by this method, and considering the simplifications made, the agreement with all-electron four-component results is noteworthy. For this reason, we will pursue a development of effective-core potentials in the four-component approach in order to fully account for the valence spin-orbit effects at a computational cost that enables applications to organometallic systems of technological interest.

ACKNOWLEDGMENT

The authors acknowledge a grant for computing time at the National Supercomputer Centre (NSC), Sweden.

[1] *Nonlinear Optical Properties of Matter: From Molecules to Condensed Phases*, edited by M. Papadopoulos, J. Leszczynski, and A. J. Sadlej, (Kluwer Academic, Dordrecht, 2006).
[2] J. Olsen and P. Jørgensen, J. Chem. Phys. **82**, 3235 (1985).
[3] O. Christiansen, P. Jørgensen, and C. Hättig, Int. J. Quantum Chem. **68**, 1 (1998).
[4] P. Norman, D. M. Bishop, H. J. Aa. Jensen, and J. Oddershede, J. Chem. Phys. **123**, 194103 (2005).
[5] H. Hettema, H. Jensen, P. Jørgensen, and J. Olsen, J. Chem. Phys. **97**, 1174 (1992).
[6] P. Norman, D. Jonsson, O. Vahtras, and H. Ågren, Chem. Phys. **203**, 23 (1996).
[7] D. Jonsson, P. Norman, and H. Ågren, J. Chem. Phys. **105**, 6401 (1996).
[8] C. Hättig, O. Christiansen, H. Koch, and P. Jørgensen, Chem. Phys. Lett. **269**, 428 (1997).
[9] J. Gauss, O. Christiansen, and J. Stanton, Chem. Phys. Lett. **296**, 117 (1998).
[10] C. Hättig, O. Christiansen, and P. Jørgensen, Chem. Phys. Lett. **282**, 139 (1998).
[11] P. Salek, O. Vahtras, T. Helgaker, and H. Ågren, J. Chem. Phys. **117**, 9630 (2002).
[12] B. Jansik, P. Salek, D. Jonsson, O. Vahtras, and H. Ågren, J. Chem. Phys. **122**, 54107 (2005).
[13] M. Douglas and N. M. Kroll, Ann. Phys. (San Diego) **82**, 89 (1974).
[14] G. Jansen and B. Hess, Phys. Rev. A **39**, 6016 (1989).
[15] R. M. Pitzer and N. M. Winter, Int. J. Quantum Chem. **40**, 773 (1991).
[16] P. Norman and H. J. Aa. Jensen, J. Chem. Phys. **121**, 6145 (2004).
[17] J. Henriksson, P. Norman, and H. J. Aa. Jensen, J. Chem. Phys. **122**, 114106 (2005).
[18] P. Norman and H. Ågren, J. Comput. Theor. Nanosci. **1**, 343 (2004).
[19] E. van Lenthe, E. J. Baerends, and J. G. Snijders, J. Chem. Phys. **101**, 9783 (1994).
[20] E. van Lenthe, J. G. Snijders, and E. J. Baerends, J. Chem. Phys. **105**, 6505 (1996).
[21] T. Saue and H. J. Aa. Jensen, J. Chem. Phys. **118**, 522 (2003).
[22] A. D. Becke, J. Chem. Phys. **98**, 5648 (1993).
[23] W. J. Hehre, R. Ditchfield, and J. A. Pople, J. Chem. Phys. **56**, 2257 (1972).
[24] V. A. Rassolov, J. Pople, M. A. Ratner, and T. L. Windus, J. Chem. Phys. **109**, 1223 (1998).
[25] M. Kaupp, P. Schleyer, H. Stoll, and H. Preuss, J. Am. Chem. Soc. **113**, 6012 (1991).
[26] M. J. Frisch, G. W. Trucks, H. B. Schlegel *et al.*, GAUSSIAN 03, Revision B05, Gaussian, Inc., Pittsburgh PA, 2003.
[27] H. J. Aa. Jensen, T. Saue, L. Visscher *et al.*, DIRAC, a relativistic *ab initio*

electronic structure program, release DIRAC04.0, 2004.
[28] DALTON, a molecular electronic structure program, Release 2.0, 2005, see http://www.kjemi.uio.no/software/dalton/dalton.html
[29] A. J. Sadlej, Collect. Czech. Chem. Commun. **53**, 1995 (1988).
[30] L. Visscher and T. Saue, J. Chem. Phys. **113**, 3996 (2000).
[31] P. Norman, B. Schimmelpfennig, K. Ruud, H. J. Aa. Jensen, and H. Ågren, J. Chem. Phys. **116**, 6914 (2002).
[32] W. McClain, J. Chem. Phys. **55**, 2789 (1971).

Paper VI

Theoretical simulations of clamping levels in optical power limiting

Alexander Baev
Patrick Norman
Johan Henriksson
Hans Ågren

The Journal of Physical Chemistry B **110**, 20912 (2006)

VI

20912 *J. Phys. Chem. B* **2006,** *110,* 20912−20916

Theoretical Simulations of Clamping Levels in Optical Power Limiting

Alexander Baev

Institute for Lasers, Photonics and Biophotonics, SUNY at Buffalo, Buffalo, New York 14260

Patrick Norman* and Johan Henriksson

Department of Physics, Chemistry and Biology, Linköping University, SE-581 83 Linköping, Sweden

Hans Ågren

Theoretical Chemistry, Royal Institute of Technology, SE-100 44 Stockholm, Sweden

Received: July 3, 2006; In Final Form: August 22, 2006

Multiphysics modeling, combining quantum mechanical and classical wave mechanical theories, of clamping levels has been performed for a platinum(II) organic compound in a sol−gel glass matrix. A clamping level of 2.5 μJ is found for a pulse duration of 10 ns. The excited-state absorption in the triplet manifold is shown to be crucial for clamping to occur.

I. Introduction

Laser light propagation through an optically active medium can favorably be analyzed by means of multiphysics modeling that involves an interplay of quantum mechanical and classical electromagnetic theories. In the present work we exploit this notion and address optical power limiting (OPL), induced by randomly oriented molecular materials, by combining first principles quantum mechanical calculations of molecular properties with time-domain solutions of the Maxwell equations. We demonstrate our modeling approach on π-conjugated platinum(II) acetylide that in recent experimental work has been shown to function as a broadband limiter.[1] The power limiting capability is explained in terms of a Jablonski diagram,[2] several key parameters of which previously have been determined for related platinum(II) organic compounds by use of first principle methods[3,4] and in a more general context by experiment.[5−7] In the present work we significantly widen the scope for the theoretical simulations of OPL by also including quantum mechanical simulations of excited-state properties both in the singlet and in the triplet manifold of states and by combining the molecular property calculations with a light propagation model[8,9] to retrieve estimates of the final property of interest, namely, the clamping level of the material. If successful, such a development is expected to have a large impact on the possibility to design molecular materials for OPL applications by theoretical simulations. The basic principle is that knowledge of the intrinsic molecular properties must be combined with classical pulse propagation to address the strong dependence of clamping levels on the laser pulse characteristics, such as intensity, shape, and duration time.

II. Methodology

We demonstrate the use of our simulation approach by studying the clamping levels for platinum(II) acetylide with thiophene units in the ligands under different lasing conditions. We consider the linear and nonlinear interactions between an ensemble of randomly oriented chromophores with number density N and an optical electric field. The field is phase coherent in the xy-plane (i.e., a plane wave) and propagates in the z-direction through a glass medium doped with chromophores and with thickness d according to

$$\mathbf{E}(\mathbf{r},t) = \mathcal{E}(\mathbf{r},t)\, e^{i(kz+\omega t)} + \text{c.c.} \tag{1}$$

where $k = 2\pi n/\lambda$ is the wavenumber (n is the refractive index) of the laser field and $\mathcal{E}$ is the amplitude function that corresponds to an intensity $I = c\epsilon_0|\mathcal{E}|^2/2$. The incident laser pulse is, at time $t = 0$, assumed to have a Gaussian profile characterized by its peak power and a given full width at half-maximum (fwhm) in the time domain, and with the amplitude function $\mathcal{E}(\mathbf{r},t)$, at time $t > 0$ during the propagation through the medium, determined from the paraxial wave equation[10]

$$\left(\frac{\partial}{\partial z} + \frac{1}{c}\frac{\partial}{\partial t} - \frac{i}{2k}\Delta_\perp\right)\mathcal{E}(\mathbf{r},t) = \frac{ik}{\epsilon_0}\mathcal{P}(\mathbf{r},t) \tag{2}$$

where $\mathbf{P}(\mathbf{r},t) = \mathcal{P}(\mathbf{r},t)\, e^{i(kz+\omega t)} + \text{c.c.}$ is the polarization of the medium.

The polarization of the medium has two contributions, namely the polarizations of the host $\mathcal{P}_\text{h}$ and the chromophore $\mathcal{P}_\text{c}$

$$\mathcal{P}(\mathbf{r},t) = \mathcal{P}_\text{h}(\mathbf{r},t) + \mathcal{P}_\text{c}(\mathbf{r},t) \tag{3}$$

The host material can for instance be a solvent, sol−gel glass, or polymer matrix, which should be nonabsorbing at the frequency of interest. In addition, the polarization of the host is assumed to be linear so that it can be written as

$$\mathcal{P}_\text{h}(\mathbf{r},t) = \epsilon_0\chi_\text{h}^{(1)}(\omega)\, \mathcal{E}(\mathbf{r},t) \tag{4}$$

where $\chi_\text{h}^{(1)}$ is the electric linear susceptibility. The host susceptibility relates to the corresponding refractive index according to $\chi_\text{h}^{(1)} = n^2 - 1$.

The polarization of the chromophore governs the optical power limiting capabilities of the material. This polarization will obviously have nonlinear components, and macroscopic

* Address correspondence to this author. E-mail: panor@ifm.liu.se.

10.1021/jp064167b CCC: $33.50
Published on Web 09/26/2006

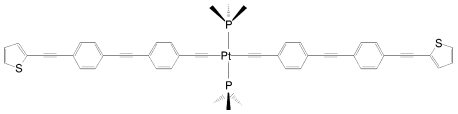

Figure 1. Molecular structure.

excited-state populations will appear during the action of the laser pulse. It is the aim of the present work to interrelate the power limiting performance and the electronic structure of the ground and excited states of the chromophore. We determine the polarization of the chromophore by use of the quantum mechanical density matrix formalism and the Liouville equation[11]

$$\frac{\partial}{\partial t}\rho_{mn} = \frac{1}{i\hbar}(H_{mk}\rho_{kn} - \rho_{mk}H_{kn}) - \gamma_{mn}(\rho_{mn} - \rho_{00}\delta_{n0}\delta_{m0}) \quad (5)$$

where the Hamiltonian matrix is a sum of the unperturbed molecular Hamiltonian (diagonal matrix with excitation energies on the diagonal) and a perturbation due to the external electric field. In the electric-dipole approximation (which applies to a given chromophore at position $\mathbf{r}_0$), the perturbation is equal to

$$\hat{V}(t) = -\hat{\mu}_\alpha E_\alpha(\mathbf{r}_0,t) \quad (6)$$

where we have introduced the electric dipole moment operator $\hat{\mu}_\alpha$ along the molecular axis α. Given the solution to eq 5, the polarization as due to the chromophore at point $\mathbf{r}_0$ is

$$\mathscr{P}_c(\mathbf{r}_0,t) = N\,\mathrm{Tr}\{\hat{\mu}\hat{\rho}\} \quad (7)$$

where N is the number density of chromophores in the medium. Our calculations account for an averaging of the molecular orientations with respect to the external electric field.

The matrix elements of the molecular Hamiltonian and the dipole moment operator as well as radiative absorption and relaxation parameters in the Liouville equation [eq 5] are determined by the use of first principles quantum chemical calculations, whereas the nonradiative relaxation parameters are set to values that are generally representative for large-sized chromophores. A detailed presentation of our methodology is found in ref 8, with underlying theory given in refs 9 and 12.

III. Computational Details

The molecular structure of the platinum(II) chromophore (ATP) is shown in Figure 1. The structure was optimized at the density functional theory (DFT) level by using the B3LYP hybrid exchange-correlation functional[13] with effective-core potentials for platinum[14] and phosphorus[15] and all-electron 6-31G[16] basis sets for the light elements. Apart from the exchange-correlation functional, an identical parametrization of the Kohn−Sham determinant was chosen for the property calculations where the time-dependent DFT (TD-DFT) approach was employed. All property calculations were performed at the ground-state optimized structure (vertical transitions), employing the Coulomb-attenuated B3LYP (CAM-B3LYP) exchange-correlation functional.[17] The geometry optimization has been performed with the Gaussian program,[18] whereas all molecular property calculations have been carried out with the Dalton program.[19]

The optimized structure of ATP belongs to the C_{2h} point group. The molecular point group of this compound is ambiguous, depending on the orientation of the phosphine and thiophene groups, see Figure 1. However, this choice is of no importance to the optical properties of the molecules, so our choice of conformer for the theoretical work is made with respect to computational efficiency. With our choice made the molecule will be strictly planar in the optimized configuration, and due to inversion symmetry, the diagonal elements of the dipole moment matrix $\langle n|\,\hat{\mu}|\,n\rangle$ vanish. The y-axis is chosen to be the long in-plane molecular axis and the z-axis to be the out-of-plane axis. As a consequence of this choice, the components of the electric dipole operator $\hat{\mu}_x$, $\hat{\mu}_y$, and $\hat{\mu}_z$ will span the irreducible representations B_u, B_u, and A_u, respectively.

The pulse propagation simulations are performed assuming a sample thickness $d = 1$ mm and a chromophore concentration of 0.02 M. We have used fwhm values of 100 fs and 10 ns for the laser pulses, and we have considered the photon wavelengths of 532 and 694 nm. The refractive index of the medium is set to $n = 1.457$ for the two wavelengths under consideration, which corresponds to a situation where the chromophores are embedded in a sol−gel glass. In our simulations of the transmittance curves we used a 20 μm beam waist radius to estimate the pulse energy. The relaxation parameters, or inverse lifetimes, of the excited states are set to 10^6, 10^9, and 10^{12} s^{-1} for the first excited triplet state, the first excited singlet state, and other excited singlet and triplet states, respectively, and the intersystem crossing rate between the singlet and triplet manifolds is set to 10^{11} s^{-1}.

IV. Results and Discussion

A. Electronic Structure Calculations. The electronic ground state of ATP is closed-shell in nature, and therefore of singlet spin symmetry. The dominating state in the linear absorption spectrum is the $1\,^1B_u$ state, which to a large extent is described by a one-electron transition from the highest occupied molecular orbital of b_g symmetry to the lowest unoccupied molecular orbital of a_u symmetry. ATP is "one-dimensional" in the sense that the absorption is induced by an electric field oscillating along the molecular long in-plane y-axis—the x- and z-directed absorption can to a good approximation be ignored. This observation holds for one-photon as well as two-photon induced absorption and implies that only states of A_g symmetry are two-photon active.

As far as the quantum chemical calculations of linear and nonlinear optical properties are concerned we have chosen to adopt the density functional theory approach with the CAM-B3LYP functional. This choice is motivated by the documented good performance of this functional for response properties (including the description of charge-transfer transitions).[20,21]

The vertical electronic transition energy of the $1\,^1B_u$ state is predicted to be 3.39 eV (366 nm) at this level of theory, and the corresponding electric dipole transition matrix element is 8.124 au (see Table 1). In atomic units, the oscillator strength—which is proportional to the absorption strength—for the transition from the ground state S_0 to the excited state S_n is given by

$$f^{0n} = \frac{2\Delta E}{3}\sum_\alpha |M_\alpha|^2 \quad (8)$$

and for the discussed transistion to the $1\,^1B_u$ state the oscillator strength is as large as 5.48. This theoretical result is in good agreement with the experimental spectrum recorded in solution (tetrahydrofuran).[22] The experiment shows a highly intense and broad absorption between 350 and 420 nm that completely dominates the near-visible and visible spectrum, and the sample is accordingly slightly colored. The chromophore used in the

TABLE 1: Vertical Transition State Energies, ΔE (eV), One-Photon Moments,[a] M_α (au), and Two-photon Moments, $S_{\alpha\beta}$ (au) that Are of Predominant Importance for Optical Power Limiting at 532 and 694 nm for Molecular Compound ATP

ψ_i	ψ_f	ΔE	$\lvert M_y\rvert$	$\lvert S_{yy}\rvert$
X ^1A_g	1 ^1B_u	3.39	8.124	0
	1 ^1A_g	3.63	0	327.2
	2 ^1B_u	4.02	1.409	0
	2 ^1A_g	4.23	0	155.2
	4 ^1A_g	4.39	0	723.9
	3 ^1B_u	4.62	0.500	0
	5 ^1A_g	4.76	0	3504.4
	9 ^1A_g	5.18	0	1936.4
1 ^3B_u[b]	4 ^3A_g	1.75	0.058	0
	6 ^3A_g	2.20	0.496	0
	7 ^3A_g	2.28	0.123	0
	10 ^3A_g	2.44	2.154	0
1 ^1B_u	1 ^1A_g	0.24	1.426	0
	2 ^1A_g	0.84	0.490	0
	3 ^1A_g	0.86	0.252	0
	4 ^1A_g	1.00	2.026	0
	5 ^1A_g	1.37	9.074	0
	9 ^1A_g	1.79	2.916	0
	10 ^1A_g	2.02	0.430	0

[a] The corresponding oscillator strength is $f = 2\Delta E\sum_\alpha |M_\alpha|^2/3$. [b] The transition energy of 1 ^3B_u relative to the ground state is 1.93 eV.

experiment is that illustrated in Figure 1 but with phosphine groups that contain butyl rather than hydrogens. At the DFT/B3LYP level of theory we have determined the red-shift associated with such a change in the phosphine groups to be equal to 20 nm and we would thus expect a transition wavelength of 386 nm at the CAM-B3LYP level. A smaller red-shift is also associated with the solvent.

The conditions for our laser pulse propagation simulations will mimic those most commonly used in the experiment with respect to the laser source, that means a frequency-doubled Nd:YAG laser operating at 532 nm (2.33 eV). The laser detuning thus amounts to 31% when compared to the vertical electronic transition energy of the 1 ^1B_u state, but considering the enormous oscillator strength of the $S_0 \rightarrow S_1$ transition, the large size of the molecule, and the effects of the environment, there are several factors that will significantly broaden this absorption. The experimental linear absorption spectrum[22] shows a tail that stretches to about 550 nm. Due to this broadening, there will be an important contribution to the OPL characteristics from nonresonant linear absorption in ATP at the wavelength of the laser.

Resonant two-photon absorption (TPA) is in general believed to be of greater importance to the population of the excited states at longer wavelengths, or short pulse lengths; the reason for this assumption is that at longer wavelenths (or shorter pulse lengths) the off-resonant one-photon population of the excited states is supressed. We further assume that TPA directly followed by excited state absorption (ESA) is a relatively unlikely event. We motivate this assumption with the fact that the TP states are of gerade symmetry and above the 1 ^1B_u state in energy, and since the lifetime of the higher excited states will be short and nonradiative relaxation will occur, a macroscopic population of these states will be effectively prevented. We have therefore targeted our calculations of excited-to-excited state transition dipole moments to include only those where the 1^1B_u state acts as an initial state, see Figure 2. Furthermore, since the molecular conjugation axis is of B_u symmetry the excited-to-excited state transitions will be effective only for final states of A_g symmetry. We have determined the transition matrix elements from the 1 ^1B_u state to the 10 lowest singlet states of

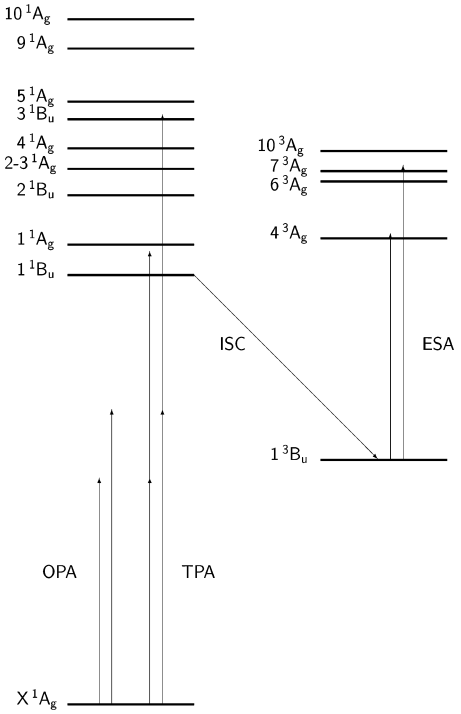

Figure 2. Electronic states of predominant importance in the simulation of the optical power limiting at 532 (2.33 eV) and 694 nm (1.79 eV) of ATP. The absorption is electric field induced whereas the relaxation processes and the intersystem crossing (ISC) are nonradiative. The figure is correctly scaled with respect to photon and transition energies; the long and short vectors correspond to photon wavelengths of 532 and 694 nm, respectively.

A_g symmetry that covers excitation energies up to 5.41 eV. The strongest absorption takes place to states 5 ^1A_g and 9 ^1A_g positioned at 4.76 and 5.18 eV, respectively, and with transition moments M_y that equal 9.07 and 2.92 au, respectively. These two states will be occupied in what we denote as a "two-step" process, which refers to nonresonant ground-to-excited states absorption followed promptly by excited-excited-state absorption (both processes having a linear dependence on the intensity of the laser field). The two individual photons involved in the two processes have a combined energy of 4.66 eV, and the two-step absorption to states 5 ^1A_g and 9 ^1A_g (via 1 ^1B_u) therefore contributes strongly to the optical power limiting performance of the material.

The population of the triplet manifold of states is important in optical power limiting applications since it causes a situation where the molecules are spin-trapped for times that are comparable to, or longer than, the duration of the laser pulse. It has been shown in experiment that the nonradiative intersystem crossing in platinum(II) organic materials is both fast and effective,[1] and it will be the predominant channel to populate the triplet manifold in our setup. Fast vibronic relaxation leads us to consider excited-to-excited-state transitions in the triplet manifold from the lowest triplet state only, i.e., the 1 ^3B_u state

at 1.93 eV. We include the 10 lowest triplet states of A_g symmetry and thereby cover excitation energies up to 4.37 eV. The most important transitions within the triplet manifold are those from 1 ^3B_u to states 4 ^3A_g and 10 ^3A_g for photon wavelengths of 694 and 532 nm, respectively. It is only in the latter case, however, that the transition moment M_y is significant (2.154 au) and the triplet state ESA should therefore be less effective at the longer of the two wavelengths. This summarizes the transitions that will govern the pulse propagation through the material. We have covered the energy region that includes nonresonant one-photon absorption and coherent two-photon absorption from the ground state and resonant excited-to-excited state one-photon transitions. We argue that the size of transition moments between a low-lying and a high-lying excited state is likely to be small due to the large number of nodes in the wave functions of the latter, which implies that the use of very extended conjugated systems may be prohibitive for the excited-to-excited-state absorption in the desired energy region, since the larger system will have a larger density of valence-excited states.

B. Pulse Propagation Calculations. The simulations of the propagation of a laser pulse through the optical power limiting material are carried out through a time integration of the combined quantum mechanical and electrodynamical equations presented in Section II. The populations of the ground and excited states of the chromophore will vary considerably during the extent of the pulse and the chromophore state propagation can therefore not be described by perturbation theory in this situation.

In a perturbational approach the coherent one- and two-photon absorption moments can be identified from the first- and second-order corrections to the expansion coefficients of the reference state in terms of the eigenstates to the zeroth-order Hamiltonian, and the corresponding one- and two-photon absorption cross sections are obtained by taking the absolute square of the moments. See for instance the book chapter by Norman and Ruud[23] for a detailed description of the perturbational approach and its application to response theory. In the past, we, and others, have made frequent use of an identification of the one- and two-photon matrix elements from the first-order residue of the linear and quadratic response functions, respectively, and it is also this approach that is used to determine the transition moments in Table 1. The one- and two-photon transition moments (M_α and $S_{\alpha\beta}$) are to be squared to obtain the corresponding absorption cross sections.

In the direct dynamical approach that is used to describe the pulse propagation in the present work there is not, and cannot be, a distinct separation between one-photon, two-photon, etc. absorption due to a mixture of excitations in the ground state and the excited state manifold. What can be clearly defined, however, are the terms in the total absorption cross section which depend linearly and nonlinearly on the intensity of the external electric field; the first two terms are typically denoted by $\sigma^{(1)}$ and $\sigma^{(2)}$. It is in the limit of short laser pulses that we can compare the absorption cross sections obtained in the perturbational approach with those obtained in the direct dynamical approach, since the short pulse will have only a small effect on the reference state. In other words, the ground-state two-photon matrix elements $S_{\alpha\beta}$ are relevant in the sense that they may describe the onset for population of the excited states by coherent multiphoton absorption, but they cannot provide the complete picture for longer pulses.

The results from simulations of the laser pulse propagation are presented in Figures 3 and 4 for the cases of short (100 fs) and long (10 ns) pulses, respectively. Two separate wavelengths of 532 and 694 nm are considered, and the relative energies of the incident light versus the electronic state separations are illustrated in Figure 2.

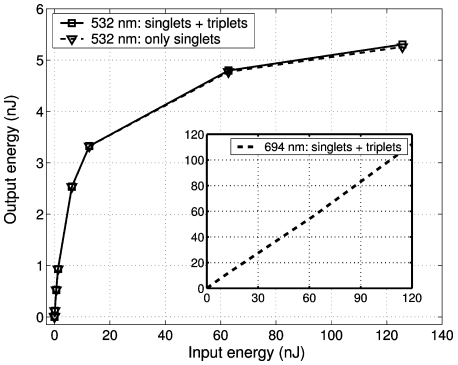

Figure 3. Optical power limiting at 532 nm with use of the ATP chromophore in a 1 mm glass at a concentration of 0.02 M. The pulse length is 100 fs.

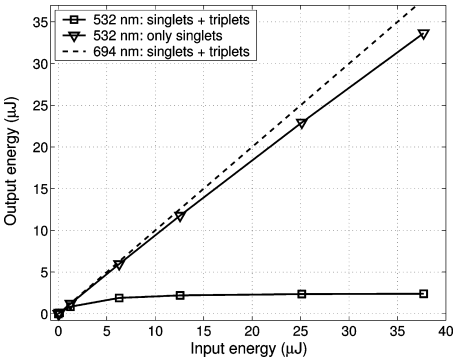

Figure 4. Optical power limiting at 532 nm with use of the ATP chromophore in a 1 mm glass at a concentration of 0.02 M. The pulse length is 10 ns.

The intersystem crossing rate is slower than the duration of the shorter pulse. In the 100 fs simulation the influence of the excited-state absorption in the triplet manifold is found negligible. An observed clamping level of about 6 nJ is found at a laser wavelength of 532 nm, regardless of whether the triplet−triplet channels are included in the simulations. For the longer wavelength the nonresonant one-photon absorption in the ground state is of course weaker than that for the short wavelength, and in addition, the two-photon resonance corresponding to state 5 ^1A_g is an order of magnitude stronger than that for state 1 ^1A_g, which further promotes a lower clamping level at 532 nm compared to the situation at 694 nm. The inset in Figure 3 also shows that clamping is not observed at 694 nm for the laser pulse energies under consideration.

The intersystem crossing rate is, on the other hand, faster than the duration of the longer pulse, and we expect therefore that the influence of the triplet manifold increases. Our simulations clearly demonstrate that this assumption is correct;

in Figure 4 it is seen that a clamping level of about 2.5 μJ is found when triplet−triplet absorption is included whereas, as triplet−triplet absorption is excluded, clamping is not reached within the energy region under consideration. This strong dependence of the optical power limiting characteristics at 532 nm on the absorption in the triplet manifold is explained by the large transition moment ($M_y = 2.154$ au) between states $1\ ^3B_u$ and $10\ ^3A_g$ (see Table 1). For the longer wavelength, on the other hand, there is no state for which the excited triplet state absorption is strong, and in the pulse propagation simulation in Figure 4 it is also seen that the absorption is virtually linear throughout the energy region of 0−40 μJ.

If we compare the results for the two pulse lengths, it is clear that the inclusion of the triplet manifold is crucial for clamping to occur with the longer of the two laser pulses but not with the shorter one. This is a result that we could not have anticipated from merely looking at the quantum mechanical results for the transition moments and excitation energies but rather it requires the consideration of the population dynamics in the chromophore medium. The reason for the requirement of the triplet manifold to obtain low-level clamping for the longer pulse is that, in this case, the excited singlet state absorption is effectively prohibited due to saturation of the high-lying singlet state. So we conclude that efficient optical power limiting relies not only on strong absorption between excited-to-excited states but also that saturation of available absorption channels (in the singlet and triplet manifolds) does not occur.

V. Concluding Remarks

We have demonstrated simulations of clamping levels in optical power limiting applications that, apart from relaxation parameters, are based on first principles. Our multiphysics modeling approach combines quantum mechanical and classical wave mechanical calculations that make it possible to pinpoint the importance of specific absorption channels to the clamping level, and that can tie the electronic structure of the chromophore to the overall performance of the material. We believe that our modeling approach provides a versatile tool to guide synthetic work.

Acknowledgment. This work received financial support from the Sensor Protection project within the NanoTek program (www.nanotek.se) that is run by the Swedish Defence Agencies. The authors acknowledge a grant for computing time at the National Supercomputer Centre (NSC), Sweden, and financial support from NordForsk (network grant No. 030262). Prof. Faris Gel'mukhanov is gratefully acknowledged for his important contributions to the theory used in the present work.

References and Notes

(1) McKay, T. J.; Bolger, J. A.; Staromlynska, J.; Davy, J. R. *J. Chem. Phys.* **1998**, *118*, 5537.

(2) Parker, C. A. *Photoluminescence of solutions*; Elsevier: New York, 1968.

(3) Cooper, T. M.; McLean, D. G.; Rogers, J. E. *Chem. Phys. Lett.* **2001**, *349*, 31.

(4) Norman, P.; Cronstrand, P.; Ericsson, J. *Chem. Phys.* **2002**, *285*, 207.

(5) Rogers, J. E.; Cooper, T. M.; Fleitz, P. A.; Glass, D. J.; McLean, D. G. *J. Phys. Chem. A* **2002**, *106*, 10108.

(6) Rogers, J. E.; Nguyen, K. A.; Hufnagle, D. C.; McLean, D. G.; Su, W.; Gossett, K. M.; Burke, A. R.; Vinogradov, S. A.; Pachter, R.; Fleitz, P. A. *J. Phys. Chem. A* **2003**, *107*, 11331.

(7) Rogers, J. E.; Slagle, J. E.; McLean, D. G.; Sutherland, R. L.; Sankaran, B.; Kannan, R.; Tan, L.-S.; Fleitz, P. A. *J. Phys. Chem. A* **2004**, *108*, 5514.

(8) Baev, A.; Gel'mukhanov, F.; Kimberg, V.; Ågren, H. *J. Phys. B: At. Mol. Opt. Phys.* **2003**, *36*, 3761.

(9) Baev, A.; Gel'mukhanov, F.; Macak, P.; Ågren, H.; Luo, Y. *J. Chem. Phys.* **2002**, *117*, 6214.

(10) Jackson, J. D. *Classical Electrodynamics*, 3rd ed.; Wiley: New York, 1999.

(11) Boyd, R. W. *Nonlinear Optics*; Academic Press: San Diego, CA, 1992.

(12) Gel'mukhanov, F.; Baev, A.; Macak, P.; Luo, Y.; Ågren, H. *J. Opt. Soc. Am. B* **2002**, *19*, 937.

(13) Becke, A. D. *J. Chem. Phys.* **1993**, *98*, 5648.

(14) Bergner, A.; Dolg, M.; Kuchle, W.; Stoll, H.; Preuss, H. *Mol. Phys.* **1993**, *80*, 1431.

(15) Andrae, D.; Haussermann, U.; Dolg, M.; Stoll, H.; Preuss, H. *Theor. Chim. Acta* **1990**, *77*, 123.

(16) Hehre, W. J.; Ditchfield, R.; Pople, J. A. *J. Chem. Phys.* **1972**, *56*, 2257.

(17) Yanai, T.; Tew, D. P.; Handy, N. C. *Chem. Phys. Lett.* **2004**, *393*, 51.

(18) Frisch, M. J.; Trucks, G. W.; Schlegel, H. B.; Scuseria, G. E.; Robb, M. A.; Cheeseman, J. R.; Zakrzewski, V. G.; Montgomery, J. A., Jr.; Stratmann, R. E.; Burant, J. C.; Dapprich, S.; Millam, J. M.; Daniels, A. D.; Kudin, K. N.; Strain, M. C.; Farkas, O.; Tomasi, J.; Barone, V.; Cossi, M.; Cammi, R.; Mennucci, B.; Pomelli, C.; Adamo, C.; Clifford, S.; Ochterski, J.; Petersson, G. A.; Ayala, P. Y.; Cui, Q.; Morokuma, K.; Malick, D. K.; Rabuck, A. D.; Raghavachari, K.; Foresman, J. B.; Cioslowski, J.; Ortiz, J. V.; Stefanov, B. B.; Liu, G.; Liashenko, A.; Piskorz, P.; Komaromi, I.; Gomperts, R.; Martin, R. L.; Fox, D. J.; Keith, T.; Al-Laham, M. A.; Peng, C. Y.; Nanayakkara, A.; Gonzalez, C.; Challacombe, M.; Gill, P. M. W.; Johnson, B.; Chen, W.; Wong, M. W.; Andres, J. L.; Gonzalez, C.; Head-Gordon, M.; Replogle, E. S.; Pople, J. A. *Gaussian 98*; Gaussian, Inc.: Pittsburgh, PA, 1998.

(19) Dalton, a molecular electronic structure program, release 2.0, 2005.

(20) Peach, M. J. G.; Helgaker, T.; Salek, P.; Keal, T. W.; Lutnæs, O. B.; Tozer, D. J.; Handy, N. C. *Phys. Chem. Chem. Phys.* **2006**, *8*, 558.

(21) Paterson, M. J.; Christiansen, O.; Pawlowski, F.; Jørgensen, P.; Hättig, C.; Helgaker, T.; Salek, P. *J. Chem. Phys.* **2006**, *124*, 054322.

(22) Lopes, C. Private communication.

(23) Norman, P.; Ruud, K. In *Nonlinear optical properties of matter*: *From molecules to condensed phases*; Papadopoulos, M., Leszczynski, J., Sadlej, A. J., Eds.; Kluwer Academic Press: New York, 2006.